Modeling and Control of a Pressure-Limited Respirator and Lung Mechanics System

A Dissertation Presented to
The Academic Faculty of
The School of Aerospace Engineering

by

Hancao Li

In Partial Fulfillment of
The Requirements for the Degree of
Doctor of Philosophy in Aerospace Engineering

Georgia Institute of Technology
May 2013

Modeling and Control of a Pressure-Limited Respirator and Lung Mechanics System

Approved by:

Dr. Wassim M. Haddad, Chairman
Aerospace Engineering
Georgia Institute of Technology

Dr. J. V. R. Prasad
Aerospace Engineering
Georgia Institute of Technology

Dr. Eric Feron
Aerospace Engineering
Georgia Institute of Technology

Dr. Vitali Volovoi
Aerospace Engineering
Georgia Institute of Technology

Dr. James M. Bailey
Department of Anesthesiology
Northeast Georgia Medical Center

Date Approved: March 31, 2013

To my parents Zhengguo Li and Yueju Xu

Acknowledgements

It is my pleasure to take this opportunity and thank several people who in one way or another contributed and extended their valuable assistance for the successful completion of this work. This dissertation would not have been possible without their guidance and help.

First and foremost, I would like to express my deepest appreciation to my advisor Professor Wassim M. Haddad. His passion for understanding the natural sciences, pursuit of scientific truth, and fervor for the supreme beauty of mathematics, have deeply inspired me and impacted my scientific education. I am particularly thankful to him for introducing me to the world of mathematical control theory through and for giving me the freedom to pursue my research interests. Working with him as his doctoral student was my most valuable educational experience, which not only unlocked my research horizons but also inspired my enthusiasm towards the pursuit to scientific discovery. Besides his guidance and encouragement through my Ph.D. research, I am grateful for his friendship and guidance to all aspects of my graduate life while being thousands of miles away from home. I also thank Mrs. Lydia Haddad for her hospitality and the great time we had together.

I also would like to express my gratitude to Professors J. V. R. Prasad, Eric M. Feron and Vitali Volovoi for taking time to serve on my dissertation reading committee and for their useful comments and suggestions to improve this dissertation. I also thank Professor John McCuan for his insightful suggestions on the application of the

calculus of variations method to the lung mechanics problem.

I am deeply grateful to Dr. James M. Bailey, who has taken the time from his busy schedule to be on my dissertation committee. The initial ideas and concepts in this dissertation were initiated by him. And his clinical expertise has offered precious ideas and insights to this work. The interaction with Dr. Bailey has helped me understand the general scientific principles underlying physiological systems.

I am also greatly thankful to Dr. VijaySekhar Chellaboina, who was my advisor at the University of Tennessee and who also showed me the power of mathematics in control system research.

I thank all lab partners, Dr. Behnood Gholami, Dr. Kostyantyn Y. Volyanskyy, Andrea L'Afflitto, and Teymur Sadikhov, who shared time, space, and friendship with me at Georgia Tech. They made Knight 408 full of memories in my graduate life. I am additionally thankful to my dear friends, Dr. Liwei Zhang, Dr. Ritu Priyanka Marpu, and Derya Aksaray, for their emotional support.

I am deeply grateful to my husband, Dr. Song Yan. I am indebted to him for his encouragement and support throughout these years that made me stay with my dream firmly. I admire his exemplary perseverance and optimism in the face of difficulties and challenges. I also thank my uncle Dr. Le Li and aunt Grace Ying for every cherishable winter break I spent with them since coming to US.

Lastly, but by no means least, I would like to express my most sincere gratitude to my parents Zhengguo Li and Yueju Xu, for their unconditional love, patience, and support. Without their sacrifice and inspiration, I could not have achieved the educational pinnacle. With tremendous pride and appreciation I dedicated this work to them.

Table of Contents

List of Figures

Summary

Acute respiratory failure due to infection, trauma, and major surgery is one of the most common problems encountered in intensive care units and mechanical ventilation is the mainstay of supportive therapy for such patients. This dissertation develops an analysis and control synthesis framework for a pressure-limited respirator and lung mechanics system using compartment models. Specifically, a general mathematical model is developed for the dynamic behavior of a multicompartment respiratory system. Then, based on this multicompartment model, an optimal respiratory pattern is characterized using classical calculus of variations minimization techniques for inspiratory and expiratory breathing cycles. Furthermore, model predictive controller frameworks are designed to track the given optimal respiratory air flow pattern while satisfying control input amplitude and rate constrains.

Numerous mathematical models of respiratory function that have been presented in the medical and scientific literature have typically viewed the lungs as a single compartment characterized by its compliance (the ratio of compartment volume to pressure) and the resistance to airflow into the compartment. However, the lungs are comprised of many subunits, or compartments, that differ in their capacities for gas exchange. In this dissertation, we develop a general mathematical model for the dynamic behavior of a multicompartment respiratory system in response to an arbitrary applied inspiratory pressure. Specifically, we use compartmental dynamical system theory and Poincaré maps to model and analyze the dynamics of a pressure-

limited respirator and lung mechanics system, and show that the periodic orbit generated by this system is globally asymptotically stable. Furthermore, we show that the individual compartmental volumes, and hence the total lung volume, converge to steady-state end-inspiratory and end-expiratory values. In addition, we develop a model reference direct adaptive controller framework for the multicompartmental model of a pressure-limited respirator and lung mechanics system where the plant and reference model involve switching and time-varying dynamics. We then apply the proposed adaptive feedback controller framework to stabilize a given limit cycle corresponding to a clinically plausible respiratory pattern.

The prediction of the optimal respiratory airflow pattern is critical for the mechanical ventilation to ensure adequate ventilation and adequate oxygenation. In this dissertation, we develop optimal respiratory airflow patterns using a nonlinear multicompartment model for a lung mechanics system. Specifically, we use classical calculus of variations minimization techniques to derive an optimal airflow pattern for inspiratory and expiratory breathing cycles. The physiological interpretation of the optimality criteria used involve the minimization of work of breathing and lung volume acceleration for the inspiratory phase, and the minimization of the elastic potential energy and rapid airflow rate changes for the expiratory phase. Furthermore, we numerically integrate the resulting nonlinear two-point boundary value problems to determine the optimal airflow patterns over the inspiratory and expiratory breathing cycles.

The goal of mechanical ventilation is to ensure adequate ventilation, which involves a magnitude of gas exchange that leads to the desired blood level of carbon dioxide, and adequate oxygenation, which involves a blood concentration of oxygen that will ensure organ function. In this dissertation, first, we develop a model predictive controller for a time-varying, linear periodic multicompartment respiratory

system. Specifically, for a given periodic reference volume pattern, we design a tracking controller using a framework that merges repetitive control and model predictive control. In particular, the periodic multicompartment model is transformed into a lifted run-to-run invariant model and a model predictive controller with nonnegative control input constraints is designed. The proposed tracking control framework is applied to a two-compartment lung mechanics model to demonstrate the efficacy of the proposed approach.

Finally, we develop a model predictive controller based on a nonlinear multicompartment lung mechanics model with the aim to automatically adjust the pressure generated by mechanical ventilation such that the system output tracks a given clinically plausible breathing pattern. Specifically, we formulate a quadratic optimal control problem subject to control input amplitude and rate constraints that minimizes the deviation of the multicompartment respiratory system output from the given reference volume pattern. Then, we derive the predictive control law by minimizing a performance criterion involving the prediction of the future system response over a prescribed time step. The derived optimal control law is given by an explicit form, and thus, avoids an online optimization and reduces the computational effort.

Chapter 1

Introduction

The lungs are particularly vulnerable to acute critical illness. Respiratory failure can result not only from primary lung pathology, such as pneumonia, but also as a secondary consequence of heart failure or inflammatory illness, such as sepsis or trauma. When this occurs, it is essential to support patients while the fundamental disease process is addressed. For example, a patient with pneumonia may require mechanical ventilation while the pneumonia is being treated with antibiotics, which will eventually effectively cure the disease. Since the lungs are vulnerable to critical illness and respiratory failure is common, support of patients with mechanical ventilation is very common in the intensive care unit.

The goal of mechanical ventilation is to ensure adequate ventilation, which involves a magnitude of gas exchange that leads to the desired blood level of carbon dioxide (CO_2), and adequate oxygenation, which involves a blood concentration of oxygen that ensures organ function. Achieving these goals is complicated by the fact that mechanical ventilation can actually cause acute lung injury, either by inflating the lungs to excessive volumes or by using excessive pressures to inflate the lungs. The challenge to mechanical ventilation is to produce the desired blood levels of CO_2 and oxygen without causing further acute lung injury.

The earliest primary modes of ventilation can be classified, approximately, as

volume-controlled or pressure-controlled [65]. In volume-controlled ventilation, the lungs are inflated (by the mechanical ventilator) to a specified volume and then allowed to passively deflate to the baseline volume. The mechanical ventilator controls the volume of each breath and the number of breaths per minute. In pressure-controlled ventilation, the lungs are inflated to a given peak pressure. The ventilator controls this peak pressure as well as the number of breaths per minute. In early ventilation technology, *negative pressure ventilation* was employed, wherein a patient's thoracic area is enclosed in an airtight chamber and the volume of the chamber is expanded, inflating the patient's lungs. Such ventilator devices include tank ventilators, jacket ventilators, and cuirassess [54].

The primary determinant of the level of CO_2 in the blood is *minute ventilation*, which is defined as the *tidal volume* (the volume of each breath) multiplied by the number of breaths per minute [45,69]. With volume-controlled ventilation, both tidal volume and the number of breaths are determined by the machine (the ventilator), and typically, the tidal volumes and breaths per minute are selected by the clinician caring for the patient. In pressure-controlled ventilation, the tidal volume is not directly controlled. The ventilator determines the pressure that inflates the lungs and the tidal volume is proportional to this driving pressure and the compliance or stiffness, of the lungs. Consequently, the minute ventilation is not directly controlled by the ventilator and any change in lung compliance (such as improvement or deterioration in the underlying lung pathology) can result in changes in tidal volume, minute ventilation, and ultimately, the blood concentration of CO_2.

With the increasing availability of microchip technology, it has been possible to design mechanical ventilators that have control algorithms which are more sophisticated than simple volume or pressure control. Examples are proportional-assist ventilation [73,74], adaptive support ventilation [37], SmartCare ventilation [15], and

neutrally adjusted ventilation [59]. In proportional-assist ventilation, the ventilator measures the patients volume and rate of inspiratory gas flow, and then applies pressure support in proportion to the patients inspiratory effort [72]. In this mode of ventilation, inspired oxygen and positive end-expiratory pressure are manually adjusted by the clinician.

In adaptive support ventilation, tidal volume and respiratory rate are automatically adjusted [63]. In particular, the patients respiratory pattern is measured pointwise in time and fed back to the controller to provide the required (target) tidal volume and patient respiratory rate. Adaptive support ventilation does not provide continuous control of minute ventilation, positive end-expiratory pressure, and inspired oxygen, these parameters need to be adjusted manually.

SmartCare ventilation monitors tidal volume, respiratory rate, and end-tidal pressure of CO_2 to maintain the patient in a respiratory "comfort" zone by automatically adjusting the level of pressure support [8, 39]. SmartCare ventilators do not account for patient respiratory variations and do not generally guarantee adequate minute ventilation during weaning. In addition, positive end-expiratory pressure and inspired oxygen need to be manually adjusted.

Neurally adjusted ventilation is fundamentally different from the aforementioned automatic ventilation technologies in the sense that it uses the patients respiratory neural drive as a measurement signal to the ventilator [30]. In this mode of ventilation, rather than controlling pressure, the patients respiratory neural drive signal to the diaphragmatic electromyogram is controlled using electrodes placed on an esophageal catheter [3]. Even though this approach has been shown to be effective in some recent clinical studies [4, 50], its effectiveness is affected if the patient is highly sedated. In addition, as in the aforementioned ventilator technologies, positive end-expiratory pressure and inspired oxygen need to be manually controlled.

The common theme in modern ventilation control algorithms is the use of pressure-limited ventilation while also guaranteeing adequate minute ventilation. One of the challenges in the design of efficient control algorithms is that the fundamental physiological variables defining lung function, i.e., the resistance to gas flow and the compliance of the lung units, are not constant but rather vary with lung volume. For example, the compliance is strictly defined as $\mathrm{d}V/\mathrm{d}P$, where V is the lung unit volume and P is the pressure driving inflation. More simply, lung volume is a nonlinear function of driving pressure. In addition, these physiological variables vary from patient to patient, as well as within the same patient under different conditions, making it very challenging to develop models and effective control law architectures for active mechanical ventilations.

1.1. Brief Outline of the Dissertation

In this dissertation, we develop mathematical modeling and control design methods for a pressure-limited respirator and lung mechanics system. The contents of the dissertation are as follows. In Chapter 2 we develop a general mathematical model for the dynamic behavior of a multicompartment respiratory system in response to an arbitrary applied inspiratory pressure. Specifically, we use compartmental dynamical system theory and Poincaré maps to model and analyze the dynamics of a pressure-limited respirator and lung mechanics system. Then, we present a model reference direct adaptive controller framework for the multicompartmental model of a pressure-limited respirator and lung mechanics system where the plant and reference model involve switching and time-varying dynamics.

In Chapter 3, we use classical calculus of variations minimization techniques to characterize optimal respiratory airflow patterns using a nonlinear multicompartment model for a lung mechanics system. In Chapter 4, we consider a model predictive

controller framework for a time-varying, linear periodic multicompartment respiratory system such that for a given periodic reference volume pattern, a tracking controller is designed using a framework that merges repetitive control and model predictive control. Then, in Chapter 5, we develop a predictive tracking controller for a nonlinear multicompartment lung mechanics model by minimizing a quadratic performance criterion involving a prediction of the system response over a prescribed time step. Specifically, the proposed tracking control framework is applied to a lung mechanics model with nonlinear compliances. Finally, in Chapter 6, we discuss ongoing research and future extensions of the research.

Chapter 2

Limit Cycle Stability Analysis and Adaptive Control of a Multicompartment Model for a Pressure-Limited Respirator and Lung Mechanics System

2.1. Introduction

Acute respiratory failure due to infection, trauma, and major surgery is one of the most common problems encountered in intensive care units and mechanical ventilation is the mainstay of supportive therapy for such patients. Numerous mathematical models of respiratory function have been developed in the hope of better understanding pulmonary function and the process of mechanical ventilation [2, 9, 17, 44, 67]. However, the models that have been presented in the medical and scientific literature have typically assumed homogenous lung function. For example, in analogy to a simple electrical circuit, the most common model has assumed that the lungs can be viewed as a single compartment characterized by its compliance (the ratio of compartment volume to pressure) and the resistance to air flow into the compartment [9, 44, 67].

While a few investigators have considered two compartment models, reflecting the fact that there are two lungs (right and left), there has been little interest in more detailed models [13, 29, 58]. However, the lungs, especially diseased lungs, are hetero-

geneous, both functionally and anatomically, and are comprised of many subunits, or compartments, that differ in their capacities for gas exchange. Realistic models should take this heterogeneity into account. While more sophisticated models entail greater complexity, since the models are readily presented in the context of dynamical systems theory, sophisticated mathematical tools can be applied to their analysis. Compartmental lung models are described by a state vector, whose components are the volumes of the individual compartments. One interesting and important question is the stability, in the sense of dynamical systems theory, of the model.

For a simple one compartment model, it is easy to demonstrate that the model exhibits an asymptotically stable limit cycle behavior. And indeed, in clinical practice it appears that the total lung volume converges to the steady-state end-inspiratory and end-expiratory values after the institution of mechanical ventilation. However, a more subtle question for a multicompartment lung model is whether the volumes in the individual compartments could be unstable, even when the total volume of the lung (the sum of all the compartment volumes) converges to a steady-state value. That is, Is it possible that individual compartment volumes oscillate or even demonstrate chaotic behavior while the total lung volume is stable?

This question has interesting clinical implications as there is also heterogeneity in the amount of blood flowing to individual subunits of the lung. If there is significant disparity in the ratio of ventilation (reflected in the compartment volume) to blood flow, gas exchange is impaired, resulting in decreases in the oxygen or increases in the carbon dioxide content of blood, which is a serious clinical problem. Instability of the compartment volumes could be reflected in unstable measures of basic pulmonary function, such as oxygen or carbon dioxide levels in the blood. In this chapter, we first develop a generalized multicompartment lung model and subsequently analyze its stability properties. Specifically, we use compartmental dynamical system theory

and Poincaré maps to model and analyze the dynamics of a pressure-limited respirator and lung mechanics system, and show that the periodic orbit generated by this system is globally asymptotically stable. Furthermore, we show that the individual compartmental volumes, and hence the total lung volume, converge to steady-state end-inspiratory and end-expiratory values.

As noted above, mechanical ventilation of a patient with respiratory failure is one of the most common life-saving procedures performed in the intensive care unit. However, mechanical ventilation is physically uncomfortable due to the noxious interface between the ventilator and patient, and mechanical ventilation evokes substantial anxiety on the part of the patient. This will often be manifested by the patient "fighting the ventilator." In this situation, there is dyssynchrony between the ventilatory effort of the patient and the ventilator. The patient will attempt to exhale at the time the ventilator is trying to expand the lungs or the patient will try to inhale when the ventilator is decreasing airway pressure to allow an exhalation.

When patient-ventilator dyssynchrony occurs, at the very least there is excessive work of breathing with subsequent ventilatory muscle fatigue and in the worst case, elevated airway pressures that can actually rupture lung tissue. In this situation, it is a very common clinical practice to sedate patients to minimize "fighting the ventilator." Sedative-hypnotic agents act on the central nervous system to ameliorate the anxiety and discomfort associated with mechanical ventilation and facilitate patient-ventilator synchrony.

Using the multicompartmental model of a pressure-limited respirator and lung mechanics systems developed in the first part of the chapter, we also develop an adaptive feedback controller for addressing this dyssynchrony for intensive care unite sedation. In particular, we develop a model reference direct adaptive controller framework where the plant and reference model involve switching and time-varying dynamics. Then,

we apply the proposed adaptive framework to the multicompartmental model of a pressure-limited respirator and lung mechanics system. Specifically, we develop an adaptive feedback controller that stabilizes a given limit cycle corresponding to a clinically plausible breathing pattern. Finally, we apply the proposed adaptive control framework to a mechanical ventilation model to quantify patient-ventilator dyssynchrony for intensive care unit sedation.

2.2. Notation and Mathematical Preliminaries

In this section, we introduce notation, several definitions, and some key results that are necessary for developing the main results of this dissertation. Specifically, $\mathbb{R}^n$ denotes the set of $n \times 1$ real column vectors and $\mathbb{R}^{n\times m}$ denotes the set of $n \times m$ real matrices, for $x \in \mathbb{R}^n$ we write $x \geq\geq 0$ (resp., $x >> 0$) to indicate that every component of x is nonnegative (resp., positive). In this case, we say that x is *nonnegative* or *positive*, respectively. Likewise, $A \in \mathbb{R}^{n\times m}$ is *nonnegative*[1] or *positive* if every entry of A is nonnegative or positive, respectively, which is written as $A \geq\geq 0$ or $A >> 0$, respectively.

Furthermore, for $A \in \mathbb{R}^{n\times n}$ we write $A \geq 0$ (resp., $A > 0$) to indicate that A is a nonnegative-definite (resp., positive-definite) matrix. In addition, $(\cdot)^{\mathrm{T}}$ denotes transpose, $(\cdot)^{-1}$ denotes inverse, "$\otimes$" denotes the Kronecker product, $(\cdot)'$ to denote Frèchet derivative, $\|\cdot\|_2$ denotes the Euclidian norm, $\|\cdot\|_Q$ denotes the weighted Euclidian norm, that is, $\|z\|_Q^2 \triangleq z^{\mathrm{T}}Qz, z \in \mathbb{R}^n$, spec$(A)$ denotes the spectrum of the square matrix A, $\rho(A)$ denotes the spectral radius of A, dim $\mathcal{S}$ denotes the dimension of the set $\mathcal{S} \subseteq \mathbb{R}^n$, and $\mathcal{N}(A)$ denotes the null space of A, 0_m denotes the zeros vector of order m, that is, $0_m = [0, \ldots, 0]^{\mathrm{T}}$, $\mathbb{Z}_+$ denotes the set of positive integers, and $\mathbb{R}_+$

[1]In this proposal it is important to distinguish between a square nonnegative (resp., positive) matrix and a nonnegative-definite (resp., positive-definite) matrix.

denotes the set of positive real numbers. Let $\overline{\mathbb{R}}^n_+$ and $\mathbb{R}^n_+$ denote the nonnegative and positive orthants of $\mathbb{R}^n$, that is, if $x \in \mathbb{R}^n$, then $x \in \overline{\mathbb{R}}^n_+$ and $x \in \mathbb{R}^n_+$ are equivalent, respectively, to $x \geq\geq 0$ and $x >> 0$. Finally, let $\mathbf{e}_n \in \mathbb{R}^n$ denotes the ones vector of order n, that is, $\mathbf{e}_n = [1, \cdots, 1]^{\mathrm{T}}$; if the order of $\mathbf{e}_n$ is clear from context we simply write $\mathbf{e}$ for $\mathbf{e}_n$.

The following definitions introduce the notions of essentially nonnegative, compartmental, and strictly ultrametric matrices.

Definition 2.1 [20]. Let $A \in \mathbb{R}^{n\times n}$. A is *essentially nonnegative* if $A_{(i,j)} \geq 0$, $i, j = 1, \ldots, n$, $i \neq j$. A is *compartmental* if A is essentially nonnegative and $A^{\mathrm{T}}\mathbf{e} \leq\leq 0$.

Definition 2.2 [46]. Let $A \in \mathbb{R}^{n\times n}$ be such that $A \geq\geq 0$. A is *strictly ultrametric* if A is symmetric, $A_{(i,i)} > \max\{A_{(i,k)} : k = 1, \ldots, n, k \neq i\}$, $i = 1, \ldots, n$, and $A_{(i,j)} \geq \min\{A_{(i,k)}, A_{(k,j)}\}$, $k = 1, \ldots, n$, $i, j = 1, \ldots, n, i \neq j$.

The following lemmas and propositions are key in establishing the main results of this chapter.

Lemma 2.1 [20]. Let $A \in \mathbb{R}^{n\times n}$. Then A is essentially nonnegative if and only if e^{At} is nonnegative for all $t \geq 0$.

Proposition 2.1. The following statements hold:

i) Let $\lambda_1, \lambda_2 \geq 0$ be such that $\lambda_1 + \lambda_2 > 0$ and let $A_1, A_2 \in \mathbb{R}^{n\times n}$ be strictly ultrametric. Then $\lambda_1 A_1 + \lambda_2 A_2$ is strictly ultrametric.

ii) Let $x \in \mathbb{R}^n$ be such that $x_i = 0$ or $1, i = 1, \ldots, n$, and let $P \in \mathbb{R}^{n\times n}$ be a positive diagonal matrix. Then $P + xx^{\mathrm{T}}$ is a strictly ultrametric matrix.

Proof. Statement i) is a direct consequence of Definition 2.2. To show ii) let $A \triangleq P + xx^{\mathrm{T}}$ and note that A is symmetric and

$$A_{(i,j)} = \begin{cases} P_{(i,i)} + x_i^2, & \text{if } i = j, \\ x_i x_j, & \text{if } i \neq j. \end{cases}$$

Hence, if $x_i = 0$, then $\max\{A_{(i,k)} : k = 1, \ldots, n, k \neq i\} = 0, i = 1, \ldots, n$, which implies that $A_{(i,i)} = P_{(i,i)} > \max\{A_{(i,k)} : k = 1, \ldots, n, k \neq i\}, i = 1, \ldots, n$. Alternatively, if $x_i = 1$, then $A_{(i,i)} = P_{(i,i)} + 1 > \max\{x_k : k = 1, \ldots, n, k \neq i\}, i = 1, \ldots, n$. Furthermore, for $i \neq j, A_{(i,j)} = x_i x_j$ and

$$\min\{A_{(i,k)}, A_{(k,j)}\} = \begin{cases} 0, & \text{if } x_i x_j = 0, \\ x_k, & \text{otherwise.} \end{cases}$$

In either case, $A_{(i,j)} \geq \min\{A_{(i,k)}, A_{(k,j)}\}, k = 1, \ldots, n, i, j = 1, \ldots, n, i \neq j$, which implies that A is strictly ultrametric. □

Lemma 2.2 [46]. Let $A \in \mathbb{R}^{n \times n}$ be such that $A \geq\geq 0$. If A is strictly ultrametric, then $-A^{-1}$ is essentially nonnegative and $A^{-1}\mathbf{e} \geq\geq 0$.

Proposition 2.2. Let $A \in \mathbb{R}^{n \times n}$ and assume that there exists an $n \times n$ matrix $P > 0$ such that

$$A^{\mathrm{T}}P + PA < 0. \tag{2.1}$$

Then $e^{A^{\mathrm{T}}} P e^{A} < P$.

Proof. Define $R \triangleq -(A^T P + PA) > 0$ and note that (2.1) implies

$$P = \int_0^\infty e^{A^{\mathrm{T}}t} R e^{At} \mathrm{d}t. \tag{2.2}$$

Next, pre- and post- multiplying (2.2) by $e^{A^{\mathrm{T}}}$ and e^{A}, respectively, yields

$$\begin{aligned} e^{A^{\mathrm{T}}} P e^{A} &= \int_0^\infty e^{A^{\mathrm{T}}(t+1)} R e^{A(t+1)} \mathrm{d}t \\ &= \int_1^\infty e^{A^{\mathrm{T}}t} R e^{At} \mathrm{d}t \end{aligned}$$

$$
\begin{aligned}
&= \int_0^\infty e^{A^{\mathrm{T}}t} R e^{At} - \int_0^1 e^{A^{\mathrm{T}}t} R e^{At} \mathrm{d}t \\
&= P - \int_0^1 e^{A^{\mathrm{T}}t} R e^{At} \mathrm{d}t \\
&< P,
\end{aligned}
$$

which proves the result. □

Remark 2.1. It is well known that A is Hurwitz if and only if e^A is Schur. Hence, it follows from Proposition 2.2 that the Lyapunov function $V(x) = x^{\mathrm{T}}Px$ can be used to establish the stability of both A and e^A.

Next, we analyze the stability of periodic orbits using Poincaré maps [19, 70]. To state Poincaré's theorem, consider the nonlinear periodic dynamical system

$$
\dot{x}(t) = f(t, x(t)), \qquad x(0) = x_0, \qquad t \in \mathcal{I}_{x_0}, \tag{2.3}
$$

where $x(t) \in \mathcal{D} \subseteq \mathbb{R}^n$, $t \in \mathcal{I}_{x_0}$, is the system state vector, $\mathcal{D}$ is an open set, $f : [0, \infty) \times \mathcal{D} \to \mathbb{R}^n$ satisfies $f(t, x) = f(t + T, x)$, $x \in \mathcal{D}$, $t \geq 0$, for some $T > 0$, and $\mathcal{I}_{x_0} = [0, \tau_{x_0})$, $0 < \tau_{x_0} \leq \infty$, is the maximal interval of existence for the solution $x(\cdot)$ of (2.3). A continuously differentiable function $x : \mathcal{I}_{x_0} \to \mathcal{D}$ is said to be a *solution* to (2.3) on the interval $\mathcal{I}_{x_0} \subseteq [0, \infty)$ with initial condition $x(0) = x_0$ if $x(t)$ satisfies (2.3) for all $t \in \mathcal{I}_{x_0}$. It is assumed that $f(\cdot, \cdot)$ is such that the solution to (2.3) is unique for every initial condition in $\mathcal{D}$ and jointly continuous in t and x_0. A sufficient condition ensuring this is Lipschitz continuity of $f(t, \cdot) : \mathcal{D} \to \mathbb{R}^n$ for all $t \in [0, t_1]$ and continuity of $f(\cdot, x) : [0, t_1] \to \mathbb{R}^n$ for all $x \in \mathcal{D}$. Here, we assume that all solutions to (2.3) are bounded over $\mathcal{I}_{x_0}$, and hence, by the Peano-Cauchy theorem can be extended to infinity.

Next, we introduce the notions of periodic solutions and periodic orbits for (2.3). For the next definition, we denote the solution $x(\cdot)$ to (2.3) with initial conditon

$x_0 \in \mathcal{D}$ by $s(t, x_0)$.[2]

Definition 2.3. A solution $s(t, x_0)$ of (2.3) is *periodic* if there exists a finite time $T > 0$ such that $s(t + T, x_0) = s(t, x_0)$ for all $t \geq 0$. A set $\mathcal{O} \subset \mathcal{D}$ is a *periodic orbit* of (2.3) if $\mathcal{O} = \{x \in \mathcal{D} : x = s(t, x_0), 0 \leq t \leq T\}$ for some periodic solution $s(t, x_0)$ of (2.3).

Next, we introduce the notions of Lyapunov and asymptotic stability of a periodic orbit of the nonlinear dynamical system (2.3). For this definition, $\operatorname{dist}(p, \mathcal{M})$ denotes the smallest distance from a point p to any point in the set $\mathcal{M}$, that is, $\operatorname{dist}(p, \mathcal{M}) \triangleq \inf_{x \in \mathcal{M}} \|p - x\|$.

Definition 2.4. A periodic orbit $\mathcal{O}$ of (2.3) is *Lyapunov stable* if, for all $\varepsilon > 0$, there exists $\delta = \delta(\varepsilon) > 0$ such that if $\operatorname{dist}(x_0, \mathcal{O}) < \delta$, then $\operatorname{dist}(s(t, x_0), \mathcal{O}) < \varepsilon, t \geq 0$. A periodic orbit $\mathcal{O}$ is *asymptotically stable* if $\mathcal{O}$ is Lyapunov stable and there exists $\varepsilon > 0$ such that if $\operatorname{dist}(x_0, \mathcal{O}) < \varepsilon$, then $\operatorname{dist}(s(t, x_0), \mathcal{O}) \to 0$ as $t \to \infty$.

To proceed, we assume that for the point $p \in \mathcal{D}$, the dynamical system (2.3) has a periodic solution $s(t, p), t \geq 0$, with period $T > 0$ that generates the periodic orbit $\mathcal{O} \triangleq \{x \in \mathcal{D} : x = s(t, p), 0 \leq t \leq T\}$. Next, let $\mathcal{U} \subset \mathcal{D}$ be a neighborhood of the point p and define the Poincaré return map $P : \mathcal{U} \to \mathcal{D}$ by

$$P(x) \triangleq s(T, x), \ x \in \mathcal{U}. \tag{2.4}$$

Furthermore, define the discrete-time dynamical system given by

$$z(k + 1) = P(z(k)), \ z(0) \in \mathcal{U}, \ k \in \overline{\mathbb{Z}}_+, \tag{2.5}$$

[2]Note that since (2.3) is a time-varying dynamical system it is typical to denote its solution as $\hat{s}(t, t_0, x_0)$ to indicate the dependence on both the initial time t_0 and the initial state x_0. In this section, we assume that $t_0 = 0$ and define $s(t, x_0) \triangleq \hat{s}(t, 0, x_0)$.

where $\overline{\mathbb{Z}}_+$ denotes the set of nonnegative integers. Clearly $x = p$ is a fixed point of (2.5) since $p = s(T, p) = P(p)$.

Theorem 2.1. Consider the nonlinear periodic dynamical system (2.3) with the Poincaré map defined by (2.4). Assume that the point $p \in \mathcal{D}$ generates the periodic orbit $\mathcal{O} \triangleq \{x \in \mathcal{D} : x = s(t, p), 0 \leq t \leq T\}$, where $s(t, p), t \geq 0$, is the periodic solution with period T. Then the following statements hold:

i) $p \in \mathcal{D}$ is a Lyapunov stable fixed point of (2.5) if and only if the periodic orbit $\mathcal{O}$ generated by p is Lyapunov stable.

ii) $p \in \mathcal{D}$ is an asymptotically stable fixed point of (2.5) if and only if the periodic orbit $\mathcal{O}$ generated by p is asymptotically stable.

Proof. Define $x_1(t) \triangleq x(t)$ and $x_2(t) \triangleq t$, and note that the solution $x(t)$, $t \geq 0$, to the nonlinear periodic dynamical system (2.3) can be equivalently characterized by the solution $x_1(t)$, $t \geq 0$, to the nonlinear autonomous dynamical system

$$\dot{x}_1(t) = f(x_2(t), x_1(t)), \quad x_1(0) = x_0, \quad t \geq 0, \tag{2.6}$$

$$x_2(t) = t \bmod T, \quad x_2(0) = 0. \tag{2.7}$$

Since $p \in \mathcal{D}$ generates a periodic solution to (2.3) it follows that the point $[p, 0]^{\mathrm{T}} \in \mathcal{D} \times [0, T]$ generates a periodic solution to (2.6) and (2.7). Next, it can be shown that the map $P : \mathcal{U} \to \mathcal{D}$ given by (2.4) is a Poincaré map for (2.6) and (2.7) (see [70, p. 127] for details). Now, the result is a direct consequence of the standard Poincaré theorem [19]. □

Finally, in this chapter, we develop a multicompartment lung model based on a directed tree architecture. The following definitions are necessary for the main results of this chapter.

Definition 2.5 [64]. A *weighted directed graph* $\mathfrak{G}$ is a triple $(\mathcal{V}, \mathcal{E}, W)$, where $\mathcal{V} = \{v_1, v_2, \ldots, v_N\}$ is the set of *vertices*, $\mathcal{E} = \{e_1, e_2, \ldots, e_M\} \subseteq \mathcal{V} \times \mathcal{V}$ is the set of *edges*, and $W \in \mathbb{R}^{N\times N}$ is the weighted *adjacency matrix*. Every edge $e_l \in \mathcal{E}$ corresponds to an ordered pair of vertices $(v_i, v_j) \in \mathcal{V} \times \mathcal{V}$, where v_i and v_j are the *initial* and *terminal vertices* of the edge e_l. In this case, e_l is *incident into* v_j and *incident out of* v_i. The adjacency matrix W is such that $W_{(i,j)} > 0, i, j = 1, \ldots, N$, if $(v_i, v_j) \in \mathcal{E}$, and $W_{(i,j)} = 0$ otherwise. The *in-degree* $d_{\mathrm{i}}(v_i)$ of v_i is the number of edges incident into v_i and the *out-degree* $d_{\mathrm{o}}(v_j)$ of v_j is the number of edges incident out of v_j. A *directed path from* v_{i_1} *to* v_{i_k} is a set of distinct vertices $\{v_{i_1}, v_{i_2}, \ldots, v_{i_k}\}$ such that $(v_{i_j}, v_{i_{j+1}}) \in \mathcal{E}, j = 1, \ldots, k-1$. A vertex v_i is a *root* of $\mathfrak{G}$ if, for every $v_j \neq v_i$, there exist directed paths from v_i to v_j. $\mathfrak{G}$ is *connected* if, for every pair of $v_i, v_j \in \mathcal{V}$, there exists $v_k \in \mathcal{V}$ such that there are directed paths from v_k to v_i and v_k to v_j. A vertex $v_i \in \mathcal{V}$ is a *leaf* of $\mathfrak{G}$ if $d_{\mathrm{o}}(v_i) = 0$.

Definition 2.6 [64]. A weighted directed graph $\mathfrak{G}$ is a *weighted directed tree* if $\mathcal{G}$ is connected and there exists a vertex $v_i \in \mathcal{V}$ such that $d_{\mathrm{i}}(v_i) = 0$ and $d_{\mathrm{i}}(v_j) = 1, v_j \in \mathcal{V} \setminus \{v_i\}$.

Remark 2.2. Note that if $\mathfrak{G}$ is a weighted directed tree, then there exists exactly one root $v_i \in \mathcal{V}$ and exactly one directed path from v_i to v_j for all $v_j \in \mathcal{V} \setminus \{v_i\}$. See [64] for details.

2.3. Compartmental Modeling of Lung Dynamics: Dichotomy Architecture

In this section, we develop a general mathematical model for the dynamic behavior of a multicompartment respiratory system in response to an arbitrary applied inspiratory pressure. Here, we assume that the bronchial tree has a *dichotomy ar-*

chitecture [68], that is, in every generation each airway unit branches in two airway units of the subsequent generation. First, however, we start by considering a single-compartment lung model as shown in Figure 2.1. In this model, the lungs are repre-

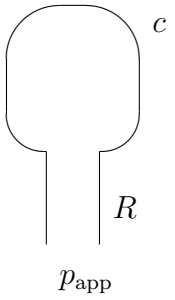

Figure 2.1: Single-compartment lung model.

sented as a single lung unit with compliance c connected to a pressure source by an airway unit with resistance (to air flow) of R. At time $t = 0$, an arbitrary pressure $p_{\text{in}}(t)$ is applied to the opening of the parent airway, where $p_{\text{in}}(t)$ is determined by the mechanical ventilator. A typical choice for $p_{\text{in}}(t)$ is $p_{\text{in}}(t) = \alpha t + \beta$, where α and β are positive constants. This pressure is applied to the airway opening over the time interval $0 \leq t \leq T_{\text{in}}$, which is the inspiratory part of the breathing cycle. At time $t = T_{\text{in}}$, the applied airway pressure is released and expiration takes place passively, that is, the external pressure is only the atmospheric pressure $p_{\text{ex}}(t)$ during the time interval $T_{\text{in}} \leq t \leq T_{\text{in}} + T_{\text{ex}}$, where T_{ex} is the duration of expiration.

The state equation for inspiration (inflation of lung) is given by

$$R_{\text{in}}\dot{x}(t) + \frac{1}{c}x(t) = p_{\text{in}}(t), \qquad x(0) = x_0^{\text{in}}, \qquad 0 \leq t \leq T_{\text{in}}, \tag{2.8}$$

where $x(t) \in \mathbb{R}$, $t \geq 0$, is the lung volume, $R_{\text{in}} \in \mathbb{R}$ is the resistance to air flow during the inspiration period, $x_0^{\text{in}} \in \mathbb{R}$ is the lung volume at the start of the inspiration and serves as the system initial condition. We assume that expiration is passive (due to elastic stretch of lung unit). During the expiration process, the state equation is given

by

$$R_{\text{ex}}\dot{x}(t) + \frac{1}{c}x(t) = p_{\text{ex}}(t), \qquad x(T_{\text{in}}) = x_0^{\text{ex}}, \qquad T_{\text{in}} \le t \le T_{\text{in}} + T_{\text{ex}}, \tag{2.9}$$

where $x(t) \in \mathbb{R}$, $t \ge 0$, is the lung volume, $R_{\text{ex}} \in \mathbb{R}$ is the resistance to air flow during the expiration period, and $x_0^{\text{ex}} \in \mathbb{R}$ is the lung volume at the start of expiration.

Next, we develop the state equations for inspiration and expiration for a 2^n-compartment model, where $n \ge 0$. In this model, the lungs are represented as 2^n lung units which are connected to the pressure source by n generations of airway units, where each airway is divided into two airways of the subsequent generation leading to 2^n compartments (see Figure 2.2 for a four-compartment model).

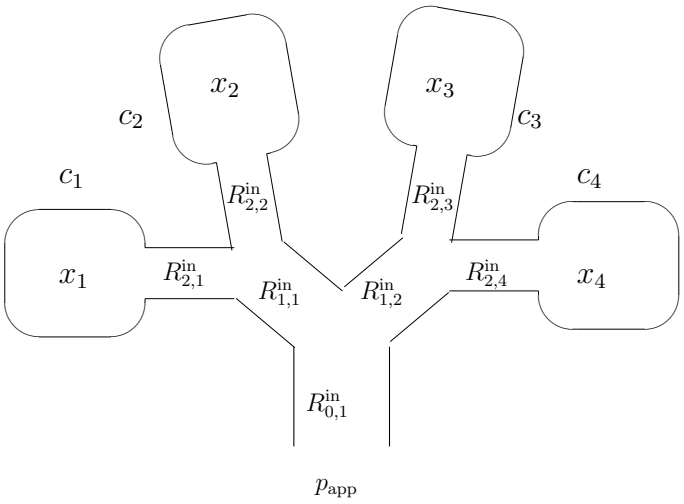

Figure 2.2: Four-compartment lung model.

Let $c_i,\ i = 1, 2, \ldots, 2^n$, denote the compliance of each compartment and let $R^{\text{in}}_{j,i}$ (resp., $R^{\text{ex}}_{j,i}$), $i = 1, 2, \ldots, 2^j,\ j = 0, \ldots, n$, denote the resistance (to air flow) of the i-th airway in the j-th generation during the inspiration (resp., expiration) period with R^{in}_{01} (resp., R^{ex}_{01}) denoting the inspiration (resp., expiration) of the *parent* (i.e., 0-th generation) airway. As in the single-compartment model we assume that a pressure of $p_{\text{in}}(t)$ is applied during inspiration. Next, let $x_i,\ i = 1, 2, \ldots, 2^n$, denote the lung

volume in the i-th compartment so that the state equations for inspiration are given by

$$R^{\text{in}}_{n,i}\dot{x}_i(t) + \frac{1}{c_i}x_i(t) + \sum_{j=0}^{n-1} R^{\text{in}}_{j,k_j} \sum_{l=(k_j-1)2^{n-j}+1}^{k_j 2^{n-j}} \dot{x}_l(t) = p_{\text{in}}(t),$$
$$x_i(0) = x^{\text{in}}_{i0}, \quad 0 \le t \le T_{\text{in}}, \quad i = 1, 2, \ldots, 2^n, \tag{2.10}$$

where

$$k_j = \left\lfloor \frac{k_{j+1} - 1}{2} \right\rfloor + 1, \quad j = 0, \ldots, n-1, \quad k_n = i, \tag{2.11}$$

and $\lfloor q \rfloor$ denotes the *floor function* which gives the largest integer less than or equal to the positive number q.

To further elucidate the inspiration state equation for a 2^n-compartment model, consider the four-compartment model shown in Figure 2.2 corresponding to a two generation lung model. Let x_i, $i = 1, 2, 3, 4$, denote the compartmental volumes. Now, the pressure $\frac{1}{c_i}x_i(t)$ due to the compliance in i-th compartment will be equal to the difference between the external pressure applied and the resistance to air flow at every airway in the path leading from the pressure source to the i-th compartment. In particular, for $i = 3$ (see Figure 2.2),

$$\frac{1}{c_3}x_3(t) = p_{\text{in}}(t) - R^{\text{in}}_{0,1}[\dot{x}_1(t) + \dot{x}_2(t) + \dot{x}_3(t) + \dot{x}_4(t)] - R^{\text{in}}_{1,2}[\dot{x}_3(t) + \dot{x}_4(t)] - R^{\text{in}}_{2,3}\dot{x}_3(t),$$

or, equivalently,

$$R^{\text{in}}_{2,3}\dot{x}_3(t) + R^{\text{in}}_{1,2}[\dot{x}_3(t) + \dot{x}_4(t)] + R^{\text{in}}_{0,1}[\dot{x}_1(t) + \dot{x}_2(t) + \dot{x}_3(t) + \dot{x}_4(t)] + \frac{1}{c_3}x_3(t) = p_{\text{in}}(t).$$

Next, we consider the state equation for the expiration process. As in the single-compartment model we assume that the expiration process is passive and the external pressure applied is $p_{\text{ex}}(t)$. Following an identical procedure as in the inspiration case, we obtain the state equation for expiration as

$$R^{\text{ex}}_{n,i}\dot{x}_i(t) + \sum_{j=0}^{n-1} R^{\text{ex}}_{j,k_j} \sum_{l=(k_j-1)2^{n-j}+1}^{k_j 2^{n-j}} \dot{x}_l(t) + \frac{1}{c_i}x_i(t) = p_{\text{ex}}(t),$$

$$x_i(T_{\rm in}) = x_{i_0}^{\rm ex}, \quad T_{\rm in} \leq t \leq T_{\rm ex} + T_{\rm in}, \quad i = 1, 2, \ldots, 2^n, \tag{2.12}$$

where k_j satisfies (3.5).

2.4. State Space Multicompartment Lung Model

In this section, we rewrite the state equations (3.3) and (3.6) for inspiration and expiration, respectively, as a switched dynamical system. To describe the dynamics of the multicompartment lung model in terms of a state space model, define the state vector $x \triangleq [x_1, x_2, \cdots, x_{2^n}]^{\rm T}$, where x_i denotes the lung volume of the i-th compartment. Now, the state equation (3.3) for inspiration can be rewritten as

$$R_{\rm in}\dot{x}(t) + Cx(t) = p_{\rm in}(t)\mathbf{e}, \quad x(0) = x_0^{\rm in}, \quad 0 \leq t \leq T_{\rm in}, \tag{2.13}$$

where $C \triangleq \mathrm{diag}[\frac{1}{c_1}, \cdots, \frac{1}{c_{2^n}}]$ and

$$R_{\rm in} \triangleq \sum_{j=0}^{n} \sum_{k=1}^{2^j} R_{j,k}^{\rm in}\ Z_{j,k}\ Z_{j,k}^{\rm T}, \tag{2.14}$$

where $Z_{j,k} \in \mathbb{R}^{2^n}$ is such that the l-th element of $Z_{j,k}$ is 1 for all $l = (k-1)2^{n-j} + 1,\ (k-1)2^{n-j} + 2, \ldots, k2^{n-j}, k = 1, \ldots, 2^j, j = 0, 1, \ldots, n$, and zero elsewhere.

Similarly, the state equation (3.6) for expiration can be rewritten as

$$R_{\rm ex}\dot{x}(t) + Cx(t) = p_{\rm ex}(t)\mathbf{e}, \quad x(T_{\rm in}) = x_0^{\rm ex}, \quad T_{\rm in} \leq t \leq T_{\rm ex} + T_{\rm in}, \tag{2.15}$$

where

$$R_{\rm ex} \triangleq \sum_{j=0}^{n} \sum_{k=1}^{2^j} R_{j,k}^{\rm ex}\ Z_{j,k}\ Z_{j,k}^{\rm T}. \tag{2.16}$$

Note that if $R_{\rm in}$ and $R_{\rm ex}$ are invertible, then (2.13) and (2.15) can be equivalently written as

$$\dot{x}(t) = A_{\rm in}x(t) + B_{\rm in}p_{\rm in}(t), \quad x(0) = x_0^{\rm in}, \quad 0 \leq t \leq T_{\rm in}, \tag{2.17}$$

$$\dot{x}(t) = A_{\rm ex}x(t) + B_{\rm ex}p_{\rm ex}(t), \quad x(T_{\rm in}) = x_0^{\rm ex}, \quad T_{\rm in} \leq t \leq T_{\rm ex} + T_{\rm in}, \tag{2.18}$$

where $A_{\text{in}} \triangleq -R_{\text{in}}^{-1}C$, $B_{\text{in}} \triangleq R_{\text{in}}^{-1}\mathbf{e}$, $A_{\text{ex}} \triangleq -R_{\text{ex}}^{-1}C$, and $B_{\text{ex}} \triangleq R_{\text{ex}}^{-1}\mathbf{e}$.

The following proposition states and proves several important properties of R_{in}, R_{ex}, A_{in}, and A_{ex} that are essential for the main results of this section.

Proposition 2.3. Consider the dynamical system (2.13) and (2.15). Then the following statements hold:

i) $R_{\text{in}} > 0$ and $R_{\text{ex}} > 0$.

ii) $A_{\text{in}}^{\text{T}}C + CA_{\text{in}} < 0$.

iii) $A_{\text{ex}}^{\text{T}}C + CA_{\text{ex}} < 0$.

iv) R_{in} and R_{ex} are strictly ultrametric.

v) A_{in} and A_{ex} are compartmental and Hurwitz, and $B_{\text{in}} \geq\geq 0$ and $B_{\text{ex}} \geq\geq 0$.

Proof. Statement *i*) follows from (2.14) by noting

$$R_{\text{in}} \geq \sum_{k=1}^{2^n} R_{n,k}^{\text{in}}\, Z_{n,k}\, Z_{n,k}^{\text{T}} = \text{diag}[R_{n,1}^{\text{in}}, \cdots, R_{n,2^n}^{\text{in}}] > 0,$$

since the l-th element of $Z_{n,k}$ is 1 if $l = k$ and zero otherwise. Similarly, it can be shown that $R_{\text{ex}} > 0$.

Statements *ii*) and *iii*) follow immediately by noting that

$$A_{\text{in}}^{\text{T}}C + CA_{\text{in}} = -2CR_{\text{in}}^{-1}C < 0$$

and

$$A_{\text{ex}}^{\text{T}}C + CA_{\text{ex}} = -2CR_{\text{ex}}^{-1}C < 0.$$

To show *iv*), define

$$R_j^{\text{in}} \triangleq \varepsilon R_n^{\text{in}} + \sum_{k=1}^{2^j} R_{j,k}^{\text{in}} Z_{j,k} Z_{j,k}^{\text{T}}, \qquad j = 1, \ldots, n-1,$$

where $R_n^{\text{in}} \triangleq \text{diag}[R_{n,1}^{\text{in}}, \cdots, R_{n,2^n}^{\text{in}}]$ and $\varepsilon = \frac{1}{n-1}$. Note that it follows from Proposition 2.1 that, for each $j \in \{1, \cdots, n\}$, R_j^{in} is strictly ultrametric, and hence, $R_{\text{in}} = \sum_{j=1}^{n} R_j^{\text{in}}$ is strictly ultrametric. Similarly, it can be shown that R_{ex} is strictly ultrametric.

Finally, to show *v*) note that since R_{in} and R_{ex} are strictly ultrametric it follows from Lemma 2.2 that $B_{\text{in}} = R_{\text{in}}^{-1}\mathbf{e} \geq\geq 0, B_{\text{ex}} = R_{\text{ex}}^{-1}\mathbf{e} \geq\geq 0$, and $-R_{\text{in}}^{-1}$ and $-R_{\text{ex}}^{-1}$ are essentially nonnegative. Hence, since C is a positive diagonal matrix, A_{in} and A_{ex} are essentially nonnegative. Now, since $R_{\text{in}}^{-1}\mathbf{e} \geq\geq 0$ and $R_{\text{ex}}^{-1}\mathbf{e} \geq\geq 0$ it follows that $A_{\text{in}}^{\text{T}}\mathbf{e} = -CR_{\text{in}}^{-1}\mathbf{e} \leq\leq 0$ and $A_{\text{ex}}^{\text{T}}\mathbf{e} = -CR_{\text{ex}}^{-1}\mathbf{e} \leq\leq 0$, which implies that A_{in} and A_{ex} are compartmental and, by *ii*) and *iii*), A_{in} and A_{ex} are Hurwitz. □

Remark 2.3. It follows from Proposition 2.3 that R_{in} and R_{ex} are invertible. Hence, A_{in} and A_{ex} are well defined, which implies that the state equations for inspiration and expiration given by (2.17) and (2.18), respectively, are well defined.

In this chapter, we assume that the inspiration process starts from a given initial state x_0^{in} followed by the expiration process where its initial state will be the final state of the inspiration. An inspiration followed by the expiration is called a single *breathing cycle*. We assume that each breathing cycle is followed by another breathing cycle where the initial condition for the latter breathing cycle is the final state of the former breathing cycle. Furthermore, we assume that the duration of inspiration is T_{in} and that of expiration is T_{ex} so that the total duration of a breathing cycle is $T_{\text{in}} + T_{\text{ex}}$. It is clear that this process generates a periodic dynamical system with a period $T \triangleq T_{\text{in}} + T_{\text{ex}}$. Furthermore, the system dynamics switch from inspiration to expiration and back to inspiration. Hence, the dynamics for a breathing cycle can be characterized by the periodic switched dynamical system $\mathcal{G}$ given by

$$\dot{x}(t) = A(t)x(t) + B(t)u(t), \quad x(0) = x_0^{\text{in}}, \quad t \geq 0, \tag{2.19}$$

where

$$A(t) = A(t+T), \qquad u(t) = u(t+T), \qquad t \geq 0, \tag{2.20}$$

$$A(t) = \begin{cases} A_{\mathrm{in}}, & 0 \leq t < T_{\mathrm{in}}, \\ A_{\mathrm{ex}}, & T_{\mathrm{in}} \leq t < T, \end{cases} \tag{2.21}$$

$$B(t) = \begin{cases} B_{\mathrm{in}}, & 0 \leq t < T_{\mathrm{in}}, \\ B_{\mathrm{ex}}, & T_{\mathrm{in}} \leq t < T, \end{cases} \tag{2.22}$$

$$u(t) = \begin{cases} p_{\mathrm{in}}(t), & 0 \leq t < T_{\mathrm{in}}, \\ p_{\mathrm{ex}}(t), & T_{\mathrm{in}} \leq t < T. \end{cases} \tag{2.23}$$

The following result shows that the solution to the switched dynamical system (2.19) is *nonnegative*, that is, for every $x_0^{\mathrm{in}} \in \overline{\mathbb{R}}_+^{2^n}$, the solution $x(t)$, $t \geq 0$, to (2.19) satisfies $x(t) \geq\geq 0$, $t \geq 0$.

Theorem 2.2. Consider the switched dynamical system (2.19) where $x_0^{\mathrm{in}} \geq\geq 0$. Then $x(t) \geq\geq 0$, $t \geq 0$, where $x(t)$ denotes the solution to (2.19).

Proof. Note that the solution to (2.19) over the time interval $[0, T]$ is given by

$$x(t) = \begin{cases} e^{A_{\mathrm{in}}t}x_0^{\mathrm{in}} + \int_0^t e^{A_{\mathrm{in}}(t-\tau)}B_{\mathrm{in}}p_{\mathrm{in}}(\tau)\mathrm{d}\tau, & 0 \leq t \leq T_{\mathrm{in}}, \\ e^{A_{\mathrm{ex}}(t-T_{\mathrm{in}})}x_0^{\mathrm{ex}} + \int_{T_{\mathrm{in}}}^t e^{A_{\mathrm{ex}}(t-\tau)}B_{\mathrm{ex}}p_{\mathrm{ex}}(\tau)\mathrm{d}\tau, & T_{\mathrm{in}} \leq t \leq T, \end{cases} \tag{2.24}$$

where $x_0^{\mathrm{ex}} = x(T_{\mathrm{in}})$. Now, since A_{in} and A_{ex} are essentially nonnegative (by Proposition 2.3), it follows from Lemma 2.1 that $e^{A_{\mathrm{in}}t} \geq\geq 0$ and $e^{A_{\mathrm{ex}}t} \geq\geq 0$ for all $t \geq 0$. Hence, $x(t) \geq\geq 0$, $0 \leq t \leq T$. Now, the nonnegativity of $x(t)$ for all $t \geq 0$ follows by mathematical induction. □

2.5. Limit Cycle Analysis of the Multicompartment Lung Model

In this section, we characterize and analyze the stability of periodic orbits of the switched dynamical system $\mathcal{G}$ given by (2.19). First, note that it follows from (2.24) that

$$x_0^{\mathrm{ex}} = x(T_{\mathrm{in}}) = \Gamma_{\mathrm{in}}x_0^{\mathrm{in}} + \theta, \tag{2.25}$$

where

$$\Gamma_{\text{in}} \triangleq e^{A_{\text{in}}T_{\text{in}}}, \tag{2.26}$$

$$\theta \triangleq e^{A_{\text{in}}T_{\text{in}}} \int_0^{T_{\text{in}}} e^{-A_{\text{in}}t} B_{\text{in}} p_{\text{in}}(t) \mathrm{d}t. \tag{2.27}$$

Furthermore, note that

$$x(T) = \Gamma_{\text{ex}} x_0^{\text{ex}} + \delta, \tag{2.28}$$

where

$$\Gamma_{\text{ex}} \triangleq e^{A_{\text{ex}}T_{\text{ex}}}, \tag{2.29}$$

$$\delta \triangleq e^{A_{\text{ex}}T} \int_{T_{\text{in}}}^{T} e^{-A_{\text{ex}}t} B_{\text{ex}} p_{\text{ex}}(t) \mathrm{d}t. \tag{2.30}$$

Next, let x_m^{in} denote the initial condition for the m-th inspiration (and hence the m-th breathing cycle) and let x_m^{ex} denote the initial condition for the m-th expiration, that is, $x_m^{\text{in}} = x(mT)$ and $x_m^{\text{ex}} = x(mT + T_{\text{in}})$, $m = 0, 1, \ldots$. Hence, it follows from (2.25) and (2.28) that

$$x_1^{\text{in}} = \Gamma_{\text{ei}} x_0^{\text{in}} + \Gamma_{\text{ex}} \theta + \delta, \tag{2.31}$$

where $\Gamma_{\text{ei}} \triangleq \Gamma_{\text{ex}} \Gamma_{\text{in}}$. Similarly, it can be shown that

$$x_1^{\text{ex}} = \Gamma_{\text{ie}} x_0^{\text{ex}} + \Gamma_{\text{in}} \delta + \theta, \tag{2.32}$$

where $\Gamma_{\text{ie}} \triangleq \Gamma_{\text{in}} \Gamma_{\text{ex}}$. More generally,

$$x_{m+1}^{\text{in}} = \Gamma_{\text{ei}} x_m^{\text{in}} + \Gamma_{\text{ex}} \theta + \delta, \quad m = 0, 1, \ldots, \tag{2.33}$$

$$x_{m+1}^{\text{ex}} = \Gamma_{\text{ie}} x_m^{\text{ex}} + \Gamma_{\text{in}} \delta + \theta, \quad m = 0, 1, \ldots. \tag{2.34}$$

The following proposition states and proves two key properties for Γ_{ei} and Γ_{ie} which are useful in characterizing a periodic orbit for the switched dynamical system $\mathcal{G}$.

Proposition 2.4. The following statements hold:

i) $\Gamma_{\mathrm{ex}}^{\mathrm{T}} C \Gamma_{\mathrm{ex}} < C$ and $\Gamma_{\mathrm{in}}^{\mathrm{T}} C \Gamma_{\mathrm{in}} < C$.

ii) $\Gamma_{\mathrm{ei}}^{\mathrm{T}} C \Gamma_{\mathrm{ei}} < C$ and $\Gamma_{\mathrm{ie}}^{\mathrm{T}} C \Gamma_{\mathrm{ie}} < C$.

Proof. It follows from Proposition 2.3 that

$$T_{\mathrm{in}}(A_{\mathrm{in}}^{\mathrm{T}} C + C A_{\mathrm{in}}) < 0,$$

$$T_{\mathrm{ex}}(A_{\mathrm{ex}}^{\mathrm{T}} C + C A_{\mathrm{ex}}) < 0.$$

Hence, it follows from Proposition 2.2 that

$$e^{A_{\mathrm{in}}^{\mathrm{T}} T_{\mathrm{in}}} C e^{A_{\mathrm{in}} T_{\mathrm{in}}} < C,$$

$$e^{A_{\mathrm{ex}}^{\mathrm{T}} T_{\mathrm{ex}}} C e^{A_{\mathrm{ex}} T_{\mathrm{ex}}} < C,$$

which proves *i)*.

To prove *ii)*, pre- and post- multiply the first inequality of *i)* by $\Gamma_{\mathrm{in}}^{\mathrm{T}}$ and Γ_{in}, respectively, to obtain

$$\Gamma_{\mathrm{in}}^{\mathrm{T}} \Gamma_{\mathrm{ex}}^{\mathrm{T}} C \Gamma_{\mathrm{ex}} \Gamma_{\mathrm{in}} \leq \Gamma_{\mathrm{in}}^{\mathrm{T}} C \Gamma_{\mathrm{in}} < C,$$

where the last inequality follows from *i)*. This establishes the first inequality of *ii)*. The second inequality follows in an identical manner. □

For the next result, define $\hat{x}_{\mathrm{in}} \triangleq (I - \Gamma_{\mathrm{ei}})^{-1}(\Gamma_{\mathrm{ex}}\theta + \delta)$ and $\hat{x}_{\mathrm{ex}} \triangleq (I - \Gamma_{\mathrm{ie}})^{-1}(\Gamma_{\mathrm{in}}\delta + \theta)$.

Proposition 2.5. Consider the switched dynamical system $\mathcal{G}$ given by (2.19). Then, for every $x_0^{\mathrm{in}} \in \overline{\mathbb{R}}_+^{2^n}$, the following statements hold:

i) $\lim_{m\to\infty} x_m^{\mathrm{in}} = \hat{x}_{\mathrm{in}}$ and $\lim_{m\to\infty} x_m^{\mathrm{ex}} = \hat{x}_{\mathrm{ex}}$.

ii) For every $t \in [0, T_{\rm in}]$,

$$\lim_{m\to\infty} x(t+mT) = e^{A_{\rm in}t}\hat{x}_{\rm in} + \int_0^t e^{A_{\rm in}(t-\tau)}B_{\rm in}p_{\rm in}(\tau)\mathrm{d}\tau,$$

and, for every $t \in [T_{\rm in}, T]$,

$$\lim_{m\to\infty} x(t+mT+T_{\rm in}) = e^{A_{\rm ex}t}\hat{x}_{\rm ex} + \int_0^t e^{A_{\rm ex}(t-\tau)}B_{\rm ex}p_{\rm ex}(\tau+T_{\rm in})\mathrm{d}\tau.$$

Proof. It follows from *ii*) of Proposition 2.4 that $\Gamma_{\rm ei}$ and $\Gamma_{\rm ie}$ are Schur, and hence, $\lim_{m\to\infty}\Gamma_{\rm ei}^m = 0$ and $\lim_{m\to\infty}\Gamma_{\rm ie}^m = 0$. Furthermore, $(I-\Gamma_{\rm ei})^{-1}$ and $(I-\Gamma_{\rm ie})^{-1}$ exist and are given by

$$(I-\Gamma_{\rm ei})^{-1} = \sum_{j=0}^{\infty}\Gamma_{\rm ei}^j, \qquad (I-\Gamma_{\rm ie})^{-1} = \sum_{j=0}^{\infty}\Gamma_{\rm ie}^j.$$

Next, it follows from (2.33) and (2.34) that

$$\begin{aligned} x_m^{\rm in} &= \Gamma_{ei}^m x_0^{\rm in} + \sum_{j=0}^{m-1}\Gamma_{\rm ei}^j(\Gamma_{\rm ex}\theta+\delta),\\ x_m^{\rm ex} &= \Gamma_{ie}^m x_0^{\rm ex} + \sum_{j=0}^{m-1}\Gamma_{\rm ie}^j(\Gamma_{\rm in}\delta+\theta), \end{aligned}$$

which, by taking limits, yields *i*). Now, *ii*) follows from *i*) and (2.24). □

Remark 2.4. It follows from Proposition 2.5 that the individual compartmental volumes, and hence the total volume, converge to the steady-state end-inspiratory and end-expiratory values of $(I-\Gamma_{\rm ei})^{-1}(\Gamma_{\rm ex}\theta+\delta)$ and $(I-\Gamma_{\rm ie})^{-1}(\Gamma_{\rm in}\delta+\theta)$, respectively.

Next, let $\hat{x} \triangleq (I-\Gamma_{\rm ei})^{-1}(\Gamma_{\rm ex}\theta+\delta)$ and define the orbit

$$\mathcal{O}_{\hat{x}} \triangleq \{x \in \overline{\mathbb{R}}_+^{2^n} : x = s(t,\hat{x}), \text{ where } s(t,\hat{x}) \text{ is the solution to (2.19)}\}. \tag{2.35}$$

With $x_0^{\rm in} = \hat{x}$ note that $x_m^{\rm in} = \hat{x}$, $m = 1, 2, \ldots$, or, equivalently, $x(mT) = \hat{x}$, $m = 1, 2, \ldots$, which implies that $\mathcal{O}_{\hat{x}}$ is a periodic orbit of (2.19). The following theorem presents one of the main results of this section.

Theorem 2.3. Consider the switched dynamical system $\mathcal{G}$ given by (2.19). Then the periodic orbit $\mathcal{O}_{\hat{x}}$ of $\mathcal{G}$ generated by $x(0) = \hat{x} = (I - \Gamma_{\mathrm{ei}})^{-1}(\Gamma_{\mathrm{ex}}\theta + \delta)$ is globally asymptotically stable.

Proof. Note that for the periodic orbit $\mathcal{O}_{\hat{x}}$ generated by the point $\hat{x} = (I - \Gamma_{\mathrm{ei}})^{-1}(\Gamma_{\mathrm{ex}}\theta + \delta)$, the Poincaré map is given by

$$z(k+1) = s(T, z(k)) = \Gamma_{\mathrm{ei}} z(k) + \Gamma_{\mathrm{ex}}\theta + \delta,\ z(0) = x_0^{\mathrm{in}},\ k \in \overline{\mathbb{Z}}_+. \tag{2.36}$$

Since Γ_{ei} is Schur (by Proposition 2.4) it follows that $\hat{x}$ is an asymptotically stable fixed point of (2.36). Hence, it follows from Theorem 2.1 that $\mathcal{O}_{\hat{x}}$ is asymptotically stable.

Next, let $\varepsilon > 0$ be such that $\mathrm{dist}(s(t, x_0), \mathcal{O}_{\hat{x}}) \to 0$ for all $x_0 \in \mathcal{D}$ and $\mathrm{dist}(x_0, \mathcal{O}_{\hat{x}}) < \varepsilon$. (The existence of such an ε is guaranteed since $\mathcal{O}_{\hat{x}}$ is asymptotically stable.) Now, it follows from $i)$ of Proposition 2.5 that there exists $m \in \mathbb{Z}_+$ such that $\mathrm{dist}(s(mT, x_0^{\mathrm{in}}), \mathcal{O}_{\hat{x}}) \leq \|s(mT, x_0^{\mathrm{in}}) - \hat{x}\| < \varepsilon$. Hence,

$$\lim_{t\to\infty} \mathrm{dist}(s(t, x_0^{\mathrm{in}}), \mathcal{O}_{\hat{x}}) = \lim_{t\to\infty} \mathrm{dist}(s(t - mT, s(mT, x_0^{\mathrm{in}})), \mathcal{O}_{\hat{x}}) = 0,$$

establishing global asymptotic stability of $\mathcal{O}_{\hat{x}}$. □

Remark 2.5. Note that Theorem 2.3 is valid for arbitrary nonnegative functions (possibly discontinuous) $p_{\mathrm{in}}(t)$ and $p_{\mathrm{ex}}(t)$ as long as $\int_0^{T_{\mathrm{in}}} e^{-A_{\mathrm{in}}t} B_{\mathrm{in}} p_{\mathrm{in}}(t)\mathrm{d}t$ and $\int_{T_{\mathrm{in}}}^{T} e^{-A_{\mathrm{ex}}t} B_{\mathrm{ex}} p_{\mathrm{ex}}(t)\mathrm{d}t$ are finite. In the case where $p_{\mathrm{in}}(t) = \alpha t + \beta$ and $p_{\mathrm{ex}}(t) = \gamma$ for some positive constants α, β, and γ, θ and δ are given by

$$\begin{aligned}
\theta &= A_{\mathrm{in}}^{-2}[(\alpha I + \beta A_{\mathrm{in}})(e^{A_{\mathrm{in}}T_{\mathrm{in}}} - I) - \alpha A_{\mathrm{in}} T_{\mathrm{in}}] B_{\mathrm{in}}, \\
\delta &= \gamma A_{\mathrm{ex}}^{-1}(e^{A_{\mathrm{ex}}T_{\mathrm{ex}}} - I) B_{\mathrm{ex}}.
\end{aligned}$$

The following result provides a generalization to Theorem 2.3.

Theorem 2.4. Consider the switched dynamical system $\mathcal{G}$ given by (2.19). Let $x(t)$ and $y(t), t \geq 0$, denote the solutions to (2.19) with initial conditions $x(0) \in \overline{\mathbb{R}}_+^{2^n}$ and $y(0) = \hat{x}$. Then, $x(t) \to y(t)$ as $t \to \infty$.

Proof. Let $e(t) \triangleq x(t) - y(t)$ so that

$$\dot{e}(t) = A(t)e(t), \quad e(0) = x(0) - \hat{x}, \quad t \geq 0. \tag{2.37}$$

Now, consider the Lyapunov function candidate $V : \mathbb{R}^{2^n} \to \mathbb{R}$ given by $V(e) = e^{\mathrm{T}}Ce$ so that the Lyapunov derivative of $V(e)$ along the trajectories of (2.37) is given by

$$\begin{aligned}
\dot{V}(e(t)) = \; & e^{\mathrm{T}}(t)[A^{\mathrm{T}}(t)C + CA(t)]e(t) \\
& \leq \max\{-2e^{\mathrm{T}}(t)CR_{\mathrm{in}}^{-1}Ce(t), -2e^{\mathrm{T}}(t)CR_{\mathrm{ex}}^{-1}Ce(t)\} \\
& \leq -2\eta e^{\mathrm{T}}(t)e(t), \quad t \geq 0,
\end{aligned}$$

where $\eta \triangleq \min\{\lambda_{\min}(CR_{\mathrm{in}}^{-1}C), \lambda_{\min}(CR_{\mathrm{ex}}^{-1}C)\}$, which implies that $e(t) \to 0$ as $t \to \infty$.

□

Remark 2.6. Note that Theorem 2.4 shows that the periodic solution given by $\mathcal{O}_{\hat{x}}$ is globally asymptotically stable (in the sense of stability of motion), and hence, $\mathcal{O}_{\hat{x}}$ is orbitally stable strengthening the conclusion of Theorem 2.3.

Remark 2.7. Note that the error dynamics $e(t), t \geq 0$, given by (2.37) is a switched dynamical system where each of the switched systems is a linear dynamical system, and $V(e) = e^{\mathrm{T}}Ce$ is a *common* Lyapunov function for both linear systems.

2.6. A Regular Dichotomy Model

In this section, we present results for a special class of models with a dichotomy architecture. Specifically, we assume that the bronchial tree has a *regular* dichotomy

structure [68], that is, for a given branch generation all airflow resistances at the airway units are equal, and hence, for an n-generation model (2^n-compartment model), $R^{\rm in}_{j,k} = \hat{R}^{\rm in}_j$ and $R^{\rm ex}_{j,k} = \hat{R}^{\rm ex}_j$, $k = 1, 2, \ldots, 2^j$, $j = 0, 1, \ldots, n$, where $\hat{R}^{\rm in}_j > 0$ and $\hat{R}^{\rm ex}_j > 0$, $j = 0, \ldots, n$. Furthermore, we assume that $c_k = \hat{c}$, $k = 1, \ldots, 2^n$, that is, the compliance of each compartment is equal. In this case, it can be shown that $C = \frac{1}{\hat{c}} I_{2^n}$ and

$$R_{\rm in} = \sum_{j=0}^{n} \hat{R}^{\rm in}_j \left(I_{2^j} \otimes \mathbf{e}_{2^{n-j}} \mathbf{e}^{\rm T}_{2^{n-j}} \right), \tag{2.38}$$

$$R_{\rm ex} = \sum_{j=0}^{n} \hat{R}^{\rm ex}_j \left(I_{2^j} \otimes \mathbf{e}_{2^{n-j}} \mathbf{e}^{\rm T}_{2^{n-j}} \right), \tag{2.39}$$

so that $A_{\rm in} = -\frac{1}{\hat{c}} R^{-1}_{\rm in}$, $B_{\rm in} = R^{-1}_{\rm in}\mathbf{e}$, $A_{\rm ex} = -\frac{1}{\hat{c}} R^{-1}_{\rm ex}$, and $B_{\rm ex} = R^{-1}_{\rm ex}\mathbf{e}$. Furthermore, note that $R_{\rm in}\mathbf{e} = 2^n \hat{R}_{\rm in}\mathbf{e}$ and $R_{\rm ex}\mathbf{e} = 2^n \hat{R}_{\rm ex}\mathbf{e}$, where $\hat{R}_{\rm in} \triangleq \sum_{j=0}^{n} \frac{\hat{R}^{\rm in}_j}{2^j}$ and $\hat{R}_{\rm ex} \triangleq \sum_{j=0}^{n} \frac{\hat{R}^{\rm ex}_j}{2^j}$, so that $B_{\rm in} = \frac{1}{2^n \hat{R}_{\rm in}}\mathbf{e}$, $B_{\rm ex} = \frac{1}{2^n \hat{R}_{\rm ex}}\mathbf{e}$, and

$$e^{A_{\rm in}(T_{\rm in}-t)} B_{\rm in} = \frac{1}{2^n \hat{R}_{\rm in}} e^{-\frac{(T_{\rm in}-{\rm t})}{\hat{c} 2^n \hat{R}_{\rm in}}}\ \mathbf{e}. \tag{2.40}$$

Hence,

$$\theta = \frac{e^{-\frac{T_{\rm in}}{\hat{c} 2^n \hat{R}_{\rm in}}}}{2^n \hat{R}_{\rm in}} \int_0^{T_{\rm in}} e^{\frac{t}{\hat{c} 2^n \hat{R}_{\rm in}}} p_{\rm app}(t) {\rm d}t\ \mathbf{e}. \tag{2.41}$$

Now, using (2.41) it can be shown that $\hat{x}_{\rm in}$ is of the form $\gamma\mathbf{e}$, where $\gamma > 0$, and hence, the limit cycle $\mathcal{O}_{\hat{x}} \subset \{\gamma\mathbf{e} : \gamma \geq 0\}$. Thus, it follows that the limiting behavior of a regular dichotomy lung model exhibits *equipartioning* of the total volume, that is, $x_i(t) \to x_j(t)$ as $t \to \infty$ for all $i, j = 1, 2, \ldots, 2^n$.

Next, we provide a relation between m-generation and n-generation regular dichotomy models, where $m < n$. Let $\hat{R}^{\rm in}_{m,j}$ and $\hat{R}^{\rm ex}_{m,j}$ denote the resistances to airflow at a j-th generation airway unit, let $\hat{c}_m$ denote the compliance of each compartment, and let x^m_i denote the i-th compartmental volume in an m-generation model. Here, we assume that

$$x^m_i = \sum_{j=1}^{L} x^n_{(i-1)L+j}, \quad i = 1, \ldots, M, \tag{2.42}$$

where $L \triangleq 2^{n-m}$ and $M \triangleq 2^m$, that is, each compartment of m-generation model is equivalent to L compartments of the n-generation model so that the total volumes in both models are equal. Note that (2.42) may be written as

$$x^m = (I_M \otimes \mathbf{e}_L^{\mathrm{T}})x^n, \tag{2.43}$$

where $x^m = [x_1^m, \ldots, x_M^m]$ and $x^n = [x_1^n, \ldots, x_N^n]$, and where $N \triangleq 2^n$.

Now, consider the n-generation state equation for inspiration given by

$$R_{\mathrm{in}}^n \dot{x}^n(t) + \frac{1}{\hat{c}_n} x^n(t) = p_{\mathrm{in}}(t)\mathbf{e}_N, \qquad x^n(0) = x_{\mathrm{in},0}^n, \qquad 0 \leq t \leq T_{\mathrm{in}}, \tag{2.44}$$

where

$$R_{\mathrm{in}}^n = \sum_{j=0}^{n} \hat{R}_{n,j}^{\mathrm{in}} (I_{2^j} \otimes \mathbf{e}_{2^{n-j}} \mathbf{e}_{2^{n-j}}^{\mathrm{T}}). \tag{2.45}$$

In this case, it can be shown that

$$(I_M \otimes \mathbf{e}_L^{\mathrm{T}})(I_{2^j} \otimes \mathbf{e}_{2^{n-j}} \mathbf{e}_{2^{n-j}}^{\mathrm{T}}) = \begin{cases} 2^L (I_{2^j} \otimes \mathbf{e}_{2^{m-j}} \mathbf{e}_{2^{m-j}}^{\mathrm{T}}), & j < m \\ 2^{n-j} (I_M \otimes \mathbf{e}_L^{\mathrm{T}}), & j \geq m. \end{cases} \tag{2.46}$$

Now, pre-multiplying (2.45) by $(I_M \otimes \mathbf{e}_L^{\mathrm{T}})$ and using (2.43) and (2.46) yields

$$\sum_{j=0}^{m-1} 2^L \hat{R}_{n,j}^{\mathrm{in}} (I_{2^j} \otimes \mathbf{e}_{2^{n-j}} \mathbf{e}_{2^{n-j}}^{\mathrm{T}}) \dot{x}^n(t) + \sum_{j=m}^{n} 2^{n-j} \hat{R}_{n,j}^{\mathrm{in}} \dot{x}^m(t) + \frac{1}{\hat{c}^n} x^m(t) = 2^L p_{\mathrm{in}}(t) \mathbf{e}_M. \tag{2.47}$$

Next, note that $(I_{2^j} \otimes \mathbf{e}_{2^{m-j}} \mathbf{e}_{2^{n-j}}^{\mathrm{T}}) \dot{x}^n(t) = (I_{2^j} \otimes \mathbf{e}_{2^{m-j}} \mathbf{e}_{2^{m-j}}^{\mathrm{T}}) \dot{x}^m(t)$ so that (2.47) can be written as

$$\sum_{j=0}^{m-1} \hat{R}_{n,j}^{\mathrm{in}} (I_{2^j} \otimes \mathbf{e}_{2^{m-j}} \mathbf{e}_{2^{m-j}}^{\mathrm{T}}) \dot{x}^m(t) + \sum_{j=m}^{n} 2^{m-j} \hat{R}_{n,j}^{\mathrm{in}} \dot{x}^m(t) + \frac{1}{2^L \hat{c}^n} x^m(t) = p_{\mathrm{in}}(t) \mathbf{e}_M. \tag{2.48}$$

Comparing (2.48) with the m-generation model given by

$$R_{\mathrm{in}}^m \dot{x}^m(t) + \frac{1}{\hat{c}_m} x^m(t) = p_{\mathrm{in}}(t) \mathbf{e}_M, \tag{2.49}$$

yields $\hat{c}_m = 2^{n-m} \hat{c}_n$ and

$$R_{\mathrm{in}}^m = \sum_{j=0}^{m-1} \hat{R}_{n,j}^{\mathrm{in}} (I_{2^j} \otimes \mathbf{e}_{2^{m-j}} \mathbf{e}_{2^{m-j}}^{\mathrm{T}}) + \sum_{j=m}^{n} 2^{m-j} \hat{R}_{n,j}^{\mathrm{in}} I_M,$$

or, equivalently,

$$\hat{R}^{\text{in}}_{m,j} = \hat{R}^{\text{in}}_{n,j}, \qquad j = 0, 1, \ldots, m-1, \tag{2.50}$$

$$\hat{R}^{\text{in}}_{m,m} = \sum_{j=m}^{n} \frac{\hat{R}^{\text{in}}_{n,j}}{2^{j-m}}. \tag{2.51}$$

Similarly, it can be shown that

$$\hat{R}^{\text{ex}}_{m,j} = \hat{R}^{\text{ex}}_{n,j}, \qquad j = 0, 1, \ldots, m-1, \tag{2.52}$$

$$\hat{R}^{\text{ex}}_{m,m} = \sum_{j=m}^{n} \frac{\hat{R}^{\text{ex}}_{n,j}}{2^{j-m}}. \tag{2.53}$$

2.7. A General Tree Structure Model

In this section, we extend the model presented in Sections 2.3–2.5 to the case where the bronchial tree has a general tree architecture [27,28,34]. The general tree structure includes the regular and irregular dichotomy [68]. Specifically, let the bronchial tree be represented by a weighted directed tree $\mathfrak{G} = (\mathcal{V}, \mathcal{E}, R)$, where each vertex corresponds to a branching point of an airway unit or the terminal compartment (alveolus) of the lung. In this case, the trachea corresponds to the root v_1 of the tree and all the alveoli correspond to the leaves of the tree. Every edge, $(v_l, v_m) \in \mathcal{E}$ corresponds to an airway unit and $R_{(l,m)}$, the weight of the edge, corresponds to the resistance of the airway unit; we use $R_{(l,m)} = R^{\text{in}}_{l,m}$ and $R_{(l,m)} = R^{\text{ex}}_{l,m}$ for resistance during inspiration and expiration, respectively.

Let $\mathcal{L} \triangleq \{v_i \in \mathcal{V} : v_i \text{ is a leaf of } \mathfrak{G}\}$ and let the number of leaves of $\mathfrak{G}$ (or, equivalently, compartments of the lung) be n so that $\mathcal{L} = \{v_{i_1}, v_{i_2}, \ldots, v_{i_n}\}$, where $i_k \in \{1, 2, \ldots, N\}$, $k = 1, 2, \ldots, n$, and N is the number of vertices of the graph. To develop the dynamical model for the inspiration process, let $c_k, k = 1, 2, \ldots, n$, denote the compliance of each compartment, and let $x_k, k = 1, 2, \ldots, n$, denote the lung volume in the k-th compartment so that the state equations for inspiration are

given by

$$\frac{1}{c_k}x_k(t) + \sum_{(v_l,v_m)\in\mathcal{P}_k} R^{\rm in}_{l,m} \sum_{v_{i_j}\in\mathcal{L}_{l,m}} \dot{x}_j(t) = p_{\rm in}(t), \quad x_i(0) = x^{\rm in}_{k0}, \quad 0 \le t \le T_{\rm in}, \\ k = 1, 2, \ldots, n, \tag{2.54}$$

where

$$\mathcal{P}_k \triangleq \{(v_l, v_m) \in \mathcal{E} : (v_l, v_m) \text{ belongs to the directed path from the root of } \mathfrak{G} \text{ to } v_{i_k}\} \tag{2.55}$$

and, for each $l, m \in \{1, \ldots, N\}$ such that $(v_l, v_m) \in \mathcal{E}$,

$$\mathcal{L}_{l,m} \triangleq \{v_{i_k} \in \mathcal{L} : \text{ there exits a directed path from } v_m \text{ to } v_{i_k},\ k = 1, \ldots, n\}. \tag{2.56}$$

Next, let $x \triangleq [x_1, \ldots, x_n]^{\rm T}$ so that (2.54) can be written as

$$R_{\rm in}\dot{x}(t) + Cx(t) = p_{\rm in}(t)\mathbf{e}, \quad x(0) = x^{\rm in}_0, \quad 0 \le t \le T_{\rm in},$$

where $C \triangleq \operatorname{diag}[\frac{1}{c_1}, \ldots, \frac{1}{c_n}]$ and

$$R_{\rm in} = \sum_{(v_l,v_m)\in\mathcal{E}} R^{\rm in}_{l,m} Z_{l,m} Z^{\rm T}_{l,m}, \tag{2.57}$$

where $Z_{l,m} \in \mathbb{R}^n$ is such that the k-th eletment of $Z_{l,m}$ is 1 if $v_{i_k} \in \mathcal{L}_{l,m}$ and 0 otherwise.

An identical procedure yields the state equations for expiration given by

$$R_{\rm ex}\dot{x}(t) + Cx(t) = p_{\rm ex}(t)\mathbf{e}, \quad x(T_{\rm in}) = x^{\rm ex}_0,\ T_{\rm in} \le t \le T, \tag{2.58}$$

where

$$R_{\rm ex} = \sum_{(v_l,v_m)\in\mathcal{E}} R^{\rm ex}_{l,m} Z_{l,m} Z^{\rm T}_{l,m}. \tag{2.59}$$

Note that it can be easily shown that $R_{\rm in} > 0$ and $R_{\rm ex} > 0$ and it follows from (2.57), (2.59), and Proposition 2.1 that $R_{\rm in}$ and $R_{\rm ex}$ are strictly ultrametric. Hence, for a

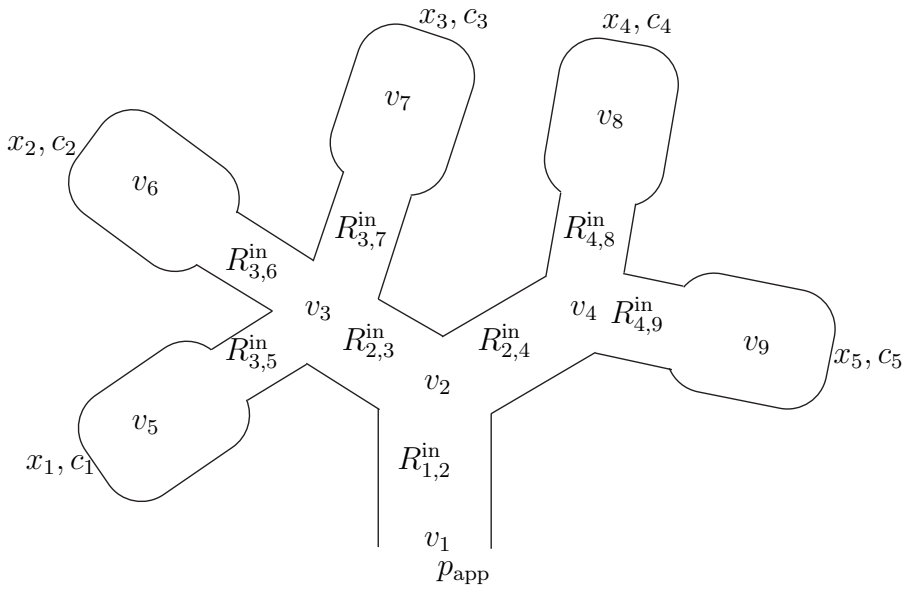

Figure 2.3: Five-compartment tree structure model.

general tree structure model all of the results of Sections 2.4 and 2.5 are valid with R_{in} and R_{ex} given by (2.57) and (2.59), respectively.

To illustrate the general tree structure lung model, consider the five-compartment model shown in Figure 2.3. Here, the bronchial tree is represented by a weighted directed tree $\mathfrak{G} = (\mathcal{V}, \mathcal{E}, R)$ consisting of nine nodes $\mathcal{V} = \{v_1, v_2, \ldots, v_9\}$ and eight edges $\mathcal{E} = \{(v_1, v_2), (v_2, v_3), (v_2, v_4), (v_3, v_5), (v_3, v_6), (v_3, v_7), (v_4, v_8), (v_4, v_9)\}$. In this case, the set of leaves $\mathcal{L} = \{v_5, v_6, \ldots, v_9\}$ corresponds to the five compartments of the lung. Let $v_{i_k} = v_{k+4}, k = 1, \ldots, 5$. Now, the pressure $\frac{1}{c_k}x_k(t)$ due to the compliance in k-th compartment will be equal to the difference between the external pressure applied and the resistance to air flow at every airway in the path leading from the pressure source (the root v_1) to the k-th compartment. In particular, for $k = 3$ (see Figure 2.3),

$$\begin{aligned}\frac{1}{c_3}x_3(t) = \; & p_{\text{in}}(t) - R^{\text{in}}_{1,2}[\dot{x}_1(t) + \dot{x}_2(t) + \dot{x}_3(t) + \dot{x}_4(t) + \dot{x}_5(t)] \\ & -R^{\text{in}}_{2,3}[\dot{x}_1(t) + \dot{x}_2(t) + \dot{x}_3(t)] - R^{\text{in}}_{3,7}\dot{x}_3(t),\end{aligned}$$

or, equivalently,

$$\frac{1}{c_3}x_3(t) + \sum_{(v_l,v_m)\in\mathcal{P}_3} R^{\text{in}}_{l,m} \sum_{v_{i_j}\in\mathcal{L}_{l,m}} \dot{x}_j(t) = p_{\text{in}}(t), \tag{2.60}$$

where

$$\begin{aligned}
\mathcal{P}_3 &= \{(v_1, v_2), (v_2, v_3), (v_3, v_7)\},\\
\mathcal{L}_{1,2} &= \{v_5, v_6, v_7, v_8, v_9\},\\
\mathcal{L}_{2,3} &= \{v_5, v_6, v_7\},\\
\mathcal{L}_{3,7} &= \{v_7\}.
\end{aligned}$$

2.8. Direct Adaptive Control for Switched Linear Time-Varying Systems

In this section, we consider the problem of adaptive tracking of uncertain linear time-varying switching systems. Specifically, consider the controlled uncertain switched linear time-varying system $\mathcal{G}$ given by

$$\dot{x}_{\text{p}}(t) = A_{\text{p}}(t)x_{\text{p}}(t) + B_{\text{p}}(t)u(t), \quad x_{\text{p}}(0) = x_{\text{p0}}, \quad t \geq 0, \tag{2.61}$$

where $x_{\text{p}}(t) \in \mathbb{R}^n, t \geq 0$, is the state vector, $u(t) \in \mathbb{R}^p, t \geq 0$, is the control input, and $A_{\text{p}}(t) \in \mathbb{R}^{n\times n}, t \geq 0$, and $B_{\text{p}}(t) \in \mathbb{R}^{n\times p}, t \geq 0$, are *unknown* time-varying matrices. The control input $u(\cdot)$ in (2.61) is restricted to the class of *admissible controls* consisting of measurable functions such that $u(t) \in \mathbb{R}^p, t \geq 0$. Furthermore, for the uncertain linear time-varying system $\mathcal{G}$, we assume that $A_{\text{p}}(\cdot)$ and $B_{\text{p}}(\cdot)$ are piecewise continuous functions and we assume that the required properties for the existence and uniqueness of solutions are satisfied; that is, $A_{\text{p}}(\cdot), B_{\text{p}}(\cdot)$, and $u(\cdot)$ satisfy sufficient regularity conditions such that (2.61) has a unique solution forward in time.

Next, consider a reference model given by

$$\dot{x}_{\text{m}}(t) = A_{\text{m}}(t)x_{\text{m}}(t) + B_{\text{m}}(t)r(t), \quad x_{\text{m}}(0) = x_{\text{m0}}, \quad t \geq 0, \tag{2.62}$$

where $x_{\rm m}(t) \in \mathbb{R}^n, t \geq 0$, is the state vector, $r(t) \in \mathbb{R}^p, t \geq 0$, is the reference input, and $A_{\rm m}(t) \in \mathbb{R}^{n \times n}, t \geq 0$, and $B_{\rm m}(t) \in \mathbb{R}^{n \times p}, t \geq 0$, are known matrices. Moreover, let $A_{\rm m}(t), t \geq 0$, satisfy

$$A_{\rm m}^{\rm T}(t)C_{\rm m} + C_{\rm m}A_{\rm m}(t) \leq -\varepsilon_{\rm m} I, \quad t \geq 0, \tag{2.63}$$

where $\varepsilon_{\rm m} > 0$ and $C_{\rm m} \in \mathbb{R}^{n \times n}$ is positive definite. Furthermore, we assume that $A_{\rm m}(\cdot)$ and $B_{\rm m}(\cdot)$ are piecewise continuous and are such that (2.62) has a unique solution for all $t \geq 0$ and $x_{\rm m}(t)$ is uniformly bounded for all $x_{\rm m0} \in \mathbb{R}^n$ and $t \geq 0$.

For the next result, we assume that there exist a positive-definite matrix $Q^* \in \mathbb{R}^{p \times p}$ and a matrix $\Theta^* \in \mathbb{R}^{p \times n}$ such that the compatibility conditions

$$B_{\rm p}(t)Q^* = B_{\rm m}(t), \quad t \geq 0, \tag{2.64}$$

$$A_{\rm p}(t) + B_{\rm p}(t)\Theta^* = A_{\rm m}(t), \quad t \geq 0, \tag{2.65}$$

are satisfied.

Theorem 2.5. Consider the uncertain linear time-varying system $\mathcal{G}$ given by (2.61) and the reference model given by (2.62), and assume the compatibility conditions (2.64) and (2.65) hold. Then the adaptive feedback control law

$$u(t) = \Theta(t)x_{\rm p}(t) + Q(t)r(t), \tag{2.66}$$

where $\Theta(t) \in \mathbb{R}^{p \times n}, t \geq 0$, and $Q(t) \in \mathbb{R}^{p \times p}, t \geq 0$, with updated laws

$$\dot{\Theta}(t) = -B_{\rm m}^{\rm T}(t)C_{\rm m}e(t)x_{\rm p}^{\rm T}(t)\Gamma_\Theta, \quad \Theta(0) = \Theta_0, \quad t \geq 0, \tag{2.67}$$

$$\dot{Q}(t) = -B_{\rm m}^{\rm T}(t)C_{\rm m}e(t)r^{\rm T}(t)\Gamma_Q, \quad Q(0) = Q_0, \tag{2.68}$$

where $\Gamma_\Theta \in \mathbb{R}^{n \times n}$ and $\Gamma_Q \in \mathbb{R}^{p \times p}$ are positive definite and $e(t) \triangleq x_{\rm p}(t) - x_{\rm m}(t)$, guarantees that the solution $(x_{\rm p}(t), \Theta(t), Q(t))$ of the closed-loop system given by (2.61), (2.62), (2.66), (2.67), and (2.68) is uniformly bounded for all $(x_{\rm p0}, \Theta_0, Q_0) \in \mathbb{R}^n \times \mathbb{R}^{p \times n} \times \mathbb{R}^{p \times p}$ and $t \geq 0$, and $x_{\rm p}(t) \to x_{\rm m}(t)$ as $t \to \infty$.

Proof. Note that with $u(t), t \geq 0$, given by (2.66) it follows from (2.61) that

$$\dot{x}_{\mathrm{p}}(t) = A_{\mathrm{p}}(t)x_{\mathrm{p}}(t) + B_{\mathrm{p}}(t)\Theta(t)x_{\mathrm{p}}(t) + B_{\mathrm{p}}(t)Q(t)r(t), \quad x_{\mathrm{p}}(0) = x_{\mathrm{p}0}, \quad t \geq 0, \quad (2.69)$$

or, equivalently, using (2.64) and (2.65),

$$\begin{aligned}
\dot{x}_{\mathrm{p}}(t) = {} & A_{\mathrm{p}}(t)x_{\mathrm{p}}(t) + B_{\mathrm{p}}(t)[\Theta^* + \Theta(t) - \Theta^*]x_{\mathrm{p}}(t) + B_{\mathrm{p}}(t)[Q^* + Q(t) - Q^*]r(t) \\
= {} & [A_{\mathrm{p}}(t) + B_{\mathrm{p}}(t)\Theta^*]x_{\mathrm{p}}(t) + B_{\mathrm{p}}(t)[\Theta(t) - \Theta^*]x_{\mathrm{p}}(t) + B_{\mathrm{p}}(t)Q^*r(t) \\
& + B_{\mathrm{p}}(t)[Q(t) - Q^*]r(t) \\
= {} & A_{\mathrm{m}}(t)x_{\mathrm{p}}(t) + B_{\mathrm{m}}(t)r(t) + B_{\mathrm{p}}(t)[\Theta(t) - \Theta^*]x_{\mathrm{p}}(t) + B_{\mathrm{p}}(t)[Q(t) - Q^*]r(t) \\
= {} & A_{\mathrm{m}}(t)x_{\mathrm{p}}(t) + B_{\mathrm{m}}(t)r(t) + B_{\mathrm{p}}(t)\Phi^{\mathrm{T}}(t)x_{\mathrm{p}}(t) + B_{\mathrm{p}}\Psi^{\mathrm{T}}(t)(t)r(t), \\
& x_{\mathrm{p}}(0) = x_0, \ t \geq 0, \quad (2.70)
\end{aligned}$$

where $\Phi^{\mathrm{T}}(t) \triangleq \Theta(t) - \Theta^*$ and $\Psi^{\mathrm{T}}(t) \triangleq Q(t) - Q^*$. Now, it follows from (2.62) and (2.70) that

$$\dot{e}(t) = A_{\mathrm{m}}(t)e(t) + B_{\mathrm{p}}(t)\Phi^{\mathrm{T}}(t)x_{\mathrm{p}}(t) + B_{\mathrm{p}}(t)\Psi^{\mathrm{T}}(t)r(t), \ e(0) = x_{\mathrm{p}0} - x_{\mathrm{m}0}, \quad t \geq 0. \quad (2.71)$$

To show uniform boundedness of the closed-loop system (2.67), (2.68), and (2.71) consider the continuously differentiable function

$$V(e, \Phi, \Psi) = e^{\mathrm{T}}C_{\mathrm{m}}e + \mathrm{tr}\ \Gamma_Q^{-1}\Psi Q^{*-1}\Psi^{\mathrm{T}} + \mathrm{tr}\ \Gamma_\Theta^{-1}\Phi Q^{*-1}\Phi^{\mathrm{T}}, \quad (2.72)$$

and note that $V(0, 0, 0) = 0$. Since $C_{\mathrm{m}}, \Gamma_Q, \Gamma_\Theta$, and Q^* are positive definite, $V(e, \Psi, \Phi) > 0$ for all $(e, \Phi, \Psi) \neq (0, 0, 0)$. In addition, $V(e, \Phi, \Psi)$ is radially unbounded. Now, using (2.67) and (2.68), it follows that the derivative of $V(\cdot, \cdot, \cdot)$ along the closed-loop system trajectories is given by

$$\dot{V}(e(t), \Phi(t), \Psi(t)) = e^{\mathrm{T}}(t)[A_{\mathrm{m}}^{\mathrm{T}}(t)C_{\mathrm{m}} + C_{\mathrm{m}}A_{\mathrm{m}}(t)]e(t) + 2e^{\mathrm{T}}(t)C_{\mathrm{m}}B_{\mathrm{p}}(t)\Phi^{\mathrm{T}}(t)x_{\mathrm{p}}(t)$$

$$
\begin{aligned}
&+2e^{\mathrm{T}}(t)C_{\mathrm{m}}B_{\mathrm{p}}(t)\Psi^{\mathrm{T}}(t)r(t)+2\mathrm{tr}\ \Gamma_{\Theta}^{-1}\Phi(t)Q^{*-1}\dot{\Phi}^{\mathrm{T}}(t)\\
&+2\mathrm{tr}\ \Gamma_{Q}^{-1}\Psi(t)Q^{*-1}\dot{\Psi}^{\mathrm{T}}(t)\\
=\ & e^{\mathrm{T}}(t)[A_{\mathrm{m}}^{\mathrm{T}}(t)C_{\mathrm{m}}+C_{\mathrm{m}}A_{\mathrm{m}}(t)]e(t)+2e^{\mathrm{T}}(t)C_{\mathrm{m}}B_{\mathrm{p}}(t)\Phi^{\mathrm{T}}(t)x_{\mathrm{p}}(t)\\
&+2e^{\mathrm{T}}(t)C_{\mathrm{m}}B_{\mathrm{p}}(t)\Psi^{\mathrm{T}}(t)r(t)-2\mathrm{tr}\ \Psi(t)Q^{*-1}B_{\mathrm{m}}^{\mathrm{T}}(t)C_{\mathrm{m}}e(t)r^{\mathrm{T}}(t)\\
&-2\mathrm{tr}\ \Phi(t)Q^{*-1}B_{\mathrm{m}}^{\mathrm{T}}(t)C_{\mathrm{m}}e(t)x_{\mathrm{p}}^{\mathrm{T}}(t)\\
=\ & e^{\mathrm{T}}(t)[A_{\mathrm{m}}^{\mathrm{T}}(t)C_{\mathrm{m}}+C_{\mathrm{m}}A_{\mathrm{m}}(t)]e(t)\\
\leq\ & -\varepsilon_{\mathrm{m}}e^{\mathrm{T}}(t)e(t),\quad t\geq 0. \qquad (2.73)
\end{aligned}
$$

Hence, it follows from Corollary 2.4 of [21, pp. 68] that $(e(t),\Phi(t),\Psi(t))$ is uniformly bounded for all $t\geq 0$, and hence, $(x_{\mathrm{p}}(t),\Theta(t),Q(t))$ is uniformly bounded for all $(x_{\mathrm{p}0},\Theta_0,Q_0)\in\mathbb{R}^{2^n}\times\mathbb{R}^{p\times 2^n}\times\mathbb{R}^{p\times p}$ and $t\geq 0$.

Finally, with $W_1(e,\Phi,\Psi)=W_2(e,\Phi,\Psi)=V(e,\Phi,\Psi)$ and $W(e,\Phi,\Psi)=\varepsilon_{\mathrm{m}}e^{\mathrm{T}}e$, it follows from Theorem 2.5 of [21] that $(e(t),\Phi(t),\Psi(t))\to\mathcal{R}$ as $t\to\infty$, where $\mathcal{R}\triangleq\{(e,\Phi,\Psi):W(e,\Phi,\Psi)=0\}=\{(e,\Phi,\Psi):e=0\}$. In particular, note that

$$
\begin{aligned}
\dot{W}(e(t),\Phi(t),\Psi(t))=2\varepsilon_{\mathrm{m}}e^{\mathrm{T}}\dot{e}=2\varepsilon_{\mathrm{m}}e^{\mathrm{T}}(t)[&A_{\mathrm{m}}(t)e(t)+B_{\mathrm{p}}(t)\Phi^{\mathrm{T}}(t)x_{\mathrm{p}}(t)\\
&+B_{\mathrm{p}}(t)\Psi^{\mathrm{T}}(t)r(t)] \qquad (2.74)
\end{aligned}
$$

is bounded for all $t\geq 0$, and hence, all conditions of Theorem 2.5 of [21, pp. 54] are satisfied proving that $e(t)\to 0$ or, equivalently, $x_{\mathrm{p}}(t)\to x_{\mathrm{m}}(t)$ as $t\to\infty$. □

Remark 2.8. Although the form of the adaptive control law given in Theorem 2.5 is identical to that of the standard model reference adaptive controllers provided in the literature (see, for example, [51]), the dynamics of system considered in Theorem 2.5 are not Lipschitz continuous, and hence, standard proofs involving Barbalat's lemma do not hold. Consequently, Theorem 2.5 requires the more general result given by Theorem 2.5 of [21].

Remark 2.9. It is important to note that the adaptive laws (2.67) and (2.68) do *not* require explicit knowledge of Q^* or Θ^*. Furthermore, no specific structure on the uncertain dynamics $A_{\rm p}(\cdot)$ and $B_{\rm p}(\cdot)$ is required as long as the compatibility conditions (2.64) and (2.65) are satisfied.

2.9. Direct Adaptive Control for the Compartment Lung Model

In this section, we demonstrate the utility of the proposed direct adaptive control framework for the multicompartmental lung model developed in Section 2.4. First, we choose the reference model (2.62) to correspond to a respiratory system producing a plausible breathing pattern. Specifically, let $A_{\rm m}(t) = -R_{\rm m}^{-1}(t)C_{\rm m}$ and $B_{\rm m}(t) = R_{\rm m}^{-1}(t)\mathbf{e}$, where

$$R_{\rm m}(t) = \begin{cases} R_{\rm in\_m}, & 0 \leq t < T_{\rm in}, \\ R_{\rm ex\_m}, & T_{\rm in} \leq t < T, \end{cases} \tag{2.75}$$

and where $R_{\rm m}(t) = R_{\rm m}(t+T), t > T$. Here, $R_{\rm in\_m}, R_{\rm ex\_m}, C_{\rm m}$, and $r(t)$ are chosen appropriately to obtain the desirable breathing pattern. It follows from Theorem 2.3 that $x_{\rm m}(t)$ converges to a stable limit cycle, and hence, $x_{\rm m}(t)$, $t \geq 0$, is uniformly bounded.

Next, we assume that the switched linear time-varying system (2.61) is such that $A_{\rm p}(t) = -R_{\rm p}^{-1}(t)C_{\rm p}$ and $B_{\rm p}(t) = R_{\rm p}^{-1}(t)\mathbf{e}$, where

$$R_{\rm p}(t) = \begin{cases} R_{\rm in\_p}, & 0 \leq t < T_{\rm in}, \\ R_{\rm ex\_p}, & T_{\rm in} \leq t < T, \end{cases} \tag{2.76}$$

and where $R_{\rm p}(t) = R_{\rm p}(t+T), t > T$, so that (2.61) has the form of a lung mechanics model. Here, we assume that $R_{\rm in\_p}, R_{\rm ex\_p}$, and $C_{\rm p}$ are *unknown* and we use Theorem 2.5 to design an adaptive controller $u(t), t \geq 0$, such that $x_{\rm p}(t) \to x_{\rm m}(t)$ as $t \to \infty$.

In order to apply Theorem 2.5, we need to show that the compatibility conditions (2.64) and (2.65) hold. The following proposition provides sufficient conditions under

which (2.64) and (2.65) hold for the compartmental lung model. Note that in this case $p = 1$.

Proposition 2.6. Let $W \triangleq R_{\text{in\_p}} R_{\text{in\_m}}^{-1}$. Assume that the following conditions hold:

i) $R_{\text{in\_p}} R_{\text{in\_m}}^{-1} = R_{\text{ex\_p}} R_{\text{ex\_m}}^{-1}$.

ii) There exists a positive scalar Q^* such that $W\mathbf{e} = Q^*\mathbf{e}$.

iii) There exists $\Theta^* \in \mathbb{R}^{1\times 2^n}$ such that $C_{\text{p}} = WC_{\text{m}} + \mathbf{e}\Theta^*$.

Then (2.64) and (2.65) hold.

Proof. The proof follows by noting that *i*) and *ii*) imply (2.64) holds, while *i*) and *iii*) imply (2.65) holds. □

Remark 2.10. In the absence of switching, conditions *ii*) and *iii*) are standard for model reference adaptive control [51]. Condition *i*) is an additional condition that ensures Theorem 2.5 holds for the switching periodic lung mechanics model.

2.10. Numerical Simulations of a Four-Compartment Model

In this section, we numerically integrate (2.19) to illustrate convergence of the trajectories to a stable limit cycle. Here, we assume that the bronchial tree has a regular dichotomy (see Section 2.6). Anatomically the human lung has around 24 generations of airway units. A typical value for lung compliance is $0.1\,\ell/\text{cm H}_2\text{O}$, that is, $\hat{c}_0 = 0.1\,\ell/\text{cm H}_2\text{O}$. (Note that respiratory pressure is measured in terms of centimeters of water pressure.) The airway resistance varies with the branch generation and typical values can be found in [26]. Furthermore, the expiratory resistances

will be higher than the inspiratory resistance by a factor of 2 to 3. Here, we assume that the factor is 2.5. Now, based on the values for the 24-generation model and using (2.50)–(2.53) we can obtain m-generation models for all $m = 0, \ldots, 23$.

Figures 2.4 and 2.5 provide the time responses of the compartmental volumes of a 1-generation and 2-generation lung models, respectively, where we assumed that the applied pressure $p_{\rm in}(t) = 20t + 5$ cm H_2O, $p_{\rm ex}(t) = 0$ cm H_2O, the inspiration time $T_{\rm in} = 1$ sec, the expiration time $T_{\rm ex} = 2$ sec, and the initial total volume $x_{\rm tot}(0) = 0.25\,\ell$. Figures 2.4 and 2.5 clearly show that the states of the 1-generation and 2-generation models converge to limit cycles. Furthermore, after an initial transient behavior, the steady-state volume in the lung is uniformly distributed over all the compartments, that is, the steady-state value of the volume in each compartment is equal (in both the 1-generation and 2-generation models). Finally, Figure 2.6 shows the phase portrait ($x_1(t)$ versus $x_2(t)$) of the 1-generation model showing the asymptotic convergence of the state to a limit cycle.

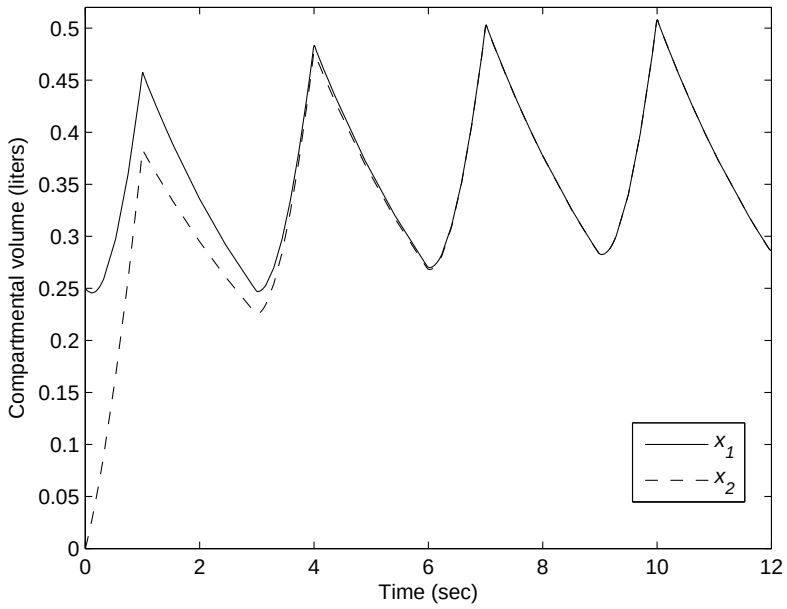

Figure 2.4: Compartmental volumes versus time: 1-generation model.

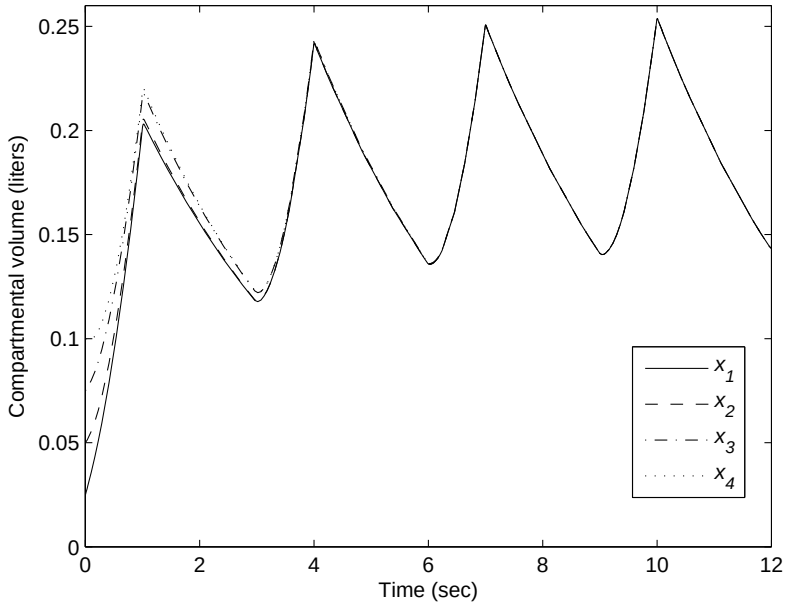

Figure 2.5: Compartmental volumes versus time: 2-generation model.

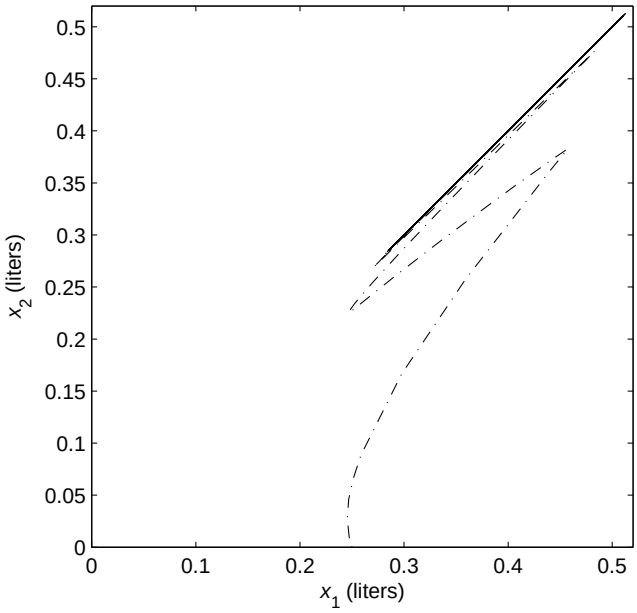

Figure 2.6: $x_1(t)$ versus $x_2(t)$: 1-generation model.

Finally, we illustrative the adaptive controller framework of Section 2.8 on our four-compartment lung mechanics model. The reference model is assumed to corre-

spond to a bronchial tree which has a regular dichotomy architecture (see Section 2.6). Furthermore, we choose a reference model so that all the conditions of Proposition 2.6, and hence, the compatibility conditions of Theorem 2.5 are satisfied. In addition, we let $\Theta_0 = [75, 75, 75, 75]$ and $Q_0 = 5$. Note that no explicit knowledge of the plant model is needed to generate the adaptive control input $u(t), t \geq 0$, given by (2.66) and the update laws given by (2.67) and (2.68). Figure 2.7 shows the error $x_{\mathrm{p}}(t) - x_{\mathrm{m}}(t)$ versus time t, verifying that $x_{\mathrm{p}}(t) \to x_{\mathrm{m}}(t)$ as $t \to \infty$. Here, we assumed that the applied pressure for the reference model is $r(t) = \sin(20t) + 5$ cm H_2O and the inspiration time is $T_{\mathrm{in}} = 1$ sec and the expiration time is $T_{\mathrm{ex}} = 2$ sec. Figures 2.8 and 2.9 show the controlled phase portrait.

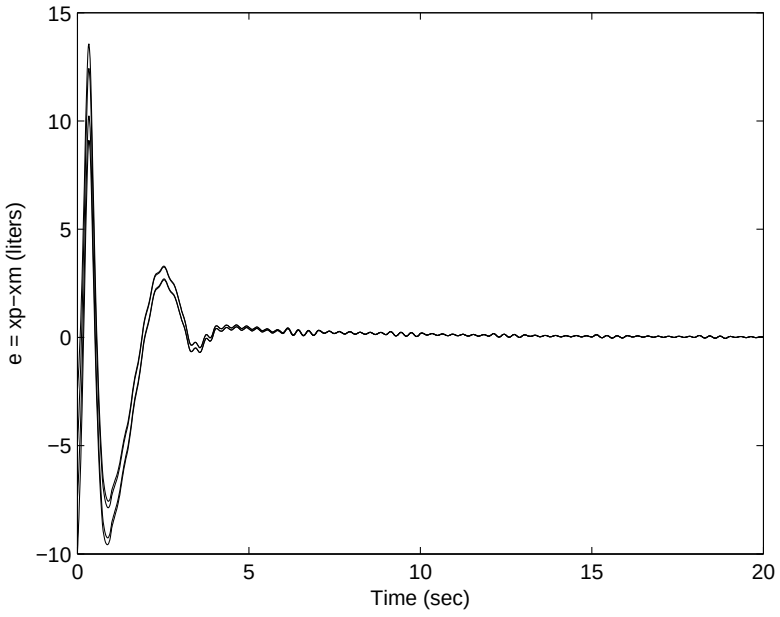

Figure 2.7: Error versus time.

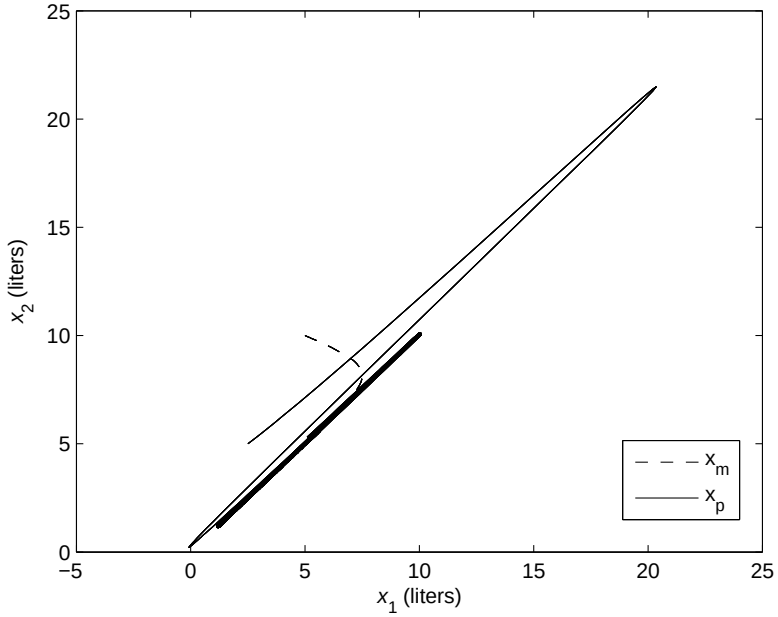

Figure 2.8: $x_1(t)$ versus $x_2(t)$: Controlled phase portrait.

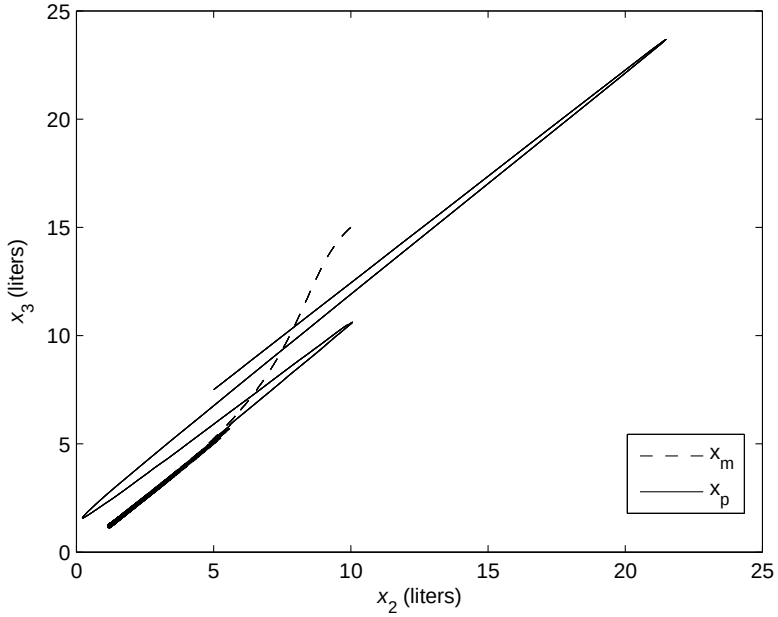

Figure 2.9: $x_2(t)$ versus $x_3(t)$: Controlled phase portrait.

Chapter 3

Optimal Determination of Respiratory Airflow Patterns using a Nonlinear Multicompartment Model for a Lung Mechanics System

3.1. Introduction

Early work on the optimality of respiratory control mechanisms using simple homogenous lung models dealt with the frequency of breathing. In particular, the authors in [53, 56, 71] predicted the frequency of breathing by using a minimum work-rate criterion. This work involves a static optimization problem and assumes that the airflow pattern is a fixed sinusoidal function. The authors in [22, 71] developed optimality criteria for the prediction of the respiratory airflow pattern with fixed inspiratory and expiratory phases of a breathing cycle. These results were extended in [23] by considering a two-level hierarchical model for the control of breathing, in which the higher-level criterion determines values for the overall control variables of the optimal airflow pattern derived from the lower-level criteria, and the lower-level criteria determine the airflow pattern with the respiratory parameters chosen by minimizing the higher-level criterion.

Although the problem for identifying optimal respiratory patterns has been addressed in the literature (see [22, 23, 53, 56, 71] and the references therein), the models on which these respiratory control mechanisms have been identified are predicated on

a single compartment lung model with constant respiratory parameters. However, as discussed in Chapter 2, the lungs, especially diseased lungs, are heterogeneous, both functionally and anatomically, and are comprised of many subunits, or compartments, that differ in their capacities for gas exchange. Realistic models should take this heterogeneity into account. In addition, the resistance to gas flow and the compliance of the lung units are not constant but rather vary with lung volume. This is particularly true for compliance. While more sophisticated models entail greater complexity, since the models are readily presented in the context of dynamical systems theory, sophisticated mathematical tools can be applied to their analysis. Compartmental lung models are described by a state vector, whose components are the volumes of the individual compartments.

A key question that arises in the consideration of nonlinear multicompartment models is whether or not experimental data support a complex model. This question can be addressed by considering an analogy to pharmakonetics. Specifically, the earliest pharmacokinetic models were typically one compartment models. This reflected the challenges of sampling and drug assay. These models were adequate for quantifying drug disposition on a long time scale. For example, simple one-compartment models were adequate in describing the total clearance or volume of distribution. However, for even open-loop control of drug concentrations the one compartment model was inadequate. More complex models (two- and three-compartment models) were needed that accounted for distribution as well as elimination processes (see [1] and the references therein).

Similarly, for adaptive control of mechanical ventilation, that is, more advanced controller architectures than simple volume- or pressure-controlled ventilation, more elaborate models are needed, especially when accounting for nonlinear compliance and resistance and lung heterogeneity [10]. In the case of pharmacokinetics, the control

algorithm can only be as complex as the data supports. This is also true for control of mechanical ventilation. Flow and pressure patterns in the airway are not simple waveforms, although clinicians to date have modeled them as such. There is considerable information embedded in these waveforms. The purpose of our work in this chapter is to provide a mathematically rigorous and general framework developing optimal determination of respiratory airflow patterns using a nonlinear multicompartment model for a lung mechanics system. It is a an easy task to simplify this framework to be congruent with the granularity of the data. The reverse process, however, is not possible without the development of a general framework.

In this chapter, we extend the work of [22, 71] to develop optimal[3] respiratory airflow patterns using a nonlinear multicompartment model for a lung mechanics system. First, we extend the linear multicompartment lung model given in Chapter 2 (see also [10]) to address system model nonlinearities. Then, we extend the performance functionals developed in [22, 71] for the inspiratory and expiratory breathing cycles to derive an optimal airflow pattern using classical calculus of variations techniques. In particular, the physiological interpretation of the optimality criteria involve the minimization of work of breathing and lung volume acceleration for the inspiratory breathing phase, and the minimization of the elastic potential energy and rapid airflow rate changes for the expiratory breathing phase. Finally, we numerically integrate the resulting nonlinear two-point boundary value problems to determine the optimal airflow patterns over the inspiratory and expiratory breathing cycles.

[3]The usage of the word *optimal* throughout the chapter refers to an optimal solution of the calculus of variations problems addressed in this chapter and not an optimal breathing pattern in the sense of respiratory physiology.

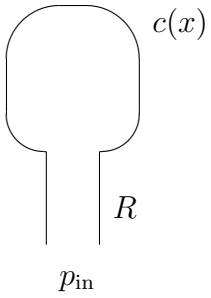

Figure 3.1: Single-compartment lung model.

3.2. A Nonlinear Multicompartment Model for Respiratory Dynamics

In this section, we extend the linear multicompartment lung model given in Section 2.3 to develop a nonlinear model for the dynamic behavior of a multicompartment respiratory system in response to an arbitrary applied inspiratory pressure. Here, we assume that the bronchial tree has a dichotomy architecture [68]; that is, in every generation each airway unit branches into two airway units of the subsequent generation. In addition, we assume that the lung compliance is a nonlinear function of lung volume.

First, for simplicity of exposition, we consider a single-compartment lung model as shown in Figure 3.1. In this model, the lungs are represented as a single lung unit with nonlinear compliance $c(x)$ connected to a pressure source by an airway unit with resistance (to air flow) of R. At time $t = 0$, a driving pressure $p_{\text{in}}(t)$ is applied to the opening of the parent airway, where $p_{\text{in}}(t)$ is generated by the respiratory muscles or a mechanical ventilator. This pressure is applied over the time interval $0 \leq t \leq T_{\text{in}}$, which is the inspiratory part of the breathing cycle. At time $t = T_{\text{in}}$, the applied airway pressure is released and expiration takes place passively, that is, the external pressure is only the atmospheric pressure $p_{\text{ex}}(t)$ during the time interval $T_{\text{in}} \leq t \leq T_{\text{in}} + T_{\text{ex}}$, where T_{ex} is the duration of expiration.

The state equation for inspiration (inflation of lung) is given by

$$R_{\text{in}}\dot{x}(t) + \frac{1}{c_{\text{in}}(x)}x(t) = p_{\text{in}}(t), \qquad x(0) = x_0^{\text{in}}, \qquad 0 \le t \le T_{\text{in}}, \tag{3.1}$$

where $x(t) \in \mathbb{R}$, $t \ge 0$, is the lung volume, $R_{\text{in}} \in \mathbb{R}$ is the resistance to air flow during the inspiration period, $c_{\text{in}} : \mathbb{R} \to \mathbb{R}_+$ is a nonlinear function defining the lung compliance at inspiration, $x_0^{\text{in}} \in \mathbb{R}_+$ is the lung volume at the start of the inspiration and serves as the system initial condition. Equation (3.1) is simply a pressure balance equation where the driving pressure $p_{\text{in}}(t), 0 \le t \le T_{\text{in}}$, applied to the compartment is proportional to the volume of the compartment via the compliance and the rate of change of the compartmental volume via the resistance. We assume that expiration is passive due to the elastic stretch of the lung unit. During the expiration process, the state equation is given by

$$R_{\text{ex}}\dot{x}(t) + \frac{1}{c_{\text{ex}}(x)}x(t) = p_{\text{ex}}(t), \qquad x(T_{\text{in}}) = x_0^{\text{ex}}, \qquad T_{\text{in}} \le t \le T_{\text{in}} + T_{\text{ex}}, \tag{3.2}$$

where $x(t) \in \mathbb{R}$, $t \ge 0$, is the lung volume, $R_{\text{ex}} \in \mathbb{R}$ is the resistance to air flow during the expiration period, $c_{\text{ex}} : \mathbb{R} \to \mathbb{R}_+$ is a nonlinear function defining the lung compliance at expiration, and $x_0^{\text{ex}} \in \mathbb{R}_+$ is the lung volume at the start of expiration.

Next, we develop the state equations for inspiration and expiration for a 2^n-compartment model, where $n \ge 0$. In this model, the lungs are represented as 2^n lung units which are connected to the pressure source by n generations of airway units, where each airway is divided into two airways of the subsequent generation leading to 2^n compartments (see Figure 3.2 for a four-compartment model).

Let $x_i,\ i = 1, 2, \ldots, 2^n$, denote the lung volume in the ith compartment, $c_i^{\text{in}}(x_i)$ (resp., $c_i^{\text{ex}}(x_i)$), $i = 1, 2, \ldots, 2^n$, denote the compliance at inspiration (resp., expiration) of each compartment as a nonlinear function of the volume of ith compartment, and let $R_{j,i}^{\text{in}}$ (resp., $R_{j,i}^{\text{ex}}$), $i = 1, 2, \ldots, 2^j,\ j = 0, \ldots, n$, denote the resistance (to air flow) of the ith airway in the jth generation during the inspiration (resp., expiration)

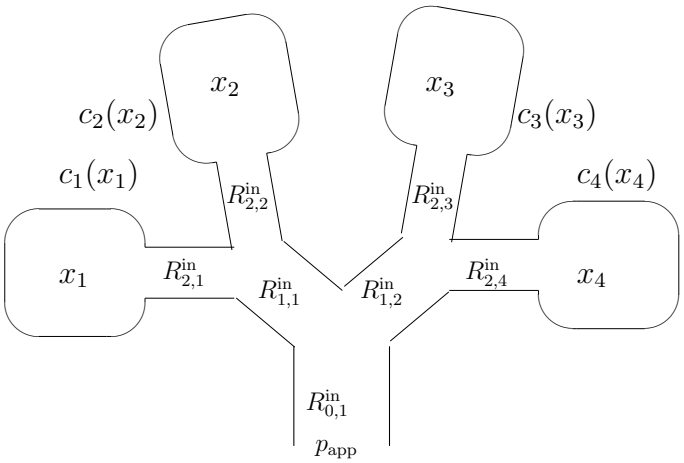

Figure 3.2: Four-compartment lung model.

period with R^{in}_{01} (resp., R^{ex}_{01}) denoting the inspiration (resp., expiration) of the *parent* (i.e., 0th generation) airway. As in the single-compartment model we assume that a pressure of $p_{\text{in}}(t), t \geq 0$, is generated (by the inspiratory muscles) or applied (by a mechanical ventilator) during inspiration.

Now, the state equations for inspiration are given by

$$R^{\text{in}}_{n,i}\dot{x}_i(t) + \frac{1}{c^{\text{in}}_i(x_i(t))}x_i(t) + \sum_{j=0}^{n-1} R^{\text{in}}_{j,k_j} \sum_{l=(k_j-1)2^{n-j}+1}^{k_j 2^{n-j}} \dot{x}_l(t) = p_{\text{in}}(t),$$
$$x_i(0) = x^{\text{in}}_{i0}, \quad 0 \leq t \leq T_{\text{in}}, \quad i = 1, 2, \ldots, 2^n, \quad (3.3)$$

where $c^{\text{in}}_i(x_i),\ i = 1, 2, \ldots, 2^n$, are nonlinear functions of x_i, $i = 1, 2, \ldots, 2^n$, given by ([14])

$$c^{\text{in}}_i(x_i) \triangleq \begin{cases} a^{\text{in}}_{i_1} + b^{\text{in}}_{i_1}x_i, & \text{if } 0 \leq x_i \leq x^{\text{in}}_{i_1}, \\ a^{\text{in}}_{i_2}, & \text{if } x^{\text{in}}_{i_1} \leq x_i \leq x^{\text{in}}_{i_2}, \\ a^{\text{in}}_{i_3} + b^{\text{in}}_{i_3}x_i, & \text{if } x^{\text{in}}_{i_2} \leq x_i \leq V_{\text{T}}, \end{cases} \qquad i = 1, \ldots, 2^n, \quad (3.4)$$

where $a^{\text{in}}_{i_j}$, $j = 1, 2, 3$, and $b^{\text{in}}_{i_j}$, $j = 1, 3$, are model parameters with $b^{\text{in}}_{i_1} > 0$ and $b^{\text{in}}_{i_3} < 0$, $x^{\text{in}}_{i_j}$, $j = 1, 2$, are volume ranges wherein the compliance is constant, V_{T} denotes tidal

volume, and

$$k_j = \left\lfloor \frac{k_{j+1} - 1}{2} \right\rfloor + 1, \quad j = 0, \ldots, n-1, \quad k_n = i, \tag{3.5}$$

where $\lfloor q \rfloor$ denotes the *floor function* which gives the largest integer less than or equal to the positive number q. Figure 3.3 shows a typical piecewise linear compliance function for inspiration. A similar compliance representation holds for expiration which is also shown in Figure 3.3.

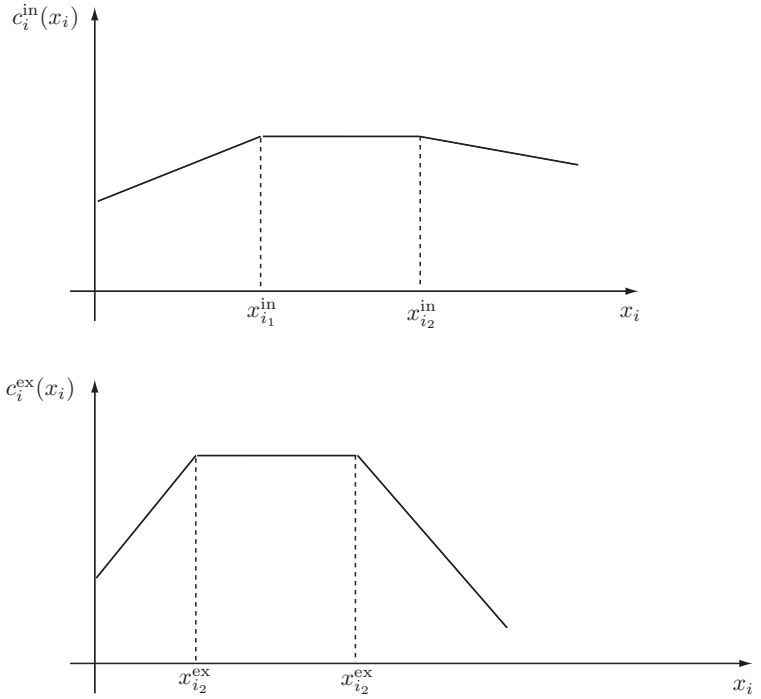

Figure 3.3: Typical inspiration and expiration compliance functions as function of compartmental volumes.

To further elucidate the inspiration state equation for a 2^n-compartment model, consider the four-compartment model shown in Figure 3.2 corresponding to a two generation lung model. Let x_i, $i = 1, 2, 3, 4$, denote the compartmental volumes. Now, the pressure $\frac{1}{c_i^{\text{in}}(x_i(t))} x_i(t)$ due to the compliance in ith compartment will be equal to the difference between the driving pressure and the resistance to air flow at every airway in the path leading from the pressure source to the ith compartment.

In particular, for $i = 3$ (see Figure 3.2),

$$\frac{1}{c_3^{\rm in}(x_3(t))}x_3(t) = p_{\rm in}(t) - R_{0,1}^{\rm in}[\dot{x}_1(t) + \dot{x}_2(t) + \dot{x}_3(t) + \dot{x}_4(t)] - R_{1,2}^{\rm in}[\dot{x}_3(t) + \dot{x}_4(t)] \\ -R_{2,3}^{\rm in}\dot{x}_3(t),$$

or, equivalently,

$$R_{2,3}^{\rm in}\dot{x}_3(t) + R_{1,2}^{\rm in}[\dot{x}_3(t) + \dot{x}_4(t)] + R_{0,1}^{\rm in}[\dot{x}_1(t) + \dot{x}_2(t) + \dot{x}_3(t) + \dot{x}_4(t)] \\ + \frac{1}{c_3^{\rm in}(x_3(t))}x_3(t) = p_{\rm in}(t).$$

Next, we consider the state equation for the expiration process. As in the single-compartment model we assume that the expiration process is passive and the external pressure applied is $p_{\rm ex}(t), t \geq 0$. Following an identical procedure as in the inspiration case, we obtain the state equation for expiration as

$$R_{n,i}^{\rm ex}\dot{x}_i(t) + \sum_{j=0}^{n-1} R_{j,k_j}^{\rm ex} \sum_{l=(k_j-1)2^{n-j}+1}^{k_j 2^{n-j}} \dot{x}_l(t) + \frac{1}{c_i^{\rm ex}(x_i(t))}x_i(t) = p_{\rm ex}(t), \\ x_i(T_{\rm in}) = x_{i_0}^{\rm ex}, \quad T_{\rm in} \leq t \leq T_{\rm ex} + T_{\rm in}, \quad i = 1, 2, \ldots, 2^n, \quad (3.6)$$

where

$$c_i^{\rm ex}(x_i) \triangleq \begin{cases} a_{i_1}^{\rm ex} + b_{i_1}^{\rm ex}x_i, & \text{if } 0 \leq x_i \leq x_{i_1}^{\rm ex}, \\ a_{i_2}^{\rm ex}, & \text{if } x_{i_1}^{\rm ex} \leq x_i \leq x_{i_2}^{\rm ex}, \\ a_{i_3}^{\rm ex} + b_{i_3}^{\rm ex}x_i, & \text{if } x_{i_2}^{\rm ex} \leq x_i \leq V_{\rm T}, \end{cases} \qquad i = 1, \ldots, 2^n, \quad (3.7)$$

$a_{i_j}^{\rm ex}$, $j = 1, 2, 3$, and $b_{i_j}^{\rm ex}$, $j = 1, 3$, are model parameters with $b_{i_1}^{\rm ex} > 0$ and $b_{i_3}^{\rm ex} < 0$, $x_{i_j}^{\rm ex}$, $j = 1, 2$, are volume ranges wherein the compliance is constant, and k_j is given by (3.5).

Next, we provide a smooth (i.e., C^∞) characterization of the nonlinear compliance using sigmoidal functions [16]. Specifically, for inspiration, $c_i^{\rm in}(x_i)$ can be approximated as

$$c_i^{\rm in}(x_i) \approx a_{i_2}^{\rm in}\left(S_{a,b}^{(\beta)}(x_i) - S_{c,d}^{(\beta)}(x_i)\right), \ i = 1, \ldots, 2^n, \quad (3.8)$$

where $a = -\frac{a^{\text{in}}_{i_1}}{b^{\text{in}}_{i_1}}$, $b = \frac{a^{\text{in}}_{i_2}}{b^{\text{in}}_{i_1}} + a$, $c = -\frac{a^{\text{in}}_{i_3}}{b^{\text{in}}_{i_3}}$, $d = \frac{a^{\text{in}}_{i_2}}{b^{\text{in}}_{i_3}} + c$, $S^{(\beta)}_{a,b}(x_i) \triangleq \frac{1}{b-a} \ln \left(\frac{\sigma_b^{(-\beta)}(x_i)}{\sigma_a^{(-\beta)}(x_i)} \right)^{1/\beta}$ with $\sigma_b^{(-\beta)}(x_i) \triangleq \frac{1}{1+e^{-\beta(x_i-a)}}$, and $\beta > 0$ is an approximation parameter. Figure 3.4 shows the smoothed approximation of the piecewise linear compliance function $c^{\text{in}}_i(x_i)$. A similar approximation holds for $c^{\text{ex}}_i(x_i)$ which is also shown in Figure 3.4.

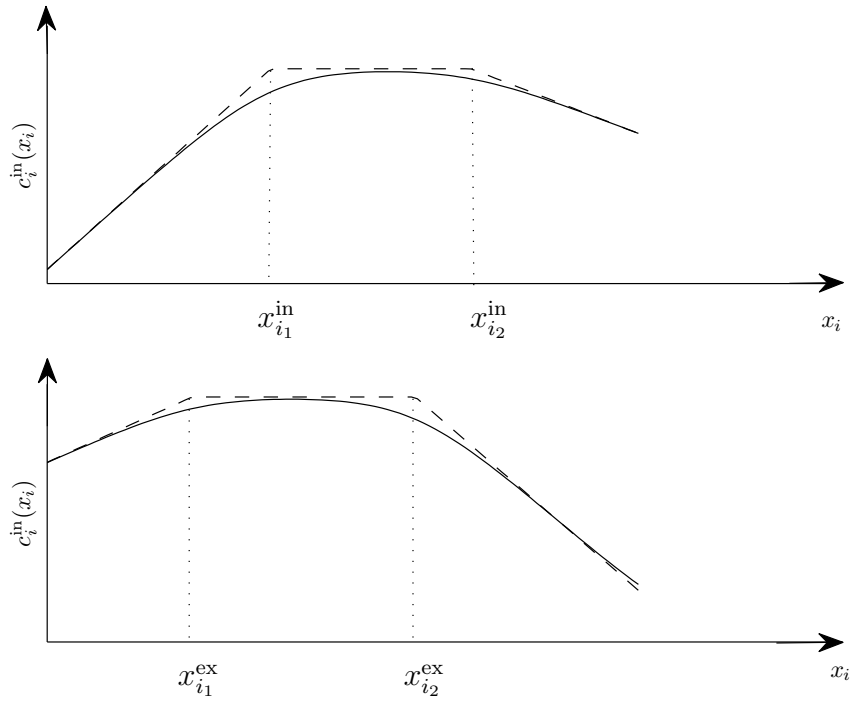

Figure 3.4: Original and the smoothed compliance functions, $\beta = 30$.

Finally, we rewrite the state equations (3.3) and (3.6) for inspiration and expiration, respectively, in vector-matrix state space form. Specifically, define the state vector $x \triangleq [x_1, x_2, \ldots, x_{2^n}]^{\text{T}}$, where x_i denotes the lung volume of the ith compartment. Now, the state equation (3.3) for inspiration can be rewritten as

$$R_{\text{in}}\dot{x}(t) + C_{\text{in}}(x(t))x(t) = p_{\text{in}}(t)\mathbf{e}, \quad x(0) = x_0^{\text{in}}, \quad 0 \leq t \leq T_{\text{in}}, \tag{3.9}$$

where $\mathbf{e} \triangleq [1, \ldots, 1]^{\text{T}}$ denotes the ones vector of order 2^n, $C_{\text{in}}(x)$ is a diagonal matrix

function given by

$$C_{\text{in}}(x) \triangleq \text{diag}\left[\frac{1}{c_1^{\text{in}}(x_1)}, \ldots, \frac{1}{c_{2^n}^{\text{in}}(x_{2^n})}\right] \tag{3.10}$$

and

$$R_{\text{in}} \triangleq \sum_{j=0}^{n} \sum_{k=1}^{2^j} R_{j,k}^{\text{in}} Z_{j,k} Z_{j,k}^{\text{T}}, \tag{3.11}$$

where $Z_{j,k} \in \mathbb{R}^{2^n}$ is such that the l-th element of $Z_{j,k}$ is 1 for all $l = (k-1)2^{n-j} + 1, (k-1)2^{n-j} + 2, \ldots, k2^{n-j}, k = 1, \ldots, 2^j, j = 0, 1, \ldots, n$, and zero elsewhere.

Similarly, the state equation (3.6) for expiration can be rewritten as

$$R_{\text{ex}}\dot{x}(t) + C_{\text{ex}}(x(t))x(t) = p_{\text{ex}}(t)\mathbf{e}, \quad x(T_{\text{in}}) = x_0^{\text{ex}}, \quad T_{\text{in}} \leq t \leq T_{\text{ex}} + T_{\text{in}}, \tag{3.12}$$

where

$$C_{\text{ex}}(x) \triangleq \text{diag}\left[\frac{1}{c_1^{\text{ex}}(x_1)}, \cdots, \frac{1}{c_{2^n}^{\text{ex}}(x_{2^n})}\right], \tag{3.13}$$

and

$$R_{\text{ex}} \triangleq \sum_{j=0}^{n} \sum_{k=1}^{2^j} R_{j,k}^{\text{ex}}\ Z_{j,k}\ Z_{j,k}^{\text{T}}. \tag{3.14}$$

Finally, it follows from Proposition 2.3 in Section 2 that R_{in} and R_{ex} are positive-definite and, hence, R_{in} and R_{ex} are invertible matrices.

3.3. Optimal Determination of Inspiratory and Expiratory Airflow in Breathing

In this section, we use the respiratory dynamical system characterized by (5.32) and (5.35) to develop an optimal model for predicting airflow patterns in breathing. The optimization criteria used allows for the minimization of oxygen expenditure of the respiratory muscles as well as rapid changes in the lung volume flow rate. The

oxygen consumption of the lung muscles is mainly due to the work carried out by the respiratory muscles to overcome the resistive forces and stretch the lung and chest wall. In [69], this work is defined as PV, where P is the pressure driving inflation and V is the lung unit volume. The efficiency of gas exchange in the lungs is related to the volume acceleration, since rapid changes in lung volume can cause discomfort and inefficacy of muscular contraction and control. Moreover, high volume acceleration can result in overexpansion of the lung resulting in lung tissue rupture as well as excessive work of breathing with subsequent ventilatory muscle fatigue.

In the ensuing discussion, we assume that the inspiration process starts from a given initial state x_0^{in} and is followed by the expiration process where its initial state will be the final state of the inspiration. An inspiration followed by an expiration is called a single *breathing cycle*. Furthermore, we assume that each breathing cycle is followed by another breathing cycle where the initial condition for the latter breathing cycle is the final state of the former breathing cycle. Since the respiratory process is periodic, we need only focus on one breathing cycle.

The next result gives the optimal solution $x^*(t), 0 \leq t \leq T_{\text{in}}$, for the inspiratory airflow breathing pattern using classical calculus of variations techniques.

Theorem 3.1. Consider the system model for inspiration given by (5.32). Let the optimal air volume $x^*(t), 0 \leq t \leq T_{\text{in}}$, be given by the solution to the minimization problem

$$\mathcal{J}_{\text{in}}(x) = \int_0^{T_{\text{in}}} \left[\ddot{x}^{\text{T}}(t)\ddot{x}(t) + \alpha_1 p_{\text{in}}(t)\mathbf{e}^{\text{T}}\dot{x}(t)\right] \mathrm{d}t, \quad \alpha_1 \geq 0, \tag{3.15}$$

subject to the natural boundary conditions

$$x(0) = V_0, \quad \dot{x}(0) = 0, \tag{3.16}$$

$$x(T_{\text{in}}) = V_0 + V_{\text{T}}, \quad \dot{x}(T_{\text{in}}) = 0, \tag{3.17}$$

where $V_0 \in \mathbb{R}^{2^n}$ is the end expiratory volume and $V_{\mathrm{T}} \in \mathbb{R}^{2^n}$ is the tidal volume. If $\alpha_1 > 0$, then $x^*(t), 0 \leq t \leq T_{\mathrm{in}}$, is given by

$$x^*(t) = d_1 + d_2 t + \exp(\sqrt{\alpha_1} R_{\mathrm{in}}^{1/2} t) d_3 + \exp(-\sqrt{\alpha_1} R_{\mathrm{in}}^{1/2} t) d_4, \quad t \geq 0, \tag{3.18}$$

and if $\alpha_1 = 0$, then

$$x^*(t) = d_1 + d_2 t + d_3 t^2 + d_4 t^3, \quad t \geq 0, \tag{3.19}$$

where d_1, d_2, d_3, and $d_4 \in \mathbb{R}^{2^n}$ are constant vectors determined by the boundary conditions (3.16) and (3.17), and $R_{\mathrm{in}}^{1/2}$ denotes the (unique) positive-definite square root of R_{in}.

Proof. First, note that $p_{\mathrm{in}}(t)\mathbf{e}, 0 \leq t \leq T_{\mathrm{in}}$, in (3.15) can be eliminated using the state equation (5.32). Thus, the integrand of the performance criterion (3.15) can be written as

$$\begin{aligned} L_{\mathrm{in}}(x(t), \dot{x}(t), \ddot{x}(t)) &= \ddot{x}^{\mathrm{T}}(t)\ddot{x}(t) + \alpha_1 \left[R_{\mathrm{in}}\dot{x}(t) + C_{\mathrm{in}}(x(t))x(t)\right]^{\mathrm{T}} \dot{x}(t) \\ &= \ddot{x}^{\mathrm{T}}(t)\ddot{x}(t) + \alpha_1 \left[\dot{x}^{\mathrm{T}}(t) R_{\mathrm{in}} \dot{x}(t) + x^{\mathrm{T}}(t) C_{\mathrm{in}}(x)\dot{x}(t)\right], \ \alpha_1 \geq 0. \end{aligned} \tag{3.20}$$

The first variation of the performance criterion $\mathcal{J}_{\mathrm{in}}(x)$ is given by

$$\begin{aligned} \delta\mathcal{J}_{\mathrm{in}}(x^*, \delta x) &= \int_0^{T_{\mathrm{in}}} \delta L_{\mathrm{in}}(x^*(t), \dot{x}^*(t), \ddot{x}^*(t)) \mathrm{d}t \\ &= \int_0^{T_{\mathrm{in}}} \left\{ \left(\frac{\partial L_{\mathrm{in}}}{\partial x}\right) \delta x(t) + \left(\frac{\partial L_{\mathrm{in}}}{\partial \dot{x}}\right) \delta\dot{x}(t) + \left(\frac{\partial L_{\mathrm{in}}}{\partial \ddot{x}}\right) \delta\ddot{x}(t) \right\} \mathrm{d}t \\ &= \left[\frac{\partial L_{\mathrm{in}}}{\partial \ddot{x}} \delta\dot{x} + \left(\frac{\partial L_{\mathrm{in}}}{\partial \dot{x}} - \frac{\mathrm{d}}{\mathrm{d}t} \frac{\partial L_{\mathrm{in}}}{\partial \ddot{x}} \right) \delta x \right]_0^{T_{\mathrm{in}}} \\ &\quad + \int_0^{T_{\mathrm{in}}} \left\{ \left(\frac{\partial L_{\mathrm{in}}}{\partial x}\right) - \frac{\mathrm{d}}{\mathrm{d}t} \left(\frac{\partial L_{\mathrm{in}}}{\partial \dot{x}}\right) + \frac{\mathrm{d}^2}{\mathrm{d}t^2} \left(\frac{\partial L_{\mathrm{in}}}{\partial \ddot{x}}\right) \right\} \delta x(t) \mathrm{d}t. \end{aligned} \tag{3.21}$$

Using the boundary conditions (3.16) and (3.17) it follows that $\delta x(0) = \delta x(T_{\mathrm{in}}) = \delta\dot{x}(0) = \delta\dot{x}(T_{\mathrm{in}}) = 0$. Now, since T_{in} is fixed, it follows from the fundamental theorem of the calculus of variations that the variation of $\mathcal{J}_{\mathrm{in}}(x)$ must vanish on x^*; that is,

the extremals optimizing the performance criterion $\mathcal{J}_{\text{in}}(x)$ satisfy the Euler-Lagrange equation

$$\left(\frac{\partial L_{\text{in}}}{\partial x}\right)^{\text{T}} - \frac{\text{d}}{\text{d}t}\left(\frac{\partial L_{\text{in}}}{\partial \dot{x}}\right)^{\text{T}} + \frac{\text{d}^2}{\text{d}t^2}\left(\frac{\partial L_{\text{in}}}{\partial \ddot{x}}\right)^{\text{T}} = 0. \tag{3.22}$$

Next, using $C_{\text{in}}(x)$ given by (5.33),

$$\left(\frac{\partial L_{\text{in}}}{\partial x}\right)^{\text{T}} = \alpha_1 C_{\text{in}}(x(t))\dot{x}(t) + \alpha_1 C'_{\text{in}}(x(t))\dot{X}(t)x(t), \quad 0 \le t \le T_{\text{in}}, \tag{3.23}$$

$$\left(\frac{\partial L_{\text{in}}}{\partial \dot{x}}\right)^{\text{T}} = 2\alpha_1 R_{\text{in}}\dot{x}(t) + \alpha_1 C_{\text{in}}(x(t))x(t), \quad 0 \le t \le T_{\text{in}}, \tag{3.24}$$

$$\left(\frac{\partial L_{\text{in}}}{\partial \ddot{x}}\right)^{\text{T}} = 2\ddot{x}(t), \quad 0 \le t \le T_{\text{in}}, \tag{3.25}$$

where $C'_{\text{in}}(x(t)) \triangleq \text{diag}\left[\frac{\partial}{\partial x_i}\left(\frac{1}{c_i^{\text{in}}(x_i(t))}\right)\right]$ and $\dot{X}(t) \triangleq \text{diag}\left[\dot{x}_i(t)\right], i = 1, \ldots, 2^n$. Thus, (3.22) yields the fourth-order differential equation

$$x^{(4)}(t) - \alpha_1 R_{\text{in}} x^{(2)}(t) = 0, \quad 0 \le t \le T_{\text{in}}, \tag{3.26}$$

where $x^{(n)}(t) \triangleq \frac{\text{d}^n x(t)}{\text{d}t^n}$, with boundary conditions given in (3.16) and (3.17). Now, using standard analysis techniques, the solution $x(t), 0 \le t \le T_{\text{in}}$, to (3.26) satisfies (3.18) if $\alpha_1 > 0$ and (3.19) if $\alpha_1 = 0$. □

Remark 3.1. The vectors d_1, d_2, d_3, and d_4 in Theorem 4.1 can be uniquely determined using the four boundary conditions given by (3.16) and (3.17). Specifically, if $\alpha_1 = 0$, it can be shown that $d_1 = V_0$, $d_2 = 0$, $d_3 = \frac{3}{T_{\text{in}}^2}V_{\text{T}}$, and $d_4 = -\frac{2}{T_{\text{in}}^3}V_{\text{T}}$. Hence, in this case, $\dot{x}(t) = d_2 + 2d_3 t + 3d_4 t^2 = \frac{6t}{T_{\text{in}}^2}V_{\text{T}}(1 - \frac{t}{T_{\text{in}}}) \geq\geq 0$, $0 \le t \le T_{\text{in}}$, which implies that the solution $x^*(t), 0 \le t \le T_{\text{in}}$, to (3.26) is increasing during inspiration, and hence, $V_{0_i} \le x_i^*(t) \le V_{0_i} + V_{\text{T}_i}, i = 1, \ldots, 2^n$, where $V_{0_i}, x_i(t)$, and V_{T_i} are the ith components of $V_0, x(t)$, and V_{T}, respectively. A similar result holds for the case where $\alpha_1 > 0$.

For the optimal breathing pattern problem in Theorem 3.1, we assume that the respiratory parameters, that is, the tidal volume V_{T} and the inspiratory period T_{in}, are given. In fact, all these parameters adjust ventilation in such a way that the chemical state of the blood is stabilized. The ventilatory demand is the input to the system controlling respiratory muscles. The muscle control system selects the breathing cycle pattern under varying metabolic and environmental conditions to generate a proper airflow pattern. And the ventilatory demand can be satisfied by this airflow pattern. Hence, there must exist interactions between the airflow pattern and the overall respiratory parameters.

For example, to identify the inspiratory parameters, the authors in [24] proposed a two-level hierarchical optimization problem with the higher level estimating inspiratory parameters and the lower level controlling the breathing. However, to understand the interaction between the higher level and lower level, we need to model the chemical state of the blood. This is further discussed in Chapter 6. In this chapter, we only focus on solving the optimal breathing pattern for a given set of respiratory parameters.

Next, we give the optimal solution $x^*(t), T_{\mathrm{in}} \leq t \leq T_{\mathrm{in}} + T_{\mathrm{ex}}$, for the expiratory airflow breathing pattern.

Theorem 3.2. Consider the system model for expiration given by (5.35). Let the optimal solution $x^*(t), T_{\mathrm{in}} \leq t \leq T_{\mathrm{in}}+T_{\mathrm{ex}}$, be given by the solution to the minimization problem

$$\mathcal{J}_{\mathrm{ex}}(x) = \int_{T_{\mathrm{in}}}^{T_{\mathrm{in}}+T_{\mathrm{ex}}} \left[\ddot{x}^{\mathrm{T}}(t)\ddot{x}(t) + \alpha_2 p_{\mathrm{ex}}^2(t)\mathbf{e}^{\mathrm{T}}\mathbf{e}\right] \mathrm{d}t, \quad \alpha_2 \geq 0, \tag{3.27}$$

subject to the natural boundary conditions

$$x(T_{\mathrm{in}}) = V_0 + V_{\mathrm{T}}, \quad \dot{x}(T_{\mathrm{in}}) = 0, \tag{3.28}$$

$$x(T_{\mathrm{in}} + T_{\mathrm{ex}}) = V_0, \quad \dot{x}(T_{\mathrm{in}} + T_{\mathrm{ex}}) = 0. \tag{3.29}$$

If $\alpha_2 > 0$, then $x^*(t), T_{\rm in} \le t \le T_{\rm in} + T_{\rm ex}$, satisfies

$$x^{(4)}(t) - \alpha_2 R_{\rm ex}^2 x^{(2)}(t) + \alpha_2 C_{\rm ex}^2(x)x(t) + \alpha_2 \left[C_{\rm ex}(x)R_{\rm ex}\dot{x}(t) - R_{\rm ex}C_{\rm ex}(x)\dot{x}(t)\right.$$
$$\left. + X(t)C'_{\rm ex}(x)R_{\rm ex}\dot{x}(t) - R_{\rm ex}C'_{\rm ex}(x)X(t)\dot{x}(t) + X(t)C'_{\rm ex}(x)C_{\rm ex}(x)x(t)\right] = 0, \quad (3.30)$$

where $X(t) \triangleq \mathrm{diag}[x_i(t)]$ and $C'_{\rm ex}(x) \triangleq \mathrm{diag}[\frac{\partial}{\partial x_i}\left(\frac{1}{c_i^{\rm ex}(x_i)}\right)], i = 1, \ldots, 2^n$, and if $\alpha_2 = 0$, then

$$x^*(t) = d_1 + d_2 t + d_3 t^2 + d_4 t^3, \quad t \ge 0, \quad (3.31)$$

where d_1, d_2, d_3, and $d_4 \in \mathbb{R}^{2^n}$ are constant vectors determined by the four boundary conditions (3.28) and (3.29).

Proof. Using (5.35), the integrand of the performance criterion (3.27) can be written as

$$\begin{aligned}
&L_{\rm ex}(x(t), \dot{x}(t), \ddot{x}(t)) \\
&\quad = \ddot{x}^{\rm T}(t)\ddot{x}(t) + \alpha_2 \left(p_{\rm ex}(t)\mathbf{e}\right)^{\rm T}\left(p_{\rm ex}(t)\mathbf{e}\right) \\
&\quad = \ddot{x}^{\rm T}(t)\ddot{x}(t) + \alpha_2 \left[R_{\rm ex}\dot{x}(t) + C_{\rm ex}(x(t))x(t)\right]^{\rm T}\left[R_{\rm ex}\dot{x}(t) + C_{\rm ex}(x(t))x(t)\right] \\
&\quad = \ddot{x}^{\rm T}(t)\ddot{x}(t) + \alpha_2 \left[\dot{x}^{\rm T}(t)R_{\rm ex}^2\dot{x}(t) + x^{\rm T}(t)C_{\rm ex}^2(x(t))x(t)\right. \\
&\qquad \left. + 2\dot{x}^{\rm T}(t)R_{\rm ex}C_{\rm ex}(x(t))x(t)\right], \quad \alpha_2 > 0. \quad (3.32)
\end{aligned}$$

Thus, the variation of $\mathcal{J}_{\rm ex}(x)$ on an extremal solution gives

$$\begin{aligned}
\delta\mathcal{J}_{\rm ex}(x^*, \delta x) &= \int_{T_{\rm in}}^{T_{\rm in}+T_{\rm ex}} \delta L_{\rm ex}(x^*(t), \dot{x}^*(t), \ddot{x}^*(t))\mathrm{d}t \\
&= \int_{T_{\rm in}}^{T_{\rm in}+T_{\rm ex}} \left\{\left(\frac{\partial L_{\rm ex}}{\partial x}\right)\delta x(t) + \left(\frac{\partial L_{\rm ex}}{\partial \dot{x}}\right)\delta\dot{x}(t) + \left(\frac{\partial L_{\rm ex}}{\partial \ddot{x}}\right)\delta\ddot{x}(t)\right\}\mathrm{d}t \\
&= \left[\frac{\partial L_{\rm ex}}{\partial \ddot{x}}\delta\dot{x} + \left(\frac{\partial L_{\rm ex}}{\partial \dot{x}} - \frac{\mathrm{d}}{\mathrm{d}t}\frac{\partial L_{\rm ex}}{\partial \ddot{x}}\right)\delta x\right]_{T_{\rm in}}^{T_{\rm in}+T_{\rm ex}} \\
&\quad + \int_{T_{\rm in}}^{T_{\rm in}+T_{\rm ex}} \left\{\left(\frac{\partial L_{\rm ex}}{\partial x}\right) - \frac{\mathrm{d}}{\mathrm{d}t}\left(\frac{\partial L_{\rm ex}}{\partial \dot{x}}\right) + \frac{\mathrm{d}^2}{\mathrm{d}t^2}\left(\frac{\partial L_{\rm ex}}{\partial \ddot{x}}\right)\right\}\delta x(t)\mathrm{d}t \\
&= 0. \quad (3.33)
\end{aligned}$$

Using the boundary conditions (3.28) and (3.29) it follows that $\delta x(T_{\rm in}) = \delta x(T_{\rm in} + T_{\rm ex}) = \delta\dot{x}(T_{\rm in}) = \delta\dot{x}(T_{\rm in} + T_{\rm ex}) = 0$. Hence, the extremals optimizing the performance criterion $\mathcal{J}_{\rm ex}(x)$ satisfy the Euler-Lagrange equation

$$\left(\frac{\partial L_{\rm ex}}{\partial x}\right)^{\rm T} - \frac{\rm d}{{\rm d}t}\left(\frac{\partial L_{\rm ex}}{\partial \dot{x}}\right)^{\rm T} + \frac{{\rm d}^2}{{\rm d}t^2}\left(\frac{\partial L_{\rm ex}}{\partial \ddot{x}}\right)^{\rm T} = 0. \tag{3.34}$$

Now, using $C_{\rm ex}(x)$ given by (5.36),

$$\begin{aligned}\left(\frac{\partial L_{\rm ex}}{\partial x}\right)^{\rm T} &= \alpha_2 \left[2C_{\rm ex}^2(x(t))x(t) + 2C_{\rm ex}(x(t))R_{\rm ex}\dot{x}(t) + 2X(t)C_{\rm ex}'(x(t))R_{\rm ex}\dot{x}(t)\right.\\ &\quad \left. +2X(t)C_{\rm ex}'(x(t))C_{\rm ex}(x(t))x(t)\right], \quad T_{\rm in} \le t \le T_{\rm in} + T_{\rm ex}, \qquad (3.35)\\ \left(\frac{\partial L_{\rm ex}}{\partial \dot{x}}\right)^{\rm T} &= \alpha_2 \left[2R_{\rm ex}^2\dot{x}(t) + 2R_{\rm ex}C_{\rm ex}(x(t))x(t)\right], \quad T_{\rm in} \le t \le T_{\rm in} + T_{\rm ex}, \qquad (3.36)\\ \left(\frac{\partial L_{\rm ex}}{\partial \ddot{x}}\right)^{\rm T} &= 2\ddot{x}(t), \quad T_{\rm in} \le t \le T_{\rm in} + T_{\rm ex}, \qquad (3.37)\end{aligned}$$

which yields (3.30). Finally, in the case where $\alpha_2 = 0$, (3.30) collapses to $x^{(4)}(t) = 0, T_{\rm in} \le t \le T_{\rm in} + T_{\rm ex}$, which satisfies (3.31). □

Remark 3.2. In the case where $\alpha_2 = 0$, the vectors d_1, d_2, d_3, and d_4 in Theorem 3.2 can be uniquely determined using the four boundary conditions (3.28) and (3.29). In particular, $d_1 = V_0 + V_{\rm T} + 3\beta T_{\rm in}^2 T_{\rm ex} V_{\rm T} + 2\beta T_{\rm in}^3 V_{\rm T}$, $d_2 = -\beta(6T_{\rm in}^2 V_{\rm T} + 6T_{\rm ex}T_{\rm in}V_{\rm T})$, $d_3 = \beta(3T_{\rm ex}V_{\rm T} + 6T_{\rm in}V_{\rm T})$, and $d_4 = -2\beta V_{\rm T}$, where $\beta = 1/(3T_{\rm ex}^3 + 12T_{\rm ex}^2 T_{\rm in} + 12T_{\rm ex}T_{\rm in}^2 + 4T_{\rm in}^3)$. Hence, $\dot{x}(t) = d_2 + 2d_3 t + 3d_4 t^2 = -6\beta V_{\rm T} t(T_{\rm in} + T_{\rm ex} - t) - 6\beta V_{\rm T} t(t - T_{\rm in}) \leq\leq 0, T_{\rm in} \le t \le T_{\rm in} + T_{\rm ex}$, which implies that the solution $x^*(t), T_{\rm in} \le t \le T_{\rm in} + T_{\rm ex}$, is decreasing during expiration, and hence, $V_{0_i} \le x_i^*(t) \le V_{0_i} + V_{{\rm T}_i}, i = 1, \ldots, 2^n$. The case where $\alpha_2 > 0$ involves the solution to (3.30), and hence, we have been unable to show that $x^*(t), T_{\rm in} \le t \le T_{\rm in} + T_{\rm ex}$, is decreasing during expiration analytically. However, this has been verified numerically.

The physiological interpretations of the performance criteria for inspiration and expiration used in Theorem 3.1 and 3.2 are slightly different. In particular, the

inspiratory criterion $\mathcal{J}_{\text{in}}(x)$ involves a weighted sum of squares of the lung volume acceleration and the mechanical work performed by the inspiratory muscles. Alternatively, during the expiratory phase the respiratory muscles remain active in the beginning of expiration since they continue their action by opposing expiration, and hence, consume oxygen thereby performing negative work. Thus, mechanical work alone is not a satisfactory criterion for describing control of breathing at rest. As in [24], we assume that oxygen consumption of expiration correlates with the integral square of the driving pressure. This assumption is supported in [49] which shows that an index of average respiratory pressure can predict the total oxygen cost of breathing. Hence, instead of mechanical work, we use the integral square of the applied pressure in the expiratory criterion $\mathcal{J}_{\text{ex}}(x)$, which corresponds to minimizing the mean standard potential energy in the lung.

It can be seen that the optimal solutions $x^*(t), t \geq 0$, depend on the variables T_{in}, T_{ex}, V_0, and V_{T} through the boundary conditions. Moreover, the nonlinearities in (3.30) are due to nonlinearities in the lung compliance $C_{\text{ex}}(x)$, which make analytical solutions to (3.30) difficult to obtain. It is interesting to note that although the optimal solutions $x^*(t), T_{\text{in}} \leq t \leq T_{\text{in}} + T_{\text{ex}}$, to (3.30) during the expiration phase depend on the nonlinear compliance of $C_{\text{ex}}(x)$, the optimal solutions $x^*(t), 0 \leq t \leq T_{\text{in}}$, to (3.26) during the inspiration phase are independent of the nonlinear system compliance $C_{\text{in}}(x)$. In the case where $n = 0$ (i.e., a single lung compartment model), $x(t) \in \mathbb{R}$, $R_{\text{ex}} \in \mathbb{R}$, and $C_{\text{ex}}(x) = C_{\text{ex}}$ is a constant, (3.30) reduces to

$$x^{(4)}(t) - \alpha_2 R_{\text{ex}}^2 x^{(2)}(t) + \alpha_2 C_{\text{ex}}^2 x(t) = 0. \tag{3.38}$$

This case is extensively discussed in [24] wherein the authors characterize four different solutions to (3.38) corresponding to $\alpha_2 = 0$, $0 < \alpha_2 < 4C_{\text{ex}}^2/R_{\text{ex}}^4$, $\alpha_2 = 4C_{\text{ex}}^2/R_{\text{ex}}^4$, and $\alpha_2 > 4C_{\text{ex}}^2/R_{\text{ex}}^4$.

3.4. Numerical Determination of Optimal Volume Trajectories

The optimal volume trajectories formulated in Section 4.3 result in two-point nonlinear boundary-value problems. Numerical methods for solving such problems include shooting methods [32] and steepest descent methods [33]. In this section, we use the collocation method implemented by *bvp4c* in MATLAB® [57] to numerically integrate the differential equations (3.26) and (3.30) to obtain the optimal volume trajectory $x^*(t), t \geq 0$.

For our simulations we first consider a two-compartment lung model and use the values for the lung compliance found in [14]. In particular, we set $a_{i_1}^{\text{in}} = 0.018\,\ell/\text{cm}$ H_2O, $b_{i_1}^{\text{in}} = 0.0233$, $a_{i_2}^{\text{in}} = 0.025\,\ell/\text{cm}$ H_2O, $a_{i_3}^{\text{in}} = 0.2532\,\ell/\text{cm}$ H_2O, $b_{i_3}^{\text{in}} = -0.01$, $x_{i_1}^{\text{in}} = 0.3\,\ell$, $x_{i_2}^{\text{in}} = 0.48\,\ell$, $a_{i_1}^{\text{ex}} = 0.02\,\ell/\text{cm}$ H_2O, $b_{i_1}^{\text{ex}} = 0.078$, $a_{i_2}^{\text{ex}} = 0.038\,\ell/\text{cm}$ H_2O, $a_{i_3}^{\text{ex}} = 0.1025\,\ell/\text{cm}$ H_2O, $b_{i_3}^{\text{ex}} = -0.15$, $x_{i_1}^{\text{ex}} = 0.23\,\ell$, $x_{i_2}^{\text{ex}} = 0.43\,\ell$, $i = 1, 2$. Here, we assume that the bronchial tree has a dichotomy structure (see Section 3.2). The airway resistance varies with the branch generation and typical values can be found in [26]. Furthermore, the expiratory resistance will be higher than the inspiratory resistance by a factor 2 to 3. Here, we assume that the factor is 2.5.

For our simulation we assume that the inspiration time $T_{\text{in}} = 2$ sec and the expiration time $T_{\text{ex}} = 3$ sec. The two weighting parameters α_1 and α_2 differ from person to person. Nominal values for the weighting parameters are $\alpha_1 = 2.0l/\text{sec}^3$ cm H_2O and $\alpha_2 = 0.1l^2/\text{sec}^4$ cm H_2O, which correspond to spontaneous breathing at rest [24]. Figure 3.5 shows the optimal air volume $\mathbf{e}^{\mathrm{T}}x^*(t), t \geq 0$, and the optimal airflow rate $\mathbf{e}^{\mathrm{T}}\dot{x}^*(t), t \geq 0$, given by the two-point nonlinear boundary-value problems (3.22) and (3.34). Note that the airflow curve for inspiration is symmetric since the nonlinearities in $C_{\text{in}}(x)$ do not appear in (3.26). However, $x^*(t), t \geq 0$, obtained using

(3.30) during expiration involves $C_{\text{ex}}(x)$, and hence, the airflow curve is asymmetric.

Figure 3.6 shows the sensitivity of the optimal volume and airflow rate patterns to changes in the parameters α_1 and α_2. As can be seen from the figure, the inspiratory airflow rate is symmetric and the maximum value of the airflow rate decreases as a function of increasing α_1. Furthermore, the asymmetric pattern of the expiratory airflow rate reflects the fact that the minimum value becomes steeper with increasing α_2. Specifically, if we set the weighting parameter $\alpha_2 = 0$, it follows from (3.30) that the airflow curve for the expiration is given by a parabolic arc. The airflow patterns in Figure 3.6 exhibit typical respiratory characteristics observed in spontaneous breathing, that is, the inspiratory airflow rate curve is relatively flat and the expiratory airflow rate waveform is asymmetric with an initial trough, and quite similar to "real" airflow signals [55].

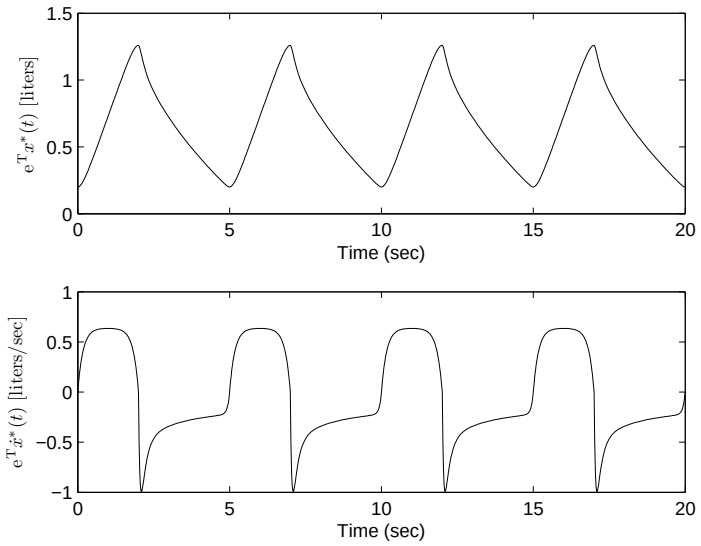

Figure 3.5: Volume and airflow rate patterns for the total lung compartments.

Figure 3.7 shows the driving pressure generated by the respiratory muscles using the optimal air volume $\mathbf{e}^{\mathrm{T}}x^*(t), t \geq 0$. Figure 3.8 compares the optimal air volume trajectory $\mathbf{e}^{\mathrm{T}}x^*(t), t \geq 0$, with a non-optimal air volume trajectory $\mathbf{e}^{\mathrm{T}}x(t), t \geq 0$,

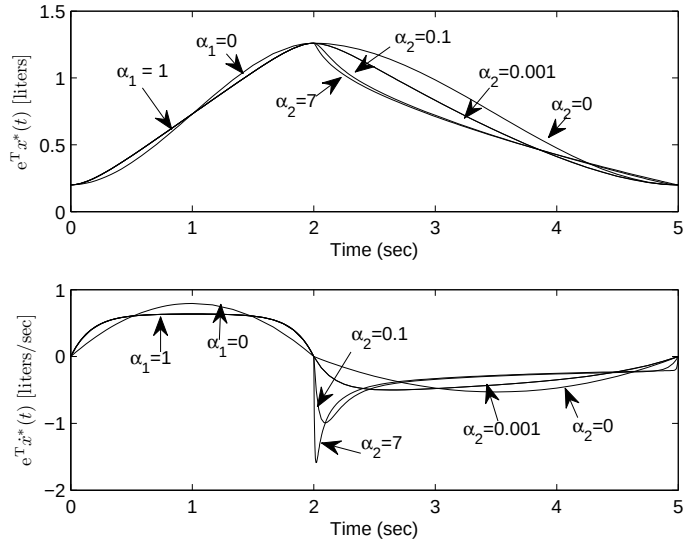

Figure 3.6: Volume and airflow rate patterns for different α_1's and α_2's.

generated by the linear pressure $p_{\text{in}}(t) = 20t + 5$ cm H_2O, $t \in [0, T_{\text{in}}]$, and $p_{\text{ex}}(t) = 0$ cm H_2O, $t \in [T_{\text{in}}, T_{\text{in}} + T_{\text{ex}}]$, [10]. Note that $\mathbf{e}^{\text{T}} x^*(t), t \geq 0$, switches between the end expiratory level $\mathbf{e}^{\text{T}} V_0 = 0.2l$ and the tidal volume $\mathbf{e}^{\text{T}} V_{\text{T}_1} = 1.2l$. Figure 3.9 shows the phase portrait of the optimal trajectories $x_1^*(t)$ and $x_2^*(t)$, and suboptimal trajectories $x_1(t)$ and $x_2(t)$. Note that both sets of trajectories asymptotically converge to a limit cycle, with the optimal solutions satisfying the boundary conditions given in (3.16), (3.17), (3.28), and (3.29). Figure 3.10 compares the value of the total performance criterion generated by the optimal air volume with the value of the total performance criterion generated by the nonoptimal air volume.

Figure 3.11 shows the optimal air volume trajectories for a four-compartment model with each air volume trajectory satisfying the boundary conditions given in (3.16), (3.17), (3.28), and (3.29). For this simulation, the compliance parameters are taken to be identical to those used for the two-compartment model with $i = 1, 2, 3, 4$, and the values for airway resistances are generated using the results of [26].

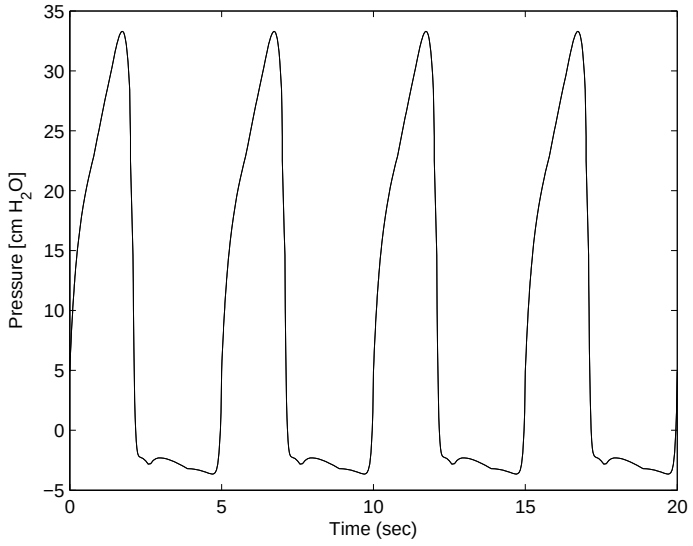

Figure 3.7: Pressure generated by optimal solution.

Finally, instead of characterizing the optimal airflow in breathing for the inspiratory and expiratory phases separately, we formulate a single optimization criterion $\mathcal{J}(x)$ for an entire breathing cycle. Specifically, we assume that the volume at the end of the inspiratory phase is unknown. Thus, considering the system models for inspiration given by (5.32) and expiration given by (5.35), we solve for the optimal air volume $x^*(t), 0 \leq t \leq T_{\text{in}} + T_{\text{ex}}$, by minimizing the following performance criterion $\mathcal{J}(x)$ given by

$$\begin{aligned}\mathcal{J}(x) = &\int_0^{T_{\text{in}}} [\ddot{x}^{\text{T}}(t)\ddot{x}(t) + \alpha_1 p_{\text{in}}(t)\mathbf{e}^{\text{T}}\dot{x}(t)]\mathrm{d}t + \int_{T_{\text{in}}}^{T_{\text{in}}+T_{\text{ex}}} [\ddot{x}^{\text{T}}(t)\ddot{x}(t) + \alpha_2 p_{\text{ex}}^2(t)\mathbf{e}^{\text{T}}\mathbf{e}]\mathrm{d}t, \\ &+\frac{1}{2}(x(T_{\text{in}}) - V_0 - V_T)^{\text{T}}(x(T_{\text{in}}) - V_0 - V_T), \quad \alpha_1 \geq 0, \alpha_2 \geq 0, \end{aligned} \tag{3.39}$$

subject to the natural boundary conditions

$$x(0) = V_0, \quad \dot{x}(0) = 0, \tag{3.40}$$

$$\dot{x}(T_{\text{in}}) = 0, \tag{3.41}$$

$$x(T_{\text{in}} + T_{\text{ex}}) = V_0, \quad \dot{x}(T_{\text{in}} + T_{\text{ex}}) = 0. \tag{3.42}$$

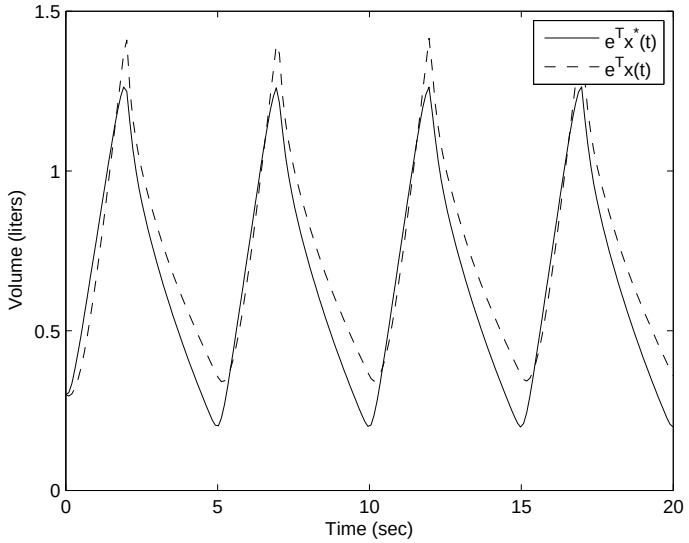

Figure 3.8: Optimal volume $\mathbf{e}^{\mathrm{T}}x^*(t)$ and nonoptimal volume $\mathbf{e}^{\mathrm{T}}x(t)$ versus time.

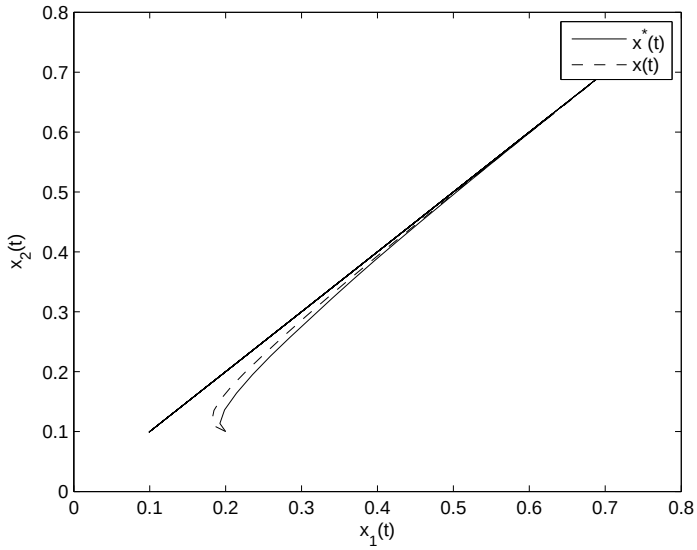

Figure 3.9: Phase portrait for $x_1^*(t)$ versus $x_2^*(t)$ and $x_1(t)$ versus $x_2(t)$.

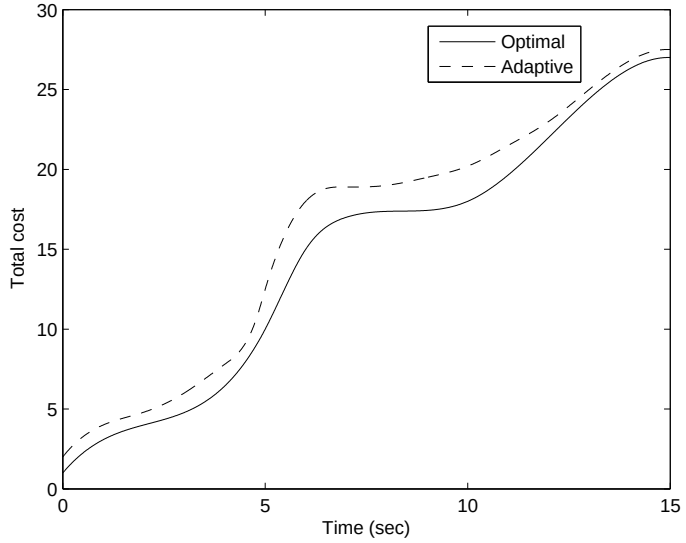

Figure 3.10: Performance criterion comparison versus time.

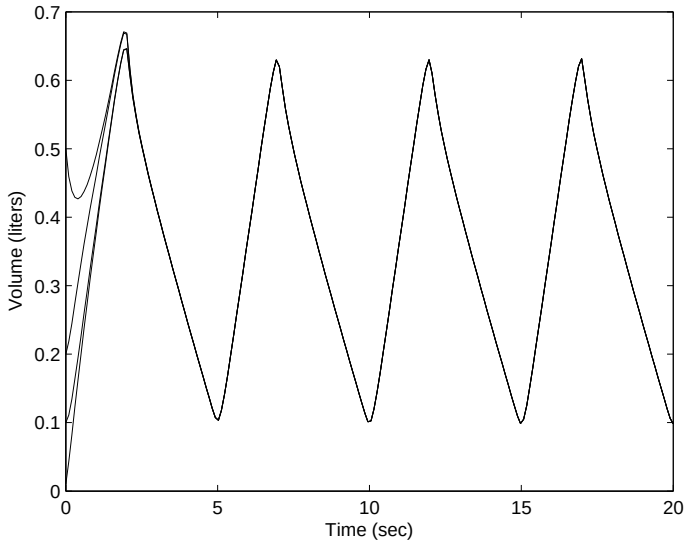

Figure 3.11: Optimal volume $x^*(t)$ versus time for a four-compartmental model.

Thus, the first variation of $\mathcal{J}(x)$ on an extremal solution gives

$$\begin{aligned}
\delta\mathcal{J}(x^*,\delta x) &= \int_0^{T_{\rm in}} \delta L_{\rm in}(x^*(t),\dot{x}^*(t),\ddot{x}^*(t))\mathrm{d}t + \int_{T_{\rm in}}^{T_{\rm in}+T_{\rm ex}} \delta L_{\rm ex}(x^*(t),\dot{x}^*(t),\ddot{x}^*(t))\mathrm{d}t \\
&\quad +(x(T_{\rm in})-V_0-V_T)^{\rm T}\delta x(T_{\rm in}) \\
&= \int_0^{T_{\rm in}} \left\{ \left(\frac{\partial L_{\rm in}}{\partial x}\right)\delta x(t) + \left(\frac{\partial L_{\rm in}}{\partial \dot{x}}\right)\delta\dot{x}(t) + \left(\frac{\partial L_{\rm in}}{\partial \ddot{x}}\right)\delta\ddot{x}(t) \right\}\mathrm{d}t \\
&\quad + \int_{T_{\rm in}}^{T_{\rm in}+T_{\rm ex}} \left\{ \left(\frac{\partial L_{\rm ex}}{\partial x}\right)\delta x(t) + \left(\frac{\partial L_{\rm ex}}{\partial \dot{x}}\right)\delta\dot{x}(t) + \left(\frac{\partial L_{\rm ex}}{\partial \ddot{x}}\right)\delta\ddot{x}(t) \right\}\mathrm{d}t \\
&\quad +(x(T_{\rm in})-V_0-V_T)^{\rm T}\delta x(T_{\rm in}) \\
&= \left[\frac{\partial L_{\rm in}}{\partial \ddot{x}}\delta\dot{x} + \left(\frac{\partial L_{\rm in}}{\partial \dot{x}} - \frac{\mathrm{d}}{\mathrm{d}t}\frac{\partial L_{\rm in}}{\partial \ddot{x}}\right)\delta x\right]_0^{T_{\rm in}} + \int_0^{T_{\rm in}} \left\{ \left(\frac{\partial L_{\rm in}}{\partial x}\right) - \frac{\mathrm{d}}{\mathrm{d}t}\left(\frac{\partial L_{\rm in}}{\partial \dot{x}}\right) \right. \\
&\quad \left. + \frac{\mathrm{d}^2}{\mathrm{d}t^2}\left(\frac{\partial L_{\rm in}}{\partial \ddot{x}}\right) \right\}\delta x(t)\mathrm{d}t + \left[\frac{\partial L_{\rm ex}}{\partial \ddot{x}}\delta\dot{x} + \left(\frac{\partial L_{\rm ex}}{\partial \dot{x}} - \frac{\mathrm{d}}{\mathrm{d}t}\frac{\partial L_{\rm ex}}{\partial \ddot{x}}\right)\delta x\right]_{T_{\rm in}}^{T_{\rm in}+T_{\rm ex}} \\
&\quad + \int_{T_{\rm in}}^{T_{\rm in}+T_{\rm ex}} \left\{ \left(\frac{\partial L_{\rm ex}}{\partial x}\right) - \frac{\mathrm{d}}{\mathrm{d}t}\left(\frac{\partial L_{\rm ex}}{\partial \dot{x}}\right) + \frac{\mathrm{d}^2}{\mathrm{d}t^2}\left(\frac{\partial L_{\rm ex}}{\partial \ddot{x}}\right) \right\}\delta x(t)\mathrm{d}t \\
&\quad +(x(T_{\rm in})-V_0-V_T)^{\rm T}\delta x(T_{\rm in}) \\
&= 0, \qquad (3.43)
\end{aligned}$$

where $L_{\rm in}(x,\dot{x},\ddot{x})$ is given by (3.20) and $L_{\rm ex}(x,\dot{x},\ddot{x})$ is given by (3.32). Using the boundary conditions (3.40)–(3.42), it follows that $\delta x(0) = \delta\dot{x}(0) = \delta\dot{x}(T_{\rm in}) = \delta x(T_{\rm in}+T_{\rm ex}) = \dot{\delta}x(T_{\rm in}+T_{\rm ex}) = 0$. Hence, the extremals optimizing the performance criterion $\mathcal{J}(x)$ satisfy the Euler-Lagrange equations given by

$$\left(\frac{\partial L_{\rm in}}{\partial x}\right)^{\rm T} - \frac{\mathrm{d}}{\mathrm{d}t}\left(\frac{\partial L_{\rm in}}{\partial \dot{x}}\right)^{\rm T} + \frac{\mathrm{d}^2}{\mathrm{d}t^2}\left(\frac{\partial L_{\rm in}}{\partial \ddot{x}}\right)^{\rm T} = 0, \quad 0 \le t \le T_{\rm in}, \qquad (3.44)$$

$$\left(\frac{\partial L_{\rm ex}}{\partial x}\right)^{\rm T} - \frac{\mathrm{d}}{\mathrm{d}t}\left(\frac{\partial L_{\rm ex}}{\partial \dot{x}}\right)^{\rm T} + \frac{\mathrm{d}^2}{\mathrm{d}t^2}\left(\frac{\partial L_{\rm ex}}{\partial \ddot{x}}\right)^{\rm T} = 0, \quad T_{\rm in} \le t \le T_{\rm in}+T_{\rm ex}, \qquad (3.45)$$

and the algebraic equation at the end of inspiration given by

$$\left[\alpha_1 C_{\rm in}(x(T_{\rm in})) - 2\alpha_2 R_{\rm ex}C_{\rm ex}(x(T_{\rm in})) + I_{2^n}\right]x(T_{\rm in}) = V_0 + V_T. \qquad (3.46)$$

Hence, it follows from (3.44)–(3.46) that α_1 and α_2 effect the breathing patterns for inspiratory and expiratory phases simultaneously. If we set $\alpha_1 = 1$ and let α_2 vary, Figure 3.12 shows that the changes of α_2 effect both inspiratory and expiratory phases.

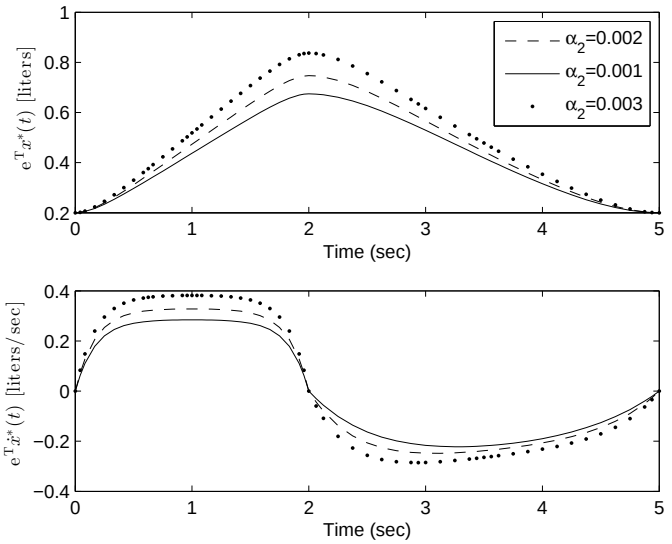

Figure 3.12: Volume and airflow rate patterns for different α_2's.

Chapter 4

Model Predictive Control for a Multicompartment Respiratory System

4.1. Introduction

Since respiratory control involves numerous state and control constraints such as air volume capacity constraints in the lungs and constraints on the sign and range of the input pressure, model predictive control is well suited for addressing mechanical ventilation control. Model predictive control is a control methodology in which an optimal control problem is solved over a receding horizon [48]. In particular, at each sampling time, an open-loop optimal control problem is solved over a finite horizon m to generate a sequence of optimal control actions $\overline{\mathbf{u}}^* = \{\mathbf{u}^*(0), \ldots, \mathbf{u}^*(m-1)\}$ based on the current system states. Next, the first control action $\mathbf{u}^*(0)$ in the generated control action sequence $\overline{\mathbf{u}}^*$ is implemented over a given sampling interval. This procedure is then repeated over the next sampling time. A key advantage of this type of control architecture is its ability to address control and state constraints.

In this chapter, we design a model predictive controller for a multicompartment respiratory system. The dynamics of the respiratory system are characterized by a linear periodic system. For a given periodic reference volume pattern, the goal of the controller is to asymptotically track the target reference. Although model predictive

control can handel periodic and time-varying systems, it can be cumbersome or at least not straightforward to use if the system is time-varying or periodic. In contrast, repetitive control [25] has been proposed to address tracking control problems involving periodic reference trajectories by transforming a periodic system into a *lifted run-to-run* invariant system. In this section, we merge model predictive control with repetitive control to address a tracking control problem involving a periodic system with nonnegative control input constraints. Specifically, we formulate a finite-time optimal control problem subject to nonnegative control input constraints that minimizes the deviation of the multicompartment respiratory system output from the given reference volume pattern. Then, we numerically compute the resulting constrained optimal control to generate an optimal control sequence, a system output trajectory, and the system states that guarantee asymptotic tracking of the target reference trajectory.

4.2. A Multicompartment Model for Respiratory Dynamics

In this section, we use the general mathematical model for capturing the dynamic behavior of a multicompartment respiratory system in response to an arbitrary applied inspiratory pressure developed in Section 2.5 of Chapter 2 and the optimal respiratory airflow pattern for the lung mechanics system defined in Chapter 3 to design a tracking controller using a model predictive controller framework.

Recall that the dynamics for a breathing cycle for a multicompartment lung model can be characterized by the periodic switched dynamical system given by (2.19). In order to account for a continuous transition of the lung resistance and compliance parameters between the inspiration and expiration phase, consider the bounded con-

tinuous periodic function $\theta(t), t \geq 0$, given by

$$\theta(t) \triangleq \begin{cases} 1, & 0 \leq t \leq T_{\rm in} - \varepsilon_{\rm in}, \\ \frac{1}{\varepsilon_{\rm in}}(T_{\rm in} - t), & T_{\rm in} - \varepsilon_{\rm in} \leq t \leq T_{\rm in}, \\ 0, & T_{\rm in} \leq t \leq T_{\rm in} + T_{\rm ex} - \varepsilon_{\rm ex}, \\ \frac{1}{\varepsilon_{\rm ex}}(t + \varepsilon_{\rm ex} - T_{\rm in} - T_{\rm ex}), & T_{\rm in} + T_{\rm ex} - \varepsilon_{\rm ex} \leq t \leq T_{\rm in} + T_{\rm ex}, \end{cases} \tag{4.1}$$

where $\varepsilon_{\rm in} > 0$ and $\varepsilon_{\rm ex} > 0$ are sufficiently small constants representing the transition times from inspiration to expiration and vice versa, respectively, and $\theta(t) = \theta(t + T_{\rm in} + T_{\rm ex})$ for all $t \geq 0$. Now, the dynamics for a breathing cycle characterized by the periodic dynamical system (2.19) can be written as

$$\dot{x}(t) = A_{\rm c}(t)x(t) + B_{\rm c}(t)u(t), \quad x(0) = x_0^{\rm in}, \quad t \geq 0, \tag{4.2}$$

$$y(t) = \mathbf{e}^{\rm T}x(t), \tag{4.3}$$

where the output (4.3) gives the total compartment lung volume, $A_{\rm c}(t) \triangleq \theta(t)A_{\rm in} + (1 - \theta(t))A_{\rm ex}$, and $B_{\rm c}(t) \triangleq \theta(t)B_{\rm in} + (1 - \theta(t))B_{\rm ex}$. Note that $A_{\rm c}(t) = A_{\rm c}(t + T)$ and $B_{\rm c}(t) = B_{\rm c}(t + T)$ for all $t \geq 0$, and hence, $A_{\rm c}(\cdot)$ and $B_{\rm c}(\cdot)$ are periodic.

Next, using a zero-order hold with a sampling time $\sigma > 0$, (4.2) and (4.3) can be discretized as

$$x_k(\tau + 1) = A(\tau)x_k(\tau) + B(\tau)u_k(\tau), \ x_k(0) = x_{0,k}^{\rm in}, \ k \in \mathbb{Z}_+, \ \tau = 0, \ldots, N - 1, \tag{4.4}$$

$$y_k(\tau) = \mathbf{e}^{\rm T}x_k(\tau), \tag{4.5}$$

where k is a run index over the periods, τ is the time step within one period, and $A(\tau)$ and $B(\tau)$ are discretized versions of $A_{\rm c}(\tau\sigma)$ and $B_{\rm c}(\tau\sigma)$. Here, each period is assumed to be divided into $N = \frac{T_{\rm in} + T_{\rm ex}}{\sigma}$ equally spaced sample intervals. Furthermore, since the system dynamics transition from inspiration to expiration and back to inspiration, a transition from the end of an expiration phase to the beginning of an inspiration phase can be expressed by

$$x_{k+1}(0) = x_k(N) = A(N - 1)x_k(N - 1) + B(N - 1)u_k(N - 1), \quad k \in \mathbb{Z}_+. \tag{4.6}$$

Next, grouping the system variables for one period into vectors as

$$\mathbf{y}_k \triangleq \begin{bmatrix} y_k(0) \\ \vdots \\ y_k(N-1) \end{bmatrix}, \quad \mathbf{u}_k \triangleq \begin{bmatrix} u_k(0) \\ \vdots \\ u_k(N-1) \end{bmatrix}, \tag{4.7}$$

and using (4.6), a *lifted run-to-run* invariant system model is given by

$$x_{k+1}(0) = \Phi x_k(0) + \Gamma \mathbf{u}_k, \quad k \in \mathbb{Z}_+, \tag{4.8}$$

$$\mathbf{y}_k = \Pi x_k(0) + G\mathbf{u}_k, \tag{4.9}$$

where $\Phi \triangleq A(N-1)A(N-2)\cdots A(0)$, $\Pi \triangleq \begin{bmatrix} \mathbf{e}^{\mathrm{T}} \\ \mathbf{e}^{\mathrm{T}}A(0) \\ \vdots \\ \mathbf{e}^{\mathrm{T}}A(N-2)\cdots A(0) \end{bmatrix}$,

$$\Gamma \triangleq \begin{bmatrix} (A(N-1)\cdots A(1)B(0)), & (A(N-1)\cdots A(2)B(1)), & \ldots, & B(N-1) \end{bmatrix},$$

$$G \triangleq \begin{bmatrix} 0 & 0 & \ldots & 0 & 0 \\ \mathbf{e}^{\mathrm{T}}B(0) & 0 & \ldots & 0 & 0 \\ \mathbf{e}^{\mathrm{T}}A(1)B(0) & \mathbf{e}^{\mathrm{T}}B(1) & \ldots & 0 & 0 \\ \vdots & \vdots & \ldots & 0 & 0 \\ \mathbf{e}^{\mathrm{T}}A(N-2)\cdots A(1)B(0) & \ldots & \ldots & \mathbf{e}^{\mathrm{T}}B(N-2) & 0 \end{bmatrix}.$$

4.3. Model Predictive Tracking Control

In this section, we develop a model predictive controller based on the lifted run-to-run invariant system dynamics model (4.8) and (4.9). The goal of this controller is to track a given reference volume pattern while enforcing a given set of control constraints. A reference volume pattern $r_{\mathrm{c}}(t), t \geq 0$, can be identified by a clinician or by solving a lung mechanics optimal respiratory trajectory generation problem as in [40] and Section 3. In Section 2.5, it was shown that the steady stable total lung volume $\mathbf{e}^{\mathrm{T}}x(t), t \geq 0$, for a pressure-limited respiratory system is a stable limit cycle.

As discussed in Section 4.1, model predictive control is an optimal control methodology which can effectively handle state and control constraints. However, model predictive control can be cumbersome to use when the reference trajectory or the system

dynamics are time-varying or periodic. Repetitive control [25] has been proposed to solve tracking control problems with periodic reference trajectories or rejection of cyclic disturbances. Specifically, instead of considering the periodic system (4.4) and (4.5) directly, the system is transformed into a *lifted run-to-run* invariant model as in (4.8) and (4.9). However, repetitive control has limitations in handling system state and control constraints. To address this, the authors in [38] develop a repetitive model predictive control framework that combines model predictive control and repetitive control.

The basic idea of repetitive model predictive control is to store the changes of the system controls, outputs, and states between two consecutive periods and use them to compute the control input actions for the next period. Specifically, define $\Delta \mathbf{u}_k \triangleq \mathbf{u}_k - \mathbf{u}_{k-1}$, $\Delta \mathbf{y}_k \triangleq \mathbf{y}_k - \mathbf{y}_{k-1}$, and $\Delta x_k(0) \triangleq x_k(0) - x_{k-1}(0),\ k \in \mathbb{Z}_+$. Then, it follows from (4.8) and (4.9) that

$$\Delta x_{k+1}(0) = \Phi \Delta x_k(0) + \Gamma \Delta \mathbf{u}_k, \quad \Delta x_1(0) = x_1^{\mathrm{in}}(0) - x_0^{\mathrm{in}}(0), \quad k \in \mathbb{Z}_+, \quad (4.10)$$

$$\Delta \mathbf{y}_k = \Pi \Delta x_k(0) + G \Delta \mathbf{u}_k. \quad (4.11)$$

Next, define the grouped reference signals over one period by $\mathbf{r} \triangleq [r(0), \ldots, r(N-1)]^{\mathrm{T}}$, where $r(\cdot)$ denotes the discretized reference signal, and define the deviation between the grouped output vector at the k-th run and the grouped reference signals by $\tilde{e}_k \triangleq \mathbf{y}_k - \mathbf{r}$. Then, a *lifted* system dynamics model follows from (4.10) and (4.11) as

$$\begin{bmatrix} \Delta x_{k+1}(0) \\ \tilde{e}_k \end{bmatrix} = \underbrace{\begin{bmatrix} \Phi & 0_{2^n \times N} \\ \Pi & I_N \end{bmatrix}}_{\overline{\Phi}} \begin{bmatrix} \Delta x_k(0) \\ \tilde{e}_{k-1} \end{bmatrix} + \underbrace{\begin{bmatrix} \Gamma \\ G \end{bmatrix}}_{\overline{\Gamma}} \Delta \mathbf{u}_k, \quad k \in \mathbb{Z}_+, \quad (4.12)$$

where the error vector over the k-th run is given by

$$\tilde{e}_k = \underbrace{\begin{bmatrix} \Pi & I_N \end{bmatrix}}_{\overline{\Pi}} \begin{bmatrix} \Delta x_k(0) \\ \tilde{e}_{k-1} \end{bmatrix} + G \Delta \mathbf{u}_k, \quad k \in \mathbb{Z}_+. \quad (4.13)$$

Defining $\mathbf{z}_k \triangleq \begin{bmatrix} \Delta x_k(0) \\ \tilde{e}_{k-1} \end{bmatrix}$, it follows from (4.12) and (4.13) that

$$\mathbf{z}_{k+1} = \overline{\Phi}\mathbf{z}_k + \overline{\Gamma}\Delta\mathbf{u}_k, \quad \mathbf{z}_1 = \begin{bmatrix} \Delta x_1(0) \\ \tilde{e}_0 \end{bmatrix}, \quad k \in \mathbb{Z}_+, \tag{4.14}$$

$$\tilde{e}_k = \overline{\Pi}\mathbf{z}_k + G\Delta\mathbf{u}_k. \tag{4.15}$$

Note that it follows from (4.14) and (4.15) that the reference trajectory has been embedded into the system dynamics through the lifted form. Hence, for a given periodic reference trajectory $r_{\mathrm{c}}(t), 0 \in [0, T_{\mathrm{in}} + T_{\mathrm{ex}}]$, a tracking control problem can be solved as a regulator control problem. The following proposition characterizes an important stability property of the lifted system matrix $\overline{\Phi}$.

Proposition 4.1. Consider the lifted run-to-run invariant system dynamics (4.14). Then the lifted system matrix $\overline{\Phi}$ is Lyapunov stable.

Proof. Since $\overline{\Phi} = \begin{bmatrix} \Phi & 0_{2^n \times N} \\ \Pi & I_N \end{bmatrix}$ is lower block triangular, it follows that $\mathrm{spec}(\overline{\Phi}) = \mathrm{spec}(\Phi) \cup \{1\}$, where $\Phi = A(N-1)A(N-2)\cdots A(0)$ and $A(\tau) = e^{A_{\mathrm{c}}(\tau\sigma)\sigma}, \tau = 0, \ldots, N-1$. Since $A_{\mathrm{c}}(\tau\sigma)$ is a convex combination of A_{in} and A_{ex}, it follows from *ii*) and *iii*) of Proposition 2.3 in Section 2 that $A_{\mathrm{c}}^{\mathrm{T}}(\tau\sigma)C + CA_{\mathrm{c}}(\tau\sigma) < 0, \tau \in \{0, \ldots, N-1\}$. Hence, it follows from Proposition 2.2 in Section 2.2 that $e^{A_{\mathrm{c}}^{\mathrm{T}}(\tau\sigma)}Ce^{A_{\mathrm{c}}(\tau\sigma)} < C$ or, equivalently, $A^{\mathrm{T}}(\tau)CA(\tau) < C, \tau \in \{0, \ldots, N-1\}$. Next, note that $\Phi^{\mathrm{T}}C\Phi = A^{\mathrm{T}}(0)\cdots A^{\mathrm{T}}(N-1)CA(N-1)\cdots A(0) < C$, where C is a positive-definite diagonal matrix. Hence, Φ is Schur stable, that is, $\rho(\Phi) < 1$. Moreover, since $\dim \mathcal{N}(\overline{\Phi} - I_{2^n+N}) = N$, it follows 1 is a semisimple eigenvalue. Thus, $\overline{\Phi}$ is Lyapunov stable. □

To achieve asymptotic tracking at each run k, that is, $\|y_k(\tau) - r(\tau)\|_{Q(\tau)} \to \infty$ as $k \to \infty$ with $Q(\tau) \in \mathbb{R}_+, \tau = 0, \ldots, N-1$, we minimize the performance criterion

$$\min_{\Delta\mathbf{u}_{k+i}, i=0,\ldots,p-1} \sum_{i=0}^{p-1} \|\tilde{e}_{k+i|k}\|_{\mathbf{Q}}^2 + \|\Delta\mathbf{u}_{k+i}\|_{\mathbf{R}}^2, \tag{4.16}$$

where $p \geq 1$ is the length of a prediction horizon, $\tilde{e}_{k+i|k}$ denotes the estimated error vector at the $k+i$-th run based on information at run k, $\mathbf{Q} \in \mathbb{R}^{N\times N}, \mathbf{Q} \geq 0$, and $\mathbf{R} \in \mathbb{R}^{N\times N}, \mathbf{R} > 0$. Here, $\Delta\mathbf{u}_{k+i}$ captures the change of the control input vector between the $k+i$-th run and the $k+i-1$-th run. Penalizing $\Delta\mathbf{u}_{k+i}$ in mechanical ventilation control is critical since rapid changes in the driving input pressure may cause discomfort and inefficacy of muscular lung contraction and control. Substituting $\tilde{e}_{k+i|k}$ with the predicted form of (4.15), the performance criterion (4.16) becomes

$$\min_{\Delta\mathbf{u}_{k+i}, i=0,\ldots,p-1} \sum_{i=0}^{p-1} \left\| \begin{bmatrix} \mathbf{z}_{k+i|k} \\ \Delta\mathbf{u}_{k+i} \end{bmatrix} \right\|_{\overline{\mathbf{Q}}}^2, \tag{4.17}$$

where

$$\overline{\mathbf{Q}} \triangleq \begin{bmatrix} \overline{\Pi}^{\mathrm{T}}\mathbf{Q}\overline{\Pi} & \overline{\Pi}^{\mathrm{T}}\mathbf{Q}G \\ G^{\mathrm{T}}\mathbf{Q}\overline{\Pi} & G^{\mathrm{T}}\mathbf{Q}G + \mathbf{R} \end{bmatrix}.$$

Finally, since the control horizon m may be different from the prediction horizon p, that is, $m \leq p$, an alternative form for the performance criterion (4.17) that can be considered is

$$\min_{\Delta\mathbf{u}_{k+i}, i=0,\ldots,m-1} \sum_{i=0}^{m-1} \left\| \begin{bmatrix} \mathbf{z}_{k+i|k} \\ \Delta\mathbf{u}_{k+i} \end{bmatrix} \right\|_{\overline{\mathbf{Q}}}^2 + \|\mathbf{z}_{k+m|k}\|_P^2, \tag{4.18}$$

where $P \in \mathbb{R}^{(2^n+N)\times(2^n+N)}$ and $P > 0$. In model predictive control, the terminal weighting matrix P is usually used to improve performance and stability [11, 48].

Next, we constrain the control input to be nonnegative and amplitude bounded, that is, $0_m \leq\leq \mathbf{u}_k \leq\leq \mathbf{u}_{\max}$, where $\mathbf{u}_{\max} = \mathbf{e}_m u_{\max}$, $u_{\max} \in \mathbb{R}_+$, and $k \in \mathbb{Z}_+$. Since the performance criterion (4.18) is in the form of $\Delta\mathbf{u}_k$ and $\mathbf{u}_k = \Delta\mathbf{u}_k + \mathbf{u}_{k-1}$, this constraint can be written as

$$M\Delta\mathbf{u}_k \leq\leq \begin{bmatrix} \mathbf{u}_{\max} - \mathbf{u}_{k-1} \\ \mathbf{u}_{k-1} \end{bmatrix}, \tag{4.19}$$

where $M \triangleq \begin{bmatrix} I \\ -I \end{bmatrix}$. Thus, at the k-th run the constrained optimal control problem

is given by

$$\min_{\Delta \mathbf{u}_{k+i}, i=0,\ldots,m-1} \sum_{i=0}^{m-1} \left\| \begin{bmatrix} \mathbf{z}_{k+i|k} \\ \Delta \mathbf{u}_{k+i} \end{bmatrix} \right\|_{\overline{\mathbf{Q}}}^2 + \|\mathbf{z}_{k+m|k}\|_P^2 \tag{4.20}$$

subject to

$$M\Delta \mathbf{u}_{k+i} \leq\leq \begin{bmatrix} \mathbf{u}_{\max} - \mathbf{u}_{k+i-1} \\ \mathbf{u}_{k+i-1} \end{bmatrix}, \tag{4.21}$$

$$\mathbf{z}_{k+i+1|k} = \overline{\Phi} \mathbf{z}_{k+i|k} + \overline{\Gamma} \Delta \mathbf{u}_{k+i}, \tag{4.22}$$

$$\mathbf{z}_{k|k} = \begin{bmatrix} \Delta x_k(0) \\ \tilde{e}_{k-1} \end{bmatrix}. \tag{4.23}$$

The following theorem gives a method for choosing the weighting matrix P for the optimal control problem (4.20)–(4.23).

Theorem 4.1. Consider the constrained optimal control problem (4.20)–(4.23). Let the weighting matrices P and $\mathbf{Q}$ be such that

$$\overline{\Phi}^{\mathrm{T}} P \overline{\Phi} + \overline{\Pi}^{\mathrm{T}} \mathbf{Q} \overline{\Pi} \leq P. \tag{4.24}$$

If there exists an optimal solution to the finite horizon optimal control problem (4.20)–(4.23), then $\lim_{k\to\infty} \|\tilde{e}_k\|_{\mathbf{Q}}^2 = 0$.

Proof. First, assume $\Delta \mathbf{u}_{k+i} = 0_N, i \geq m$, and note $\Delta \mathbf{u}_{k+i} = 0, i \geq m$, satisfies (4.21), and hence, is feasible. In this case, the error dynamics (4.15) and system dynamics (4.22) are homogenous and are given by, respectively,

$$\tilde{e}_{k+i|k} = \overline{\Pi} z_{k+i|k}, \quad z_{k+i+1|k} = \overline{\Phi} z_{k+i|k}, \quad i \geq m. \tag{4.25}$$

Next, assume that at the k-th run there exists a sequence of optimal solutions to the optimal control problem (4.20)–(4.23) given by

$$\Delta \overline{\mathbf{u}}_k^* = \left\{ \Delta \mathbf{u}_k^*, \Delta \mathbf{u}_{k+1}^*, \ldots, \Delta \mathbf{u}_{k+m-1}^* \right\}. \tag{4.26}$$

The error and state vectors that evolve from the optimal control sequence are given by

$$\overline{e}_k^* = \left\{\tilde{e}_{k|k}^*, \tilde{e}_{k+1|k}^*, \ldots, \tilde{e}_{k+m-1|k}^*\right\}, \tag{4.27}$$

$$\overline{\mathbf{z}}_k^* = \left\{\mathbf{z}_{k+1|k}^*, \mathbf{z}_{k+2|k}^*, \ldots, \mathbf{z}_{k+m|k}^*\right\}. \tag{4.28}$$

Substituting the optimal solutions (4.26)–(4.28) into (4.20), the optimal value of the performance criterion at run k is given by

$$\begin{aligned} V_k^* &= \sum_{i=0}^{m-1} \left\| \begin{bmatrix} \mathbf{z}_{k+i|k}^* \\ \Delta\mathbf{u}_{k+i}^* \end{bmatrix} \right\|_{\overline{\mathbf{Q}}}^2 + \|\mathbf{z}_{k+m|k}^*\|_P^2 \\ &= \sum_{i=0}^{m-1} \|\tilde{e}_{k+i|k}^*\|_{\mathbf{Q}}^2 + \|\Delta\mathbf{u}_{k+i}^*\|_{\mathbf{R}}^2 + \|\mathbf{z}_{k+m}^*\|_P^2. \end{aligned} \tag{4.29}$$

Next, at the $k+1$-th run consider the control sequence

$$\Delta\overline{\mathbf{u}}_{k+1} = \left\{\Delta\mathbf{u}_{k+1}^*, \Delta\mathbf{u}_{k+2}^*, \ldots, \Delta\mathbf{u}_{k+m-1}^*, 0\right\}. \tag{4.30}$$

Since $\Delta\mathbf{u}_{k+i} = 0, i \geq m$, is feasible and all the other elements of $\Delta\overline{\mathbf{u}}_{k+1}$ are obtained from the previous optimal solution $\Delta\overline{\mathbf{u}}_k^*$, it follows that $\Delta\overline{\mathbf{u}}_{k+1}$ is a feasible sequence of control inputs. Thus, using (4.25) the corresponding error and state sequences at run $k+1$ are

$$\overline{e}_{k+1} = \left\{\tilde{e}_{k+1|k}^*, \tilde{e}_{k+2|k}^*, \ldots, \tilde{e}_{k+m-1|k}^*, \overline{\Pi}\mathbf{z}_{k+m|k}^*\right\}, \tag{4.31}$$

$$\overline{\mathbf{z}}_{k+1} = \left\{\mathbf{z}_{k+2|k}^*, \mathbf{z}_{k+3|k}^*, \ldots, \mathbf{z}_{k+m|k}^*, \overline{\Phi}\mathbf{z}_{k+m|k}^*\right\}. \tag{4.32}$$

Now, the value of the performance criterion (4.20) at run $k+1$ is given by

$$\begin{aligned} V_{k+1} &= \sum_{i=1}^{m-1} \|\tilde{e}_{k+i|k}^*\|_{\mathbf{Q}}^2 + \|\Delta\mathbf{u}_{k+i}^*\|_{\mathbf{R}}^2 + \|\overline{\Pi}\mathbf{z}_{k+m|k}^*\|_{\mathbf{Q}}^2 + \|\overline{\Phi}\mathbf{z}_{k+m|k}^*\|_{\mathbf{P}}^2 \\ &= V_k^* - \|\tilde{e}_{k|k}^*\|_{\mathbf{Q}}^2 - \|\Delta\mathbf{u}_k^*\|_{\mathbf{R}}^2 + \|\mathbf{z}_{k+m|k}^*\|_{\mathbf{P}}^2 + \|\overline{\Pi}\mathbf{z}_{k+m|k}^*\|_{\mathbf{Q}}^2 + \|\overline{\Phi}\mathbf{z}_{k+m|k}^*\|_{\mathbf{P}}^2 \\ &= V_k^* - \|\tilde{e}_{k|k}^*\|_{\mathbf{Q}}^2 - \|\Delta\mathbf{u}_k^*\|_{\mathbf{R}}^2 + {\mathbf{z}^*}_{k+m|k}^{\mathrm{T}} \left[\overline{\Phi}^{\mathrm{T}} P\overline{\Phi} + \overline{\Pi}^{\mathrm{T}}\mathbf{Q}\overline{\Pi} - P\right] \mathbf{z}_{k+m|k}^*, \end{aligned} \tag{4.33}$$

and hence, the optimal value V_{k+1}^* of the performance criterion at run $k+1$ satisfies

$$V_{k+1}^* \leq V_{k+1} = V_k^* - \|\tilde{e}_{k|k}^*\|_{\mathbf{Q}}^2 - \|\Delta \mathbf{u}_k^*\|_{\mathbf{R}}^2 + \mathbf{z}^{*\mathrm{T}}_{k+m|k} \left[\overline{\Phi}^{\mathrm{T}} P \overline{\Phi} + \overline{\Pi}^{\mathrm{T}} \mathbf{Q} \overline{\Pi} - P \right] \mathbf{z}_{k+m|k}^*. \tag{4.34}$$

Finally, note that at the k-th run the model predictive control problem only applies the first element $\Delta \mathbf{u}_k^*$ in the control sequence $\Delta \overline{\mathbf{u}}_k^*$ to the system. Thus, $\tilde{e}_{k|k}^*$ is the deviation vector between the system outputs and the reference signals over the k-th run, which implies that $\tilde{e}_{k|k}^* = \tilde{e}_k$. Now, using inequality (4.24) it follows from (4.34) that

$$V_{k+1}^* \leq V_k^* - \|\tilde{e}_k\|_{\mathbf{Q}}^2, \quad k \in \mathbb{Z}_+. \tag{4.35}$$

Summing the inequalities (4.35) over $k \in \mathbb{Z}_+$, it follows that $\sum_{k=0}^{\infty} \|\tilde{e}_k\|_{\mathbf{Q}}^2 \leq V_0^* - V_\infty^*$, which implies that $\sum_{k=0}^{\infty} \|\tilde{e}_k\|_{\mathbf{Q}}^2$ is finite. Hence, it follows from the discrete-time version of Barbalat's lemma [19, p. 782] that $\lim_{k\to\infty} \|\tilde{e}_k\|_{\mathbf{Q}}^2 = 0$. □

Remark 4.1. Theorem 4.1 shows that $\lim_{k\to\infty} \|\tilde{e}_k\|_{\mathbf{Q}}^2 = 0$. Since $\mathbf{Q} \in \mathbb{R}^{N\times N}$ and $\mathbf{Q} \geq 0$, a Schur decomposition [6] of $\mathbf{Q}$ gives $\mathbf{Q} = S\Lambda_Q S^{\mathrm{T}}$, where $S \in \mathbb{R}^{N\times N}$ is orthogonal and $\Lambda_Q \in \mathbb{R}^{N\times N}$ is a nonnegative-definite diagonal matrix. Hence, $\|y_k(\tau) - r(\tau)\|_{Q(\tau)} \to 0$ as $k \to \infty$, where $Q(\tau) = \Lambda_{Q,\tau}$, $\tau = 0, \ldots, N-1$, is the τ-th diagonal entry of Λ_Q.

Remark 4.2. It is not easy to solve inequality (4.24) directly. However, since by Proposition 4.1 $\overline{\Phi}$ is Lyapunov stable, it follows that if $\lambda \in \mathrm{spec}(\overline{\Phi})$, then either $|\lambda| < 1$, or $|\lambda| = 1$ and λ is semisimple. Now, it follows from the real Jordan decomposition [6] that there exists an invertible matrix $V \in \mathbb{R}^{(2^n+N)\times(2^n+N)}$ such that $\overline{\Phi} = VJV^{-1}$, where

$$J = \begin{bmatrix} J_{\mathrm{a}} & 0 \\ 0 & J_{\mathrm{s}} \end{bmatrix}$$

with $J_{\mathrm{a}} \in \mathbb{R}^{2^n \times 2^n}$ such that $\rho(J_{\mathrm{a}}) < 1$ and $J_{\mathrm{s}} \in \mathbb{R}^{N \times N}$ being diagonal such that $|\lambda| = 1, \lambda \in \mathrm{spec}(J_{\mathrm{s}})$. Hence, forming $V^{\mathrm{T}}(4.24)V$, it follows that $J^{\mathrm{T}}\hat{P}J + (\overline{\Pi}V)^{\mathrm{T}}\mathbf{Q}(\overline{\Pi}V) \leq \hat{P}$, where $\hat{P} \triangleq V^{\mathrm{T}}PV$. Now, choosing $R_{\mathrm{a}} \in \mathbb{R}^{2^n \times 2^n}$ such that $R_{\mathrm{a}} > 0$, it follows from converse Lyapunov theory that there exists a positive-definite matrix $P_1 \in \mathbb{R}^{2^n \times 2^n}$ satisfying $J_{\mathrm{a}}^{\mathrm{T}} P_1 J_{\mathrm{a}} + R_{\mathrm{a}} = P_1$. Moreover, note that $J_{\mathrm{s}}^{\mathrm{T}} J_{\mathrm{s}} = I_N$. Thus, $J^{\mathrm{T}}\hat{P}J + R = \hat{P}$, where

$$\hat{P} = \left[\begin{array}{cc} P_1 & 0 \\ 0 & I_N \end{array} \right], \quad R = \left[\begin{array}{cc} R_{\mathrm{a}} & 0 \\ 0 & 0 \end{array} \right],$$

and hence, $P = V^{-\mathrm{T}}\hat{P}V^{-1}$. Finally, choosing $\mathbf{Q} \in \mathbb{R}^{N \times N}$ such that $\mathbf{Q} \geq 0$, we can guarantee that $0 \leq (\overline{\Pi}V)^{\mathrm{T}}\mathbf{Q}(\overline{\Pi}V) \leq R$ by solving a feasibility linear matrix inequality problem.

Remark 4.3. If P is chosen such that

$$\|\mathbf{z}_{k+m|k}\|_P^2 = \sum_{i=m}^{\infty} \left\| \left[\begin{array}{c} \mathbf{z}_{k+i|k} \\ \Delta\mathbf{u}_{k+i} \end{array} \right] \right\|_{\overline{\mathbf{Q}}}^2$$

and no constraints are posed, then the optimal control problem (4.20)–(4.23) becomes an infinite horizon linear quadratic regulation problem. In this case, a closed-form solution of $\Delta\mathbf{u}_k^*$ can be obtained by solving an algebraic Riccati equation.

4.4. Illustrative Numerical Example

In this section, we use the model predictive control results developed in Section 4.3 to obtain a tracking controller for a multi-compartment respiratory system. Here, we consider a two-compartment lung model. Specifically, we assume that the bronchial tree has a dichotomy structure (see Section 4.2). The airway resistance varies with the branch generation and typical values can be found in [26]. Furthermore, the expiratory resistance will be higher than the inspiratory resistance by a factor of 2 to 3. Here, we assume that the factor is 2. Specifically, we choose the values of

the resistances to be $R^{\text{in}}_{0,1} = 9$ cm H_2O/l/sec, $R^{\text{in}}_{1,1} = 16$ cm H_2O/l/sec, $R^{\text{in}}_{1,2} = 16$ cm H_2O/l/sec, $R^{\text{ex}}_{0,1} = 18$ cm H_2O/l/sec, $R^{\text{ex}}_{1,1} = 32$ cm H_2O/l/sec, and $R^{\text{ex}}_{1,2} = 32$ cm H_2O/l/sec. A typical value for the lung compliance is 0.1 l/cm H_2O. (Note that respiratory pressure is measured in terms of centimeters of water pressure.) The inspiration time is $T_{\text{in}} = 2$ sec and the expiration time is $T_{\text{ex}} = 3$ sec. To discretize the system, a sampling time of $\sigma = 1$ sec is chosen. Thus, each period is divided into $N = 5$ equally spaced sample intervals.

The model predictive controller is computed by using the Multi-Parameteric Toolbox [36]. Specifically, we use the repetitive control framework developed in Section 4.3 for achieving periodic tracking by transferring the periodic system dynamics into a lifted run-to-run invariant system. Consequently, on-line computation is reduced to an off-line evaluation of the control laws generated by an explicit model predictive control algorithm; see [5] for details.

The computation is composed of three phases; the design phase, the modification phase, and the computation phase. In the design phase, we choose the control horizon to be $m = 3$ and the constraints of the control input to be 0 cm $H_2O \leq u \leq$ 15 cm H_2O [66]. Since the multi-parameteric approach suffers from the curse of dimensionality, in the modification phase we set the control constraint (4.21) only on the first control vector, as it is the first control vector that will be applied to the system. The weighting matrix P is computed by solving a discrete-time Lyapunov equation and $\mathbf{Q}$ is computed through a feasibility linear matrix inequality problem using the technique outlined in Remark 4.2. However, the choices of P and $\mathbf{Q}$ are not unique and can be tuned to achieve a desired performance. The weighting matrix $\mathbf{R}$ is set to be $\mathbf{R} = \text{diag}[0.1, 0.1, 0.1, 0.1, 0.1]$. The control input vector is computed at the computation phase based on the information at the k-th run. For our simulation, we assume that the initial values $\Delta x_1(0) = [0.1, 0.2]^{\text{T}}\ l$ and $\tilde{e}_0 = [0.1, 0.2, 0.1, 0.3, 0.1]^{\text{T}}\ l$.

For our simulation, a reference trajectory $r_{\rm c}(t), 0 \leq t \leq T_{\rm in} + T_{\rm ex}$, is chosen from the solution of an optimal airflow pattern problem in [40]. Figure 4.1 shows the optimal driving pressure $u^*(t), t \geq 0$, which satisfies the nonnegativity constraints. Figure 4.2 shows the optimal driving pressure $u^*(t), t \geq 0$, when constraints are not enforced on the system input. It can be seen that $u^*(t), t \geq 0$, computed for the constrained system satisfies the constraints, whereas $u^*(t), t \geq 0$, computed without considering the input constraints can yield a negative control signal which violates the physical conditions for most mechanical ventilators. Figure 4.3 shows the input pressure generated by the adaptive controller given in [10]. It can be seen that the input pressure generated by the adaptive controller of [10] violates the given input constraints.

Figure 4.4 shows the total lung compartment volume versus the reference lung volume for the constrained system, whereas Figure 4.5 shows the total lung compartment volume for the unconstrained system. Note that the controller drives the total lung compartment volume to the reference trajectory asymptotically, even though for the constrained case the tracking takes more runs. Figure 4.6 shows the evolution of the total lung compartment volume using the adaptive controller given in [10]. Note that over the first period the tracking errors are larger, however, steady state tracking is achieved faster. Figure 9 compares the values of the total performance criterion in (4.18) using the proposed model predictive controller and the adaptive feedback controller developed in Section 2.9 of Chapter 2. Finally, Figure 4.8 shows the evolution of the air volume in each lung compartment for the constrained system.

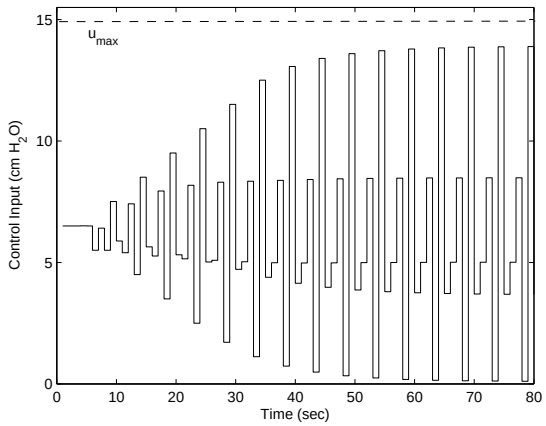

Figure 4.1: The control input for the constrained system.

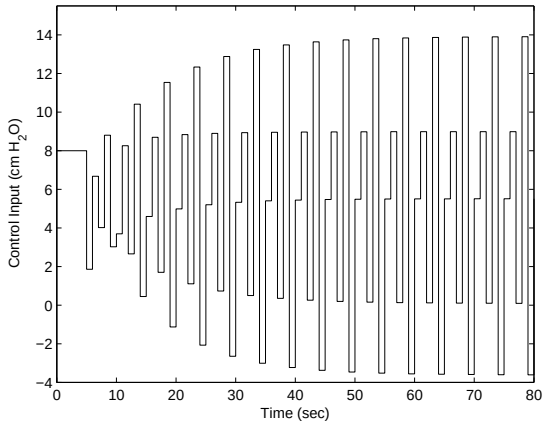

Figure 4.2: The control input for the unconstrained system.

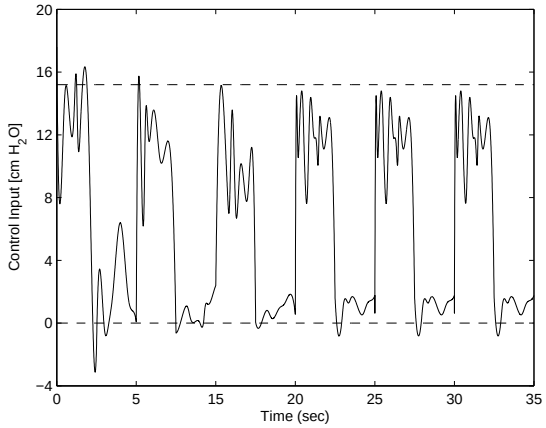

Figure 4.3: Input pressure using the adaptive controller of [10].

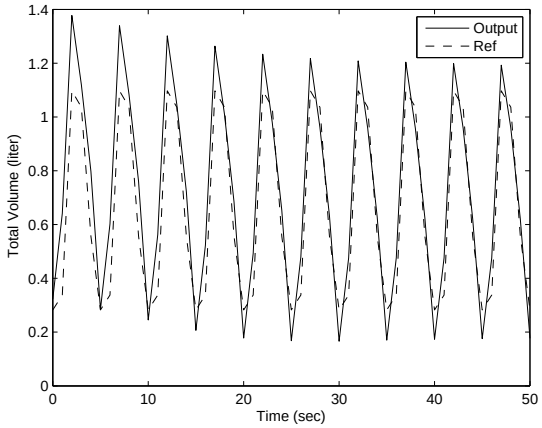

Figure 4.4: The total lung volume from the constrained system.

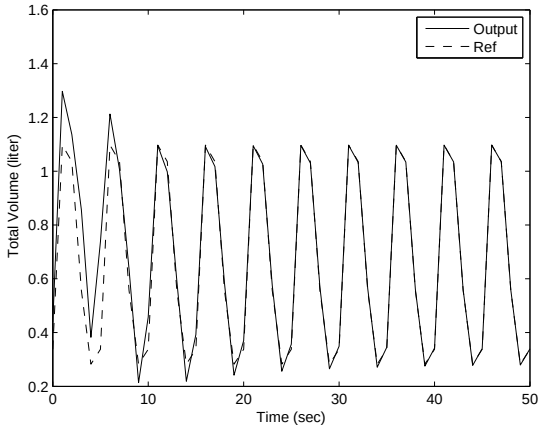

Figure 4.5: The total lung volume from the unconstrained system.

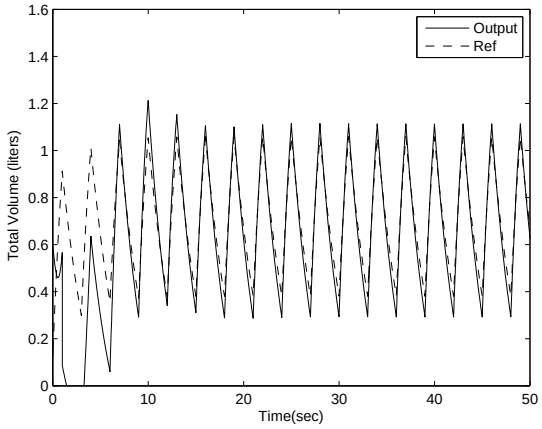

Figure 4.6: The total lung volume using the adaptive controller of [10].

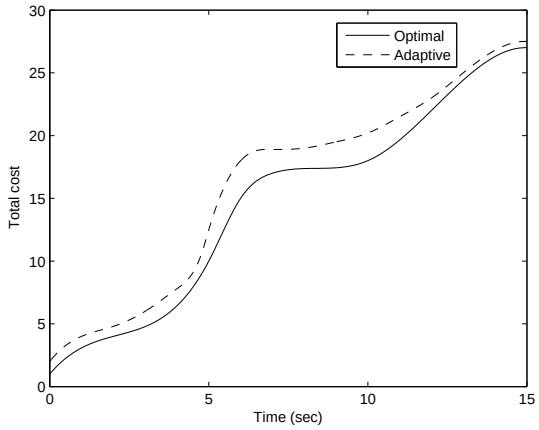

Figure 4.7: Performance criterion comparison versus time.

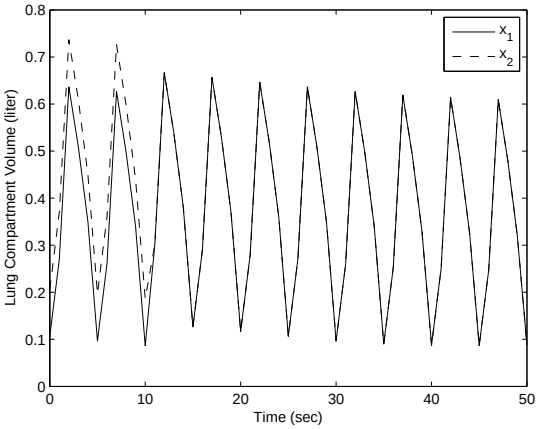

Figure 4.8: The evolution of the air volume in each compartment for the constrained system.

Chapter 5

Predictive Tracking Control for a Multicompartment Respiratory System with Amplitude and Rate Input Constraints

5.1. Introduction

Modern ventilation control algorithms have been used to provide several ventilation modes rather than simple volume or pressure control ventilation [15, 37, 59, 74]. Specifically, in Chapter 2 we developed a model reference direct adaptive control framework for a multicompartment model of a pressure-limited respiratory and lung mechanics system. In Chapter 4, a model predictive controller is designed to address control constraints on the sign and range of the input pressure in the respiratory control. This algorithm is based on a time-varying, linear periodic multicompartment lung model. However, realistic lung models should consider the fact that the lungs, especially diseased lungs, are heterogeneous, both functionally and anatomically, and are comprised of many subunits, or compartments, that differ in their capacities for gas exchange. This is particularly true for the compliance of the lung units, which are not constant but rather vary with lung volume.

In this chapter, we develop a model predictive controller based on a nonlinear multicompartment lung mechanics model with the aim to automatically adjust the

pressure generated by mechanical ventilation such that the system output tracks a given clinically plausible breathing pattern. In general, a model predictive control law is computed by an online optimization problem, and hence, when the system model involves nonlinearities, the model predictive controller requires considerable computational effort. However, for systems with stable zero dynamics, it has been possible to use short prediction horizon times to accurately predict the future system response using a given system model [60,62]. In this chapter, we formulate a quadratic optimal control problem subject to control input amplitude and rate constraints that minimizes the deviation of the multicompartment respiratory system output from the given reference volume pattern. Then, we derive the predictive control law by minimizing a performance criterion involving the prediction of the future system response over a prescribed time step. The derived optimal control law is given by an explicit form, and thus, avoids an online optimization.

5.2. Notation and Mathematical Preliminaries

In this section, we introduce notations, several definitions, and some key results that are necessary for developing the main results of this chapter. Specifically, we write $(\cdot)^{(r)}$ to denote the rth time derivative of $(\cdot)$, $L_f V(x)$ to denote the Lie derivative of a scalar function $V(x)$ along the vector field of $f(x)$, $L_f^0 V(x)$ to denote the zeroth-order Lie derivative, that is, $L_f^0 V(x) \triangleq V(x)$, and $L_f^{(r)} V(x)$ to denote the rth-order Lie derivative, that is, $L_f^{(r)} V(x) \triangleq L_f(L_f^{(r-1)} V(x))$, $L_g L_f^{(r)} V(x)$ to denote the Lie derivative of a scalar function $L_f^{(r)} V(x)$ with respect to vector field $g(x)$. Finally, we write $\lambda_{\min}(\cdot)$ (resp., $\lambda_{\max}(\cdot)$) to denote the minimum (resp., maximum) eigenvalue of a Hermitian matrix, $\sigma_{\min}(\cdot)$ to denote the minimum singular value of a matrix, and $\mathrm{mod}(\cdot,\cdot)$ for the modulo operator, that is, $\mathrm{mod}(t,T) \triangleq t - \lfloor \frac{t}{T} \rfloor T$, where $\lfloor q \rfloor$ denotes the *floor function* which gives the largest integer less than or equal to the positive

number q.

The following definitions introduce the notions of nonnegative functions and essentially nonnegative vector fields [20].

Definition 5.1. Let $T > 0$. A real function $u : [0, T] \to \mathbb{R}^m$ is a *nonnegative* (resp., *positive*) function if $u(t) \geq\geq 0$ (resp., $u(t) >> 0$) on the interval $[0, T]$.

Definition 5.2. Let $f = [f_1, \ldots, f_n]^{\mathrm{T}} : \mathcal{D} \subseteq \overline{\mathbb{R}}^n_+ \to \mathbb{R}^n$. Then f is *essentially nonnegative* if $f_i(x) \geq 0$ for all $i = 1, \ldots, n$ and $x \in \overline{\mathbb{R}}^n_+$ such that $x_i = 0, i = 1, \ldots, n$, where x_i denotes the ith component of x.

It follows from Definition 5.2 that if $f(x) = Ax$, where $A \in \mathbb{R}^{n\times n}$, then f is essentially nonnegative if and only if A is essentially nonnegative, that is, $A_{(i,j)} \geq 0, i, j = 1, \ldots, n, i \neq j$, where $A_{(i,j)}$ denotes the (i, j)th entry of A.

In this chapter, we consider controlled switched nonlinear dynamical systems $\mathcal{G}_p$ of the form

$$\dot{x}(t) = f_p(x(t)) + G_p(x(t))u(t), \quad x(0) = x_0, \quad t \geq 0 \tag{5.1}$$

$$y(t) = h(x(t)), \tag{5.2}$$

where $x(t) \in \mathbb{R}^n, t \geq 0$, is the state vector, $u(t) \in \mathbb{R}^m, t \geq 0$, is the control input, $y(t) \in \mathbb{R}^m, t \geq 0$, is the system output, p is a switching signal taking values in a finite index set $\mathcal{P} = \{1, \ldots, q\}$, and, for every $p \in \mathcal{P}$, $f_p : \mathbb{R}^n \to \mathbb{R}^n$ and $G_p : \mathbb{R}^n \to \mathbb{R}^{n\times m}$ are Lipschitz continuous functions, and $h : \mathbb{R}^n \to \mathbb{R}^m$ is a continuous output function. The family of nonlinear dynamical systems (5.1) and (5.2) can be written as the *switched dynamical systems* $\mathcal{G}_\sigma$ given by

$$\dot{x}(t) = f_{\sigma(t)}(x(t)) + G_{\sigma(t)}(x(t))u(t), \quad \sigma(\cdot) \in \Sigma, \quad x(0) = x_0, \quad t \geq 0, \tag{5.3}$$

$$y(t) = h(x(t)), \tag{5.4}$$

where $x(t) \in \mathbb{R}^n, t \geq 0, f_\sigma : \mathbb{R}^n \to \mathbb{R}^n, G_\sigma : \mathbb{R}^n \to \mathbb{R}^{n\times m}, \sigma : [0,\infty) \to \mathcal{P}$ is a piecewise constant switching signal, and Σ denotes the set of switching signals. The switching signal σ effectively switches the right-hand side of (5.3) by selecting different subsystems from the parameterized family $\{f_p(x) + G_p(x)u : p \in \mathcal{P}\}$. We denote by $t_i, i = 1, 2, \ldots$, the consecutive discontinuities of σ which we call the *switching times* of (5.3). Our convention here is that $\sigma(\cdot)$ is left-continuous, that is, $\sigma(t^-) = \sigma(t)$, where $\sigma(t^-) \triangleq \lim_{h\to 0^-}(t + h)$.

The pair $(x, \sigma) : [0,\infty) \times \Sigma \to \mathbb{R}^n$ is a solution to the switched dynamical system (5.3) if $x(\cdot)$ is absolutely continuous and satisfies (5.3) for almost all $t \geq 0$. Here, we assume that if there are infinitely many switching times, then there exists $\tau > 0$ such that for every $T \geq 0$ there exists a positive integer i such that $t_{i+1} - \tau \geq t_i \geq T$. When $t \in [t_k, t_{k+1}), \sigma(t) = i_k$, that is, the i_kth subsystem is active. Hence, the trajectory $x(t)$ of the switched dynamical system (5.3) is defined as the trajectory $x_{i_k}(t)$ of the i_kth subsystem when $t \in [t_k, t_{k+1})$.

The following definition and proposition are needed for the main results of this chapter.

Definition 5.3. The switched nonlinear dynamical system given by (5.1) is *nonnegative* if for every $x(0) \in \overline{\mathbb{R}}^n_+$ and $u(t) \geq\geq 0$, $t \geq 0$, the solution $x(t), t \geq 0$, to (5.3) is nonnegative.

Proposition 5.1. Consider the switched nonlinear dynamical system given by (5.1). If $f_p : \mathbb{R}^n \to \mathbb{R}^n, p \in \mathcal{P}$, is essentially nonnegative and $G_p(x) \geq\geq 0$ for all $x \in \overline{\mathbb{R}}^n_+$ and $p \in \mathcal{P}$, then (5.1) is nonnegative.

Proof. The proof is similar to the proof of Proposition 4.3 of [20]. □

It follows from Proposition 5.1 that if $f_p(\cdot), p \in \mathcal{P}$, is essentially nonnegative, then

a nonnegative input signal $G_p(x)u, p \in \mathcal{P}$, is sufficient to guarantee the nonnegativity of the state of (5.3).

5.3. Predictive Output Tracking Control Problem

In this section, we consider the problem of characterizing a predictive constrained output feedback control law for nonlinear essentially nonnegative dynamical systems to track a given output reference trajectory. Specifically, we consider a controlled switched nonlinear dynamical system $\mathcal{G}_p$ given by (5.1) and (5.2), where, for $p \in \mathcal{P}$, $f_p(\cdot)$ is essentially nonnegative, $G_p(\cdot)$ is nonnegative, and $h(\cdot)$ is nonnegative. Moreover, we assume that $f_p(\cdot)$, $G_p(\cdot)$, and $h(\cdot)$ are smooth (at least C^n mappings) and the control input $u(\cdot)$ is restricted to a class of admissible controls consisting of absolutely continuous functions such that $u(t) \in \mathcal{U}, t \geq 0$, where $\mathcal{U}$ is defined by

$$\mathcal{U} \triangleq \{u(t) \in \mathbb{R}^m : 0_m \leq\leq u(t) \leq\leq \mathbf{e}\overline{u},\ \mathbf{e}\underline{v} \leq\leq \dot{u}(t) \leq\leq \mathbf{e}\overline{v},\ \text{a.e. } t \geq 0\}, \tag{5.5}$$

where $\overline{u}$, $\underline{v}$, and $\overline{v}$ are given input amplitude and rate constraint bounds.

Note that since the control input $u(\cdot)$ is restricted to be nonnegative, it follows from Proposition 5.1 that $x(t) \geq\geq 0$ for all $x(0) \in \overline{\mathbb{R}}_+^n$ and $t \geq 0$. For a mechanical ventilation problem, the input rate constraint $\mathbf{e}\underline{v} \leq\leq \dot{u}(t) \leq\leq \mathbf{e}\overline{v}$ for almost every $t \geq 0$ is critical since rapid changes in the driving input pressure may cause discomfort and inefficacy of muscular lung contraction and control.

Defining $v(t) \triangleq \dot{u}(t)$ for almost every $t \geq 0$ and $z(t) \triangleq [x^{\mathrm{T}}(t),\ u^{\mathrm{T}}(t)]^{\mathrm{T}}, t \geq 0$, it follows that the augmented nonlinear dynamical system $\hat{\mathcal{G}}_p$ given by

$$\dot{z}(t) = \hat{f}_p(z(t)) + \sum_{i=1}^{m} \hat{g}_i v_i(t), \quad z(0) = [x^{\mathrm{T}}(0),\ u^{\mathrm{T}}(0)]^{\mathrm{T}}, \quad p \in \mathcal{P}, \quad \text{a.e. } t \geq 0, \tag{5.6}$$

$$y(t) = \hat{h}(z(t)), \tag{5.7}$$

where $\hat{f}_p(z) = [(f_p(x) + G_p(x)u)^{\mathrm{T}},\ 0_m^{\mathrm{T}}]^{\mathrm{T}}$, $\hat{g}_i \in \mathbb{R}^{n+m}, i = 1, \ldots, m$, is such that the

$(n+i)$th component is 1 and zero elsewhere and $\hat{h}(z(t)) = h(x(t))$, subsumes (5.3) and (5.4). Note that it follows from (5.5) that $\mathbf{e}\underline{v} \leq\leq v(t) \leq\leq \mathbf{e}\overline{v}, t \geq 0$. Furthermore, for a sufficiently small time $\delta > 0$, it follows using a first-order Talyor series expansion that

$$u_i(t+\delta) \approx u_i(t) + \delta v_i(t), \quad i = 1, \ldots, m, \quad t \geq 0, \tag{5.8}$$

where $u_i(t), t \geq 0$, denotes the ith component of $u(t), t \geq 0$. Since $u(t+\delta) \in \mathcal{U}$, it follows from (5.5) that $v_i(t)$ satisfies $-\frac{u_i(t)}{\delta} \leq v_i(t) \leq \frac{\overline{u}-u_i(t)}{\delta}, i = 1, \ldots, m$. Hence, $v(t) \in \mathcal{V}_t, t \geq 0$, where

$$\mathcal{V}_t \triangleq \{v(t) \in \mathbb{R}^m : v_{i,\min}(t) \leq v_i(t) \leq v_{i,\max}(t),\ t \geq 0,\ i = 1, \ldots, m\}, \tag{5.9}$$

$v_{i,\min}(t) \triangleq \max\{\underline{v},\ -\frac{u_i(t)}{\delta} + \varepsilon\}$, $v_{i,\max}(t) \triangleq \min\{\overline{v},\ \frac{\overline{u}-u_i(t)}{\delta} - \varepsilon\}$, and $\varepsilon > 0$ is a small positive scalar.

Next, we assume that $\hat{\mathcal{G}}_p$, for every $p \in \mathcal{P}$, has a (vector) relative degree $r \triangleq \{r_1, \ldots, r_m\}$, where r_i denotes the relative degree of $\hat{\mathcal{G}}_p$ with respect to the output $y_i, i = 1, \ldots, m$. Thus, the rth derivative of $y(t), t \geq 0$, is given by

$$y_p^{(r)}(t) = a_p(z(t)) + D_p(z(t))v(t), \quad p \in \mathcal{P}, \quad \text{a.e. } t \geq 0, \tag{5.10}$$

where $a_p(z) = [L_{\hat{f}_p}^{(r_1)}\hat{h}_1(z), \ldots, L_{\hat{f}_p}^{(r_m)}\hat{h}_m(z)]^{\mathrm{T}}$ and $D_p(z) \in \mathbb{R}^{m\times m}$ is a matrix function whose ith row is given by $D_{i_p}(z) = [L_{\hat{g}_1}L_{\hat{f}_p}^{(r_i-1)}\hat{h}_i(z), \ldots, L_{\hat{g}_m}L_{\hat{f}_p}^{(r_i-1)}\hat{h}_i(z)], i = 1, \ldots, m$. The following two assumptions are needed for the main results of this section.

Assumption 5.1. For $p \in \mathcal{P}$, *i)* $D_p(z)$ is nonsingular for all $z \in \overline{\mathbb{R}}_+^n \times \mathcal{U}$ and *ii)* the zero dynamics of $\hat{\mathcal{G}}_p$ are uniformly asymptotically stable.

Part *i)* of Assumption 5.1 guarantees that the system $\hat{\mathcal{G}}_p$ is input-output feedback linearizable for every $p \in \mathcal{P}$, whereas *ii)* ensures that the internal dynamics of $\hat{\mathcal{G}}_p$ remain asymptotically stable for every $p \in \mathcal{P}$ when the system output $y(t), t \geq 0$, is set to reference signal $y_{\mathrm{r}}(t), t \geq 0$.

Assumption 5.2. For a given bounded reference input $y_{\mathrm{r}}(t), t \geq 0$, $y_{\mathrm{r},i}^{(1)}(t), \ldots, y_{\mathrm{r},i}^{(r_i)}(t), i = 1, \ldots, m$, are bounded, where $y_{\mathrm{r},i}(t)$ is the ith element of $y_{\mathrm{r}}(t)$, and there exists $x_{\mathrm{r}}(t) \in \overline{\mathbb{R}}_+^n$ and $u_{\mathrm{r}}(t) \in \overline{\mathbb{R}}_+^m, t \geq 0$, satisfying (5.3) and (5.4) with $y_{\mathrm{r}}(t) = h(x_{\mathrm{r}}(t))$.

To achieve asymptotic tracking, we design a control law such that the system error $e(t) \triangleq y(t) - y_{\mathrm{r}}(t), t \geq 0$, is bounded and converges to zero asymptotically. Specifically, using the approach given in [60], we define a vector function $\phi_p(t) \triangleq [\phi_{1_p}(t), \ldots, \phi_{m_p}(t)]^{\mathrm{T}}, p \in \mathcal{P}$ for almost every $t \geq 0$, where

$$\phi_{i_p}(t) = e_{i_p}^{(r_i-1)}(t) + \alpha_{i,r_i-1} e_{i_p}^{(r_i-2)}(t) + \cdots + \alpha_{i,1} e_i(t) + \alpha_{i,0} \int_0^t e_i(\tau) \mathrm{d}\tau, \quad i = 1, \ldots, m, \tag{5.11}$$

$e_i(t) = y_i(t) - y_{\mathrm{r},i}(t)$, and the coefficients $\alpha_{i,j} > 0, j = 0, \ldots r_i - 1$, are chosen such that the polynomial

$$s^{r_i} + \alpha_{i,r_i-1} s^{r_i-1} + \cdots + \alpha_{i,1} s + \alpha_{i,0}, \quad i = 1, \ldots, m, \tag{5.12}$$

is Hurwitz. Differentiating (5.11) with respect to time yields, for almost every $t \geq 0$,

$$\dot{\phi}_{i_p}(t) = e_{i_p}^{(r_i)}(t) + \alpha_{i,r_i-1} e_{i_p}^{(r_i-1)}(t) + \cdots + \alpha_{i,1} \dot{e}_{i_p}(t) + \alpha_{i,0} e_i(t), \quad p \in \mathcal{P}, \quad i = 1, \ldots, m. \tag{5.13}$$

Thus, it follows from (5.10) and (5.13) that

$$\begin{aligned} \dot{\phi}_p(t) &= y_p^{(r)}(t) - y_{\mathrm{r}}^{(r)}(t) + \psi_p(t) \\ &= a_p(z(t)) + D_p(z(t))v(t) - y_{\mathrm{r}}^{(r)}(t) + \psi_p(t), \quad p \in \mathcal{P}, \quad \text{a.e. } t \geq 0, \end{aligned} \tag{5.14}$$

where $\psi_p(t) = [\psi_{1_p}^{\mathrm{T}}(t), \ldots, \psi_{m_p}^{\mathrm{T}}(t)]^{\mathrm{T}}$ with $\psi_{i_p}(t) = \alpha_{i,r_i-1} e_{i_p}^{(r_i-1)}(t) + \cdots + \alpha_{i,1} \dot{e}_{i_p}(t) + \alpha_{i,0} e_i(t), i = 1, \ldots, m$, and $y_{\mathrm{r}}^{(r)}(t) = [y_{\mathrm{r},1}^{(r_1)}(t), \ldots, y_{\mathrm{r},m}^{(r_m)}(t)]^{\mathrm{T}}$. Now, for sufficiently small $\tau > 0$, it follows from (5.14), using a first-order Talyor series expansion, that

$$\phi_p(t+\tau) \approx \phi_p(t) + \tau \dot{\phi}_p(t) = \phi_p(t) + \tau [a_p(z(t)) + D_p(z(t))v(t) - y_{\mathrm{r}}^{(r)}(t) + \psi_p(t)], \quad p \in \mathcal{P}, \quad \text{a.e. } t \geq 0. \tag{5.15}$$

Next, we use model predictive control to design a tracking controller for the dynamical system $\hat{\mathcal{G}}_p$. As discussed in [62], model predictive control involves the prediction of the future system response using a given system dynamics model and the calculation of a sequence of controller actions obtained by minimizing a given performance index. In the model predictive control literature [11, 48], a large prediction horizon has been used to address stability and unstable zero dynamics. However, large prediction horizons degrade system robustness and require significant online computational effort. For systems with stable zero dynamics, it has been shown in [42, 60, 62] that it is possible to use short prediction horizons to accurately predict the future system response using a given system dynamics model. As shown below, such a prediction equation with an appropriate reference trajectory yields a model predictive control law whose implementation does not require an online optimization.

Since the switching signal $\sigma\colon [0,\infty) \to \mathcal{P}$ is piecewise constant, there exists $p \in \mathcal{P}$ such that $\sigma(t) = p$ for a given time $t \geq 0$. To develop a model predictive controller for (5.3) and (5.4) at a given $t \geq 0$, consider the minimization problem

$$\min_{v(t)\in\mathcal{V}_t} J_p(v(t)) = \frac{1}{2}\phi_p^{\mathrm{T}}(t+\tau)Q\phi_p(t+\tau) + \frac{1}{2}v^{\mathrm{T}}(t)Rv(t), \tag{5.16}$$

where $Q > 0, Q \in \mathbb{R}^{m\times m}$, and $R \geq 0, R \in \mathbb{R}^{m\times m}$. Note that the first quadratic term in the performance criterion (5.16) captures a weighted least squares measure of the predicted tracking errors, as well as their derivatives and integrals, whereas the second quadratic term in (5.16) penalizes the control rate. Next, note that $v(t) \in \mathcal{V}_t$ can be rewritten as

$$Av(t) - b(t) \leq 0, \quad t \geq 0, \tag{5.17}$$

where

$$A = \begin{bmatrix} 1 & 0 & \dots & 0 \\ -1 & 0 & \dots & 0 \\ \vdots & \vdots & \vdots & \vdots \\ 0 & 0 & \dots & 1 \\ 0 & 0 & \dots & -1 \end{bmatrix}, \quad b(t) = \begin{bmatrix} v_{1,\max}(t) \\ -v_{1,\min}(t) \\ \vdots \\ v_{m,\max}(t) \\ -v_{m,\min}(t) \end{bmatrix}.$$

The constrained optimization problem given by (5.16) and (5.17) can be solved using Lagrange multiplier methods [33]. Specifically, introducing the Lagrange multiplier $\lambda = [\lambda_1, \hat{\lambda}_1, \dots, \lambda_m, \hat{\lambda}_m]^{\mathrm{T}} \in \mathbb{R}^{2m}$ and forming the Lagrangian

$$\mathcal{L}(J_p(v), \lambda) = J_p(v) + \lambda^{\mathrm{T}}(Av - b), \tag{5.18}$$

it follows from the Kuhn-Tucker necessary conditions [33] for optimality that, for $t \geq 0$,

$$\frac{\partial}{\partial v}\left(J_p(v(t)) + \lambda^{\mathrm{T}}(Av(t) - b(t))\right) = 0, \quad p \in \mathcal{P}, \tag{5.19}$$

$$\lambda^{\mathrm{T}}(Av(t) - b(t)) = 0, \tag{5.20}$$

$$\lambda_i = 0,\ v_i(t) < v_{i,\max}(t), \quad \hat{\lambda}_i = 0,\ v_i(t) > v_{i,\min}(t),\ i = 1, \dots, m, \tag{5.21}$$

$$\lambda_i \geq 0,\ v_i(t) = v_{i,\max}(t), \quad \hat{\lambda}_i \geq 0,\ v_i(t) = v_{i,\min}(t),\ i = 1, \dots, m. \tag{5.22}$$

Next, using (5.15) and (5.16), (5.19) can be rewritten as

$$\left(\tau^2 D_p^{\mathrm{T}}(\hat{z}(t)) Q D_p(\hat{z}(t)) + R\right) v(t) + \tau D_p^{\mathrm{T}}(\hat{z}(t)) Q \left(\phi_p(t) + \tau[a_p(\hat{z}(t)) - y_{\mathrm{r}}^{(r)}(t) + \psi(t)]\right) + A^{\mathrm{T}}\lambda = 0, \quad p \in \mathcal{P}, \quad \text{a.e. } t \geq 0, \tag{5.23}$$

where $\hat{z}(t)$ denotes the prediction of $z(t)$ at time $t \geq 0$. In order to solve (5.19)–(5.22), we use the numerical iterative approach developed in [42]. First, however, we define the saturation map $\mathcal{S} : \mathbb{R}^m \to \mathbb{R}^m$ as $\mathcal{S}(v) \triangleq [s_1(v_1),\ \dots,\ s_m(v_m)]^{\mathrm{T}}$, where

$$s_i(v_i) = \begin{cases} v_{i,\max}, & v_i \geq v_{i,\max}, \\ v_i, & v_{i,\min} < v_i < v_{i,\max}, \\ v_{i,\min}, & v_i \leq v_{i,\min}, \end{cases} \quad i = 1, \dots, m. \tag{5.24}$$

The optimal controller $v^*(t), t \geq 0$, satisfying the necessary conditions (5.19)–(5.22) is given by the following theorem. For the statement of this theorem define $\Gamma_p(\hat{z}) \triangleq \tau^2 D_p^{\mathrm{T}}(\hat{z}) Q D_p(\hat{z}) + R$ and $\beta_p \triangleq (\sum_{i=1}^m \sum_{j=1}^m \Gamma_{(i,j)_p}^2(\hat{z}))^{-1/2}$, where $\Gamma_{(i,j)_p}(\hat{z})$ denotes the (i,j)th entry of $\Gamma_p(\hat{z})$.

Theorem 5.1. For $t \geq 0$ such that $\mu(\{t \in [0,\infty) : v(t) = \dot{u}(t)\}) \neq 0$, where $\mu(\cdot)$ denotes the Lebesgue measure in $\overline{\mathbb{R}}_+$, and every $v_0 \in \mathcal{V}_t$, consider the unbounded sequence $\{v_k\}_{k=0}^{\infty}$ generated by

$$v_{k+1} = \mathcal{S}\left(\beta_p[\tau D_p^{\mathrm{T}}(\hat{z}) Q(\tau[y_{\mathrm{r}}^{(r)} - a_p(\hat{z}) - \psi_p] - \phi_p)] - [\beta_p(\tau^2 D_p^{\mathrm{T}}(\hat{z}) Q D_p(\hat{z}) + R) - I_m] v_k\right) \triangleq T(v_k). \tag{5.25}$$

Then, for sufficiently small $\tau > 0$, there exists a unique optimal controller $v^*(t)$ such that $T(v^*(t)) = v^*(t)$ and, for every $v_0 \in \mathcal{V}_t$, the sequence $\{v_k\}_{k=0}^{\infty}$ converges to $v^*(t)$.

Proof. First, we show that for a fixed time $t \geq 0$ such that $\mu(\{t \in [0,\infty) : v(t) = \dot{u}(t)\}) \neq 0$, the optimal control $v^*(t)$ satisfying (5.19)–(5.22) is a fixed point of (5.25). If $v_{i,\min}(t) < v_i^*(t) < v_{i,\max}(t)$ for a fixed $t \geq 0$ and $i = 1, \ldots, m$, then it follows from (5.21)–(5.23) that

$$\left(\tau^2 D_p^{\mathrm{T}}(\hat{z}(t)) Q D_p(\hat{z}(t)) + R\right) v(t) + \tau D_p^{\mathrm{T}}(\hat{z}(t)) Q \left(\phi_p(t) + \tau[a_p(\hat{z}(t)) - y_{\mathrm{r}}^{(r)}(t) + \psi_p(t)]\right) = 0.$$

In this case, (5.25) becomes $T(v^*(t)) = v^*(t)$. If, alternatively, $v_i^*(t) = v_{i,\max}(t)$, for a fixed $t \geq 0$ and every $i \in \{1, \ldots, m\}$, then, by (5.21) and (5.22), $\lambda_i \geq 0$ and $\hat{\lambda}_i = 0$, which implies that $(A^{\mathrm{T}}\lambda)_i = \lambda_i - \hat{\lambda}_i = \lambda_i$. Thus, the ith component of (5.23) satisfies

$$\left(\tau^2 D_p^{\mathrm{T}}(\hat{z}(t)) Q D_p(\hat{z}(t)) + R) v(t) + \tau D_p^{\mathrm{T}}(\hat{z}(t)) Q(\phi_p(t) + \tau[a_p(\hat{z}(t)) - y_{\mathrm{r}}^{(r)}(t) + \psi_p(t)]\right)_i = -\lambda_i,$$

and hence, since $\lambda_i \geq 0$, the ith component of the right-hand side of (5.25) becomes

$$s_i\left(\beta_p\lambda_i + v_i^*(t)\right) = s_i\left(\beta_p\lambda_i + v_{i,\max}(t)\right) = v_{i,\max}(t) = v_i^*(t). \tag{5.26}$$

Analogously, if $v_i^*(t) = v_{i,\min}(t)$ for a fixed $t \geq 0$ and every $i \in \{1, \ldots, m\}$, then a similar argument as given above yields

$$s_i(-\beta_p\hat{\lambda}_i + v_i^*(t)) = s_i(-\beta_p\hat{\lambda}_i + v_{i,\min}(t)) = v_{i,\min}(t) = v_i^*(t),$$

since $\hat{\lambda}_i \geq 0$. Hence, $v^*(t)$ is a fixed point of (5.25).

Next, we show that $T(\cdot)$ is a contraction mapping. To show this, define

$$\eta_p(v) \triangleq \beta_p[\tau D_p^{\mathrm{T}}(\hat{z})Q(\tau[y_{\mathrm{r}}^{(r)} - a_p(\hat{z}) - \psi_p] - \phi_p)] - [\beta_p(\tau^2 D_p^{\mathrm{T}}(\hat{z})QD_p(\hat{z}) + R) - I_m]v.$$

Then, for $p \in \mathcal{P}$ and every $v, r \in \mathbb{R}^m$,

$$\begin{aligned}
\|T(v) - T(r)\| &\leq \|\eta_p(v) - \eta_p(r)\| \\
&= \| - [\beta_p(\tau^2 D_p^{\mathrm{T}}(\hat{z})QD_p(\hat{z}) + R) - I_m](v - r)\| \\
&\leq \|I_m - \beta_p(\tau^2 D_p^{\mathrm{T}}(\hat{z})QD_p(\hat{z}) + R)\|\|v - r\| \\
&\leq \lambda_{\max}(I_m - \beta_p(\tau^2 D_p^{\mathrm{T}}(\hat{z})QD_p(\hat{z}) + R))\|v - r\| \\
&= \alpha\|v - r\|.
\end{aligned} \tag{5.27}$$

Now, since $\beta_p = (\sum_{i=1}^m \sum_{j=1}^m \Gamma_{(i,j)_p}^2(\hat{z}))^{-1/2} = \|\Gamma_p(\hat{z})\|_{\mathrm{F}}^{-1}$, where $\|\cdot\|_{\mathrm{F}}$ is the Frobenius norm, it follows that $\beta_p = (\sigma_1^2(\Gamma_p(\hat{z})) + \ldots + \sigma_m^2(\Gamma_p(\hat{z})))^{-1/2}$, where $\sigma_i(\Gamma_p(\hat{z}))$ denotes the ith singular value of $\Gamma_p(\hat{z})$. Moreover, since $\Gamma_p(\hat{z})$ is positive definite, it follows that

$$\alpha = 1 - \beta_p\lambda_{\min}(\Gamma_p(\hat{z})) = 1 - \beta_p\sigma_{\min}(\Gamma_p(\hat{z})) < 1. \tag{5.28}$$

Hence, $T : \mathbb{R}^m \to \mathbb{R}^m$ is a contraction mapping. Now, since $\mathbb{R}^m$ with spacial norm $\|\cdot\|_q, q \in [1, \infty]$, is a complete space, it follows from the Banach fixed point theorem

[19, p.68] that there exists a unique $\overline{v}^* \in \mathbb{R}^m$ such that $T(\overline{v}^*) = \overline{v}^*$, and the sequence $\{v_k\}_{k=0}^{\infty} \subseteq \mathcal{V}_t \in \mathbb{R}^m$ converges to $\overline{v}^*$. Furthermore, since $\mathcal{V}_t$ is closed, it follows from the Proposition 2.9 in [19, p.29] that $\overline{v}^* \in \mathcal{V}_t$. Since $\overline{v}^*$ is unique, $\overline{v}^* = v^*(t)$. □

If for almost every $t \geq 0$, $v^*(t)$ satisfying (5.25) is such that $v_{i,\min}(t) < v_i^*(t) < v_{i,\max}(t), i = 1, \ldots, m$, then the optimal control law $v^*(t)$ collapses to

$$v^*(t) = (\tau^2 D_p^{\mathrm{T}}(\hat{z}(t))QD_p(\hat{z}(t)) + R)^{-1}\tau D_p^{\mathrm{T}}(\hat{z}(t))Q[\tau(y_{\mathrm{r}}^{(r)}(t) - a_p(\hat{z}(t)) - \psi_p(t)) - \phi_p(t)], \quad p \in \mathcal{P}, \quad \text{a.e. } t \geq 0. \tag{5.29}$$

If, in addition, in this case the weighting matrix $R = 0_{m\times m}$, then substituting (5.29) into (5.14) yields

$$\dot{\phi}_p(t) = -\frac{1}{\tau}\phi_p(t), \quad p \in \mathcal{P}, \quad \text{a.e. } t \geq 0, \tag{5.30}$$

Hence, $\phi_p(t) \to 0$ as $t \to \infty$ almost everywhere. Now, (5.30) implies $\dot{\phi}_p(t) \to 0$ as $t \to \infty$. Furthermore, in this case substituting (5.30) into (5.13) yields

$$e_{i_p}^{(r_i)}(t) + (\alpha_{i,r_i-1} + \frac{1}{\tau})e_{i_p}^{(r_i-1)}(t) + \ldots + (\alpha_{i,0} + \frac{1}{\tau}\alpha_{i,1})e_{i_p}(t) + \frac{1}{\tau}\alpha_{i,0}\int_0^t e_i(\tau)\mathrm{d}\tau = 0, \quad i = 1, \ldots, m, \quad p \in \mathcal{P}, \quad \text{a.e. } t \geq 0. \tag{5.31}$$

Thus, since $\alpha_{i,j}, j = 0, \ldots, r_i - 1$, are chosen such that (5.12) is Hurwitz, $e_i(t) \to 0$ as $t \to \infty$, $i \in \{1, \ldots, m\}$.

Proposition 5.2. If $0 \leq\leq u(0) \leq\leq \mathbf{e}\overline{u}$ and $v^*(t)$ satisfying (5.25) is such that $T(v^*(t)) = v^*(t)$, then $u^*(t) \in \mathcal{U}$ for all $t \geq 0$.

Proof. The control rate constraint $\mathbf{e}\underline{v} \leq\leq v^*(t) \leq\leq \mathbf{e}\overline{v}, t \geq 0$, is automatically satisfied since (5.17) and (5.24) hold. Now, to show that the amplitude constraint $0_m \leq\leq u^*(t) \leq\leq \mathbf{e}\overline{u}, t \geq 0$, holds, suppose that at some time $t_1 \geq 0$, $u_i^*(t_1) = 0$ for $i \in \{1, \ldots, m\}$. Then, it follows from the definition of $v_{i,\min}(t)$ that $v_i^*(t_1) \geq$

$v_{i,\min}(t_1) > -\frac{u_i^*(t_1)}{\delta} = 0$. Thus, $u_i^*(t)$ is strictly increasing, and hence, $u_i^*(t) > 0$ for $t \geq t_1$. Similarly, suppose that for some $t_2 \geq 0$, $u_i^*(t_2) = \overline{u}$ for $i \in \{1, \ldots, m\}$. Then, $v_i^*(t_2) \leq v_{i,\max}(t_2) < \frac{\overline{u} - u_i^*(t_2)}{\delta} = 0$. Thus, $u_i^*(t)$ is strictly decreasing, and hence, $u_i^*(t) < \overline{u}$ for $t \geq t_2$. Hence, $u^*(t) \in \mathcal{U}$ for all $t \geq 0$. □

A block diagram of the constrained tracking control architecture given in Theorem 5.1 is shown in Figure 5.1.

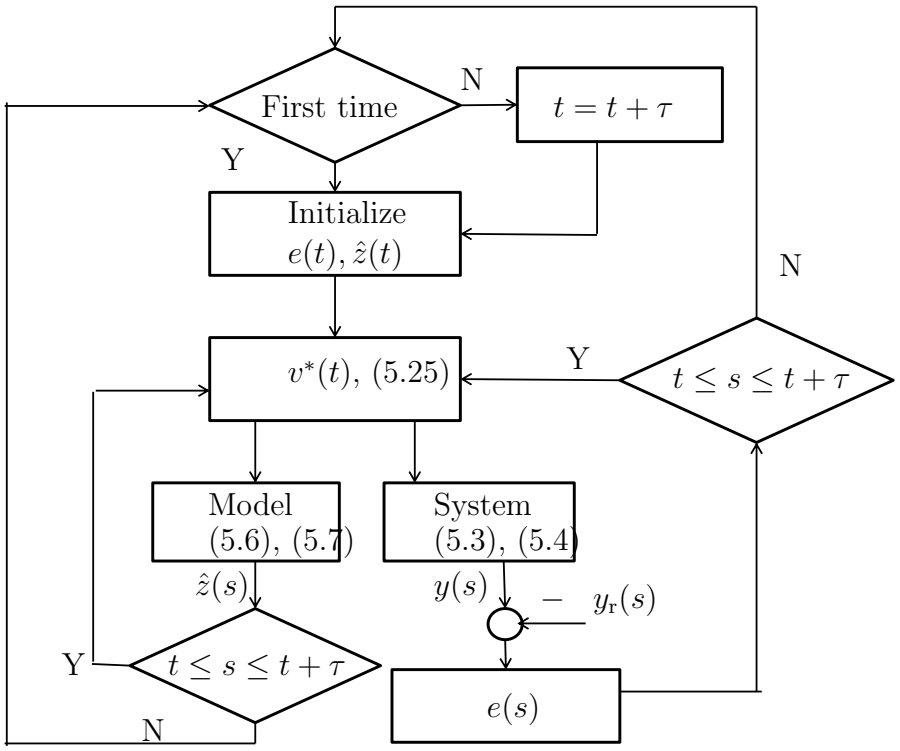

Figure 5.1: Block diagram of the constrained tracking control architecture.

5.4. Nonlinear Multicompartment Lung Model

In this section, we use the nonlinear model developed in Section 3.2 of Chapter 3 to characterize the dynamic behavior of a multicompartment respiratory system in response to an arbitrary applied inspiratory pressure. Here, we still assume that

the bronchial tree has a dichotomy architecture [68]; that is, in every generation each airway unit branches into two airway units of the subsequent generation. In addition, we assume that the lung compliance is a nonlinear function of lung volume.

Specifically, we provide a smooth characterization of the nonlinear compliance using the cubic spline data interpolation method [7]. Figure 5.2 shows the smoothed approximation of the piecewise linear compliance function $c_i^{\text{in}}(x_i)$. A similar approximation holds for $c_i^{\text{ex}}(x_i)$ which is also shown in Figure 5.2.

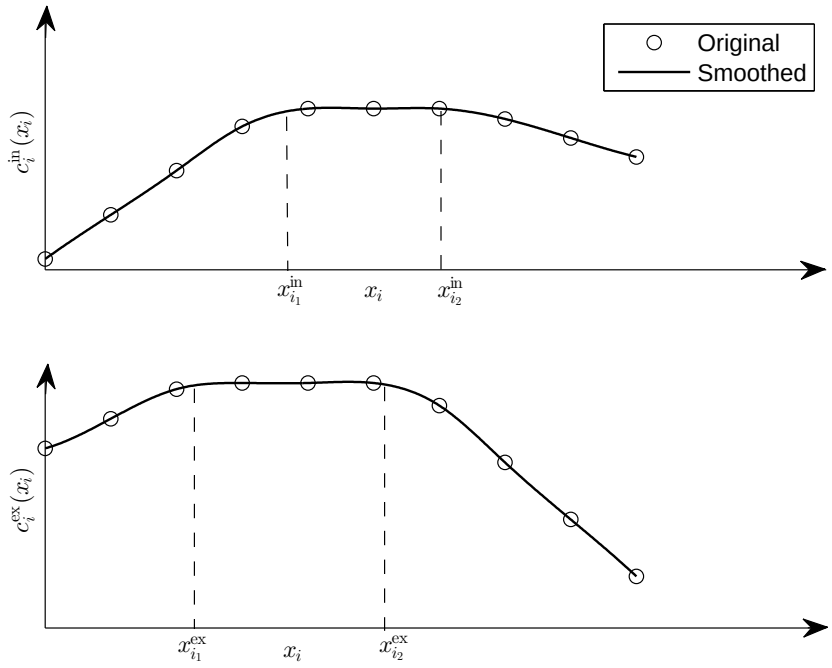

Figure 5.2: Original and the smooth compliance functions.

5.5. Tracking Control for Pressure-Limited Mechanical Ventilation

In this section, we use the constrained tracking control framework developed in Section 5.3 to design a predictive output tracking controller for the nonlinear multi-

compartmental lung mechanics model given in Section 5.4. The goal of this controller is to track a given clinically plausible volume pattern while satisfying a given set of amplitude and rate input constraints. First, however, we rewrite the state equations (3.3) and (3.6) for inspiration and expiration, respectively, into vector-matrix state space form. Specifically, define the state vector $x \triangleq [x_1, x_2, \ldots, x_{2^n}]^{\mathrm{T}}$, where x_i denotes the lung volume of the ith compartment. Now, the state equation (3.3) for inspiration can be rewritten as

$$R_{\mathrm{in}}\dot{x}(t) + C_{\mathrm{in}}(x(t))x(t) = p_{\mathrm{app}}(t)\mathbf{e}, \quad x(0) = x_0^{\mathrm{in}}, \quad 0 \leq t \leq T_{\mathrm{in}}, \tag{5.32}$$

where $C_{\mathrm{in}}(x)$ is a diagonal matrix function given by

$$C_{\mathrm{in}}(x) \triangleq \mathrm{diag}\left[\frac{1}{c_1^{\mathrm{in}}(x_1)}, \ldots, \frac{1}{c_{2^n}^{\mathrm{in}}(x_{2^n})}\right] \tag{5.33}$$

and

$$R_{\mathrm{in}} \triangleq \sum_{j=0}^{n}\sum_{k=1}^{2^j} R_{j,k}^{\mathrm{in}} Z_{j,k} Z_{j,k}^{\mathrm{T}}, \tag{5.34}$$

where $Z_{j,k} \in \mathbb{R}^{2^n}$ is such that the l-th component of $Z_{j,k}$ is 1 for all $l = (k-1)2^{n-j} + 1, (k-1)2^{n-j} + 2, \ldots, k2^{n-j}, k = 1, \ldots, 2^j, j = 0, 1, \ldots, n$, and zero elsewhere.

Similarly, the state equation (3.6) for expiration can be rewritten as

$$R_{\mathrm{ex}}\dot{x}(t) + C_{\mathrm{ex}}(x(t))x(t) = p_{\mathrm{app}}(t)\mathbf{e}, \quad x(T_{\mathrm{in}}) = x_0^{\mathrm{ex}}, \quad T_{\mathrm{in}} \leq t \leq T_{\mathrm{ex}} + T_{\mathrm{in}}, \tag{5.35}$$

where

$$C_{\mathrm{ex}}(x) \triangleq \mathrm{diag}\left[\frac{1}{c_1^{\mathrm{ex}}(x_1)}, \ldots, \frac{1}{c_{2^n}^{\mathrm{ex}}(x_{2^n})}\right], \tag{5.36}$$

and

$$R_{\mathrm{ex}} \triangleq \sum_{j=0}^{n}\sum_{k=1}^{2^j} R_{j,k}^{\mathrm{ex}}\ Z_{j,k}\ Z_{j,k}^{\mathrm{T}}. \tag{5.37}$$

Furthermore, it follows from Proposition 4.1 of [10] that $R_{\rm in}$ and $R_{\rm ex}$ are positive-definite and, hence, $R_{\rm in}$ and $R_{\rm ex}$ are invertible matrices. Hence, (5.32) and (5.35) can be rewritten as

$$\dot{x}(t) = A_{\rm in}(x(t))x(t) + B_{\rm in}u(t), \quad x(0) = x_0^{\rm in}, \quad 0 \le t \le T_{\rm in}, \tag{5.38}$$

$$\dot{x}(t) = A_{\rm ex}(x(t))x(t) + B_{\rm ex}u(t), \quad x(T_{\rm in}) = x_0^{\rm ex}, \quad T_{\rm in} \le t \le T_{\rm ex} + T_{\rm in}, \tag{5.39}$$

where $A_{\rm in}(x) = -R_{\rm in}^{-1}C_{\rm in}(x)$, $B_{\rm in} = R_{\rm in}^{-1}\mathbf{e}$, $A_{\rm ex}(x) = -R_{\rm ex}^{-1}C_{\rm ex}(x)$, and $B_{\rm ex} = R_{\rm ex}^{-1}\mathbf{e}$.

In this chapter, we assume that the inspiration process starts from a given initial state $x_0^{\rm in}$ followed by the expiration process where its initial state will be the final state of the inspiration. An inspiration followed by the expiration is called a single breathing cycle. We assume that each breathing cycle is followed by another breathing cycle where the initial condition for the latter breathing cycle is the final state of the former breathing cycle. Furthermore, we assume that the duration of inspiration is $T_{\rm in}$ and that of expiration is $T_{\rm ex}$, so that the total duration of a breathing cycle is $T \triangleq T_{\rm in}+T_{\rm ex}$. Moreover, the system dynamics switches from inspiration to expiration and back to inspiration. Hence, the dynamics for the breathing process can be characterized by a set of switched dynamical systems as

$$\dot{x}(t) = f_{\sigma(t)}(x(t)) + G_{\sigma(t)}(x(t))u(t), \quad x(0) = x_0^{\rm in}, \quad t \ge 0, \tag{5.40}$$

$$y(t) = \mathbf{e}^{\rm T}x(t). \tag{5.41}$$

Here, we define the switching signal $\sigma(t) \in \{1, 2\}$, such that

$$\sigma(t) = \begin{cases} 1, & \text{if } 0 \le \mathrm{mod}(t, T) < T_{\rm in}, \\ 2, & \text{if } T_{\rm in} \le \mathrm{mod}(t, T) < T, \end{cases} \tag{5.42}$$

and the switching system functions by

$$f_1(x) = A_{\rm in}(x)x, \quad G_1(x) = B_{\rm in}, \tag{5.43}$$

$$f_2(x) = A_{\rm ex}(x)x, \quad G_2(x) = B_{\rm ex}. \tag{5.44}$$

Note that since, by Proposition 4.1 of [10], $-R_{\text{in}}^{-1}$ and $-R_{\text{ex}}^{-1}$ are essentially nonnegative, and $C_{\text{in}}(x)$ and $C_{\text{ex}}(x)$ are diagonal, it follows that $A_{\text{in}}(x)$ and $A_{\text{ex}}(x)$ are essentially nonnegative. Thus, $f_\sigma(x)$ in (5.40) is essentially nonnegative. Moreover, it is also given in Proposition 4.1 of [10] that $B_{\text{in}} \geq\geq 0$ and $B_{\text{ex}} \geq\geq 0$. Thus, $G_\sigma(x) \geq\geq 0$.

Next, the prediction time horizon τ in the performance criterion (5.16) is chosen such that

$$\text{mod}(T_{\text{in}}, \tau) = \text{mod}(T_{\text{ex}}, \tau) = 0.$$

Thus, one period is divided into $N = \frac{T}{\tau}$ equally spaced intervals with each time interval given by

$$i\tau \leq \text{mod}(t, T) < (i+1)\tau, \quad i \in \{0, \ldots, N-1\}.$$

In this case, the switching signal $\sigma(t), t \geq 0$ in (5.42) can be rewritten as

$$\sigma(t) = \begin{cases} 1, & \text{if } \ i\tau \leq \text{mod}(t,T) < (i+1)\tau \ \text{ and } \ (i+1)\tau \leq T_{\text{in}}, \\ 2, & \text{if } \ i\tau \leq \text{mod}(t,T) < (i+1)\tau \ \text{ and } \ i\tau \geq T_{\text{in}}, \end{cases} \tag{5.45}$$

where $i \in \{0, \ldots, N-1\}$. Thus, (5.40) and (5.41), with the switching signal (5.45), are in the form of (5.3) and (5.4).

As in Section 5.3, introducing $\dot{u}(t) = v(t)$ for almost every $t \geq 0$ and states $z(t) = [x^{\text{T}}(t),\ u^{\text{T}}(t)]^{\text{T}},\ t \geq 0$, it follows that the augmented nonlinear system dynamics (5.6) and (5.7) is satisfied with

$$\hat{f}_p(z) = \begin{bmatrix} f_p(x) + G_p(x)u(t) \\ 0 \end{bmatrix},\ \hat{g} = \begin{bmatrix} 0_{2^n} \\ 1 \end{bmatrix},\ \hat{h}(z) = [\mathbf{e}^{\text{T}}\ 0]z,\ p \in \{1,2\} = \mathcal{P}.$$

Now, the time derivatives of the output are given by

$$\dot{y}_p(t) = \mathbf{e}^{\text{T}} f_p(x(t)) + \mathbf{e}^{\text{T}} G_p(x(t))u(t), \tag{5.46}$$

$$\ddot{y}_p(t) = a_p(z(t)) + D_p(z(t))v(t), \quad \text{a.e. } t \geq 0, \tag{5.47}$$

where

$$a_p(z(t)) = \begin{cases} \mathbf{e}^{\mathrm{T}}\dot{A}_{\mathrm{in}}(x(t))x(t) + \mathbf{e}^{\mathrm{T}}A_{\mathrm{in}}^2(x(t))x(t) + \mathbf{e}^{\mathrm{T}}A_{\mathrm{in}}(x(t))B_{\mathrm{in}}u(t), & p = 1, \\ \mathbf{e}^{\mathrm{T}}\dot{A}_{\mathrm{ex}}(x(t))x(t) + \mathbf{e}^{\mathrm{T}}A_{\mathrm{ex}}^2(x(t))x(t) + \mathbf{e}^{\mathrm{T}}A_{\mathrm{ex}}(x(t))B_{\mathrm{ex}}u(t), & p = 2, \end{cases}$$

$$D_p(z(t)) = \begin{cases} \mathbf{e}^{\mathrm{T}}B_{\mathrm{in}}, & p = 1, \\ \mathbf{e}^{\mathrm{T}}B_{\mathrm{ex}}, & p = 2. \end{cases}$$

Since $D_1(z(t)) = \mathbf{e}^{\mathrm{T}}R_{\mathrm{in}}^{-1}\mathbf{e} > 0$ and $D_2(z(t)) = \mathbf{e}^{\mathrm{T}}R_{\mathrm{ex}}^{-1}\mathbf{e} > 0$, $i)$ of Assumption 5.1 is satisfied. To characterize the system zero dynamics, define

$$\begin{aligned} Z_p^* &\triangleq \left\{ z = \begin{bmatrix} x \\ u \end{bmatrix} \in \overline{\mathbb{R}}_+^{2^n} \times \mathcal{U} \ : \mathbf{e}^{\mathrm{T}}x = 0 \text{ and } \mathbf{e}^{\mathrm{T}}f_p(x) + \mathbf{e}^{\mathrm{T}}G_p(x)u = 0 \right\} \\ &= \left\{ z = \begin{bmatrix} x \\ u \end{bmatrix} \in \overline{\mathbb{R}}_+^{2^n} \times \mathcal{U} \ : x = 0_{2^n},\ u = 0 \right\}. \end{aligned} \tag{5.48}$$

Thus, $ii)$ in Assumption 5.1 is automatically satisfied. Now, it follows from (5.47) that the system has relative degree two, that is, $r = 2$, and hence, by (5.11),

$$\phi_p(t) = \dot{e}_p(t) + 2e(t) + \int_0^t e(\tau)\mathrm{d}\tau, \quad p \in \mathcal{P}, \quad \text{a.e. } t \geq 0. \tag{5.49}$$

Hence, $\psi_p(t) = 2\dot{e}_p(t) + e(t),\ p \in \mathcal{P},\ \text{a.e. } t \geq 0.$

For our simulation, we consider a two-compartment lung model and use the values for lung resistance and compliance found in [14]. In particular, we set $a_{i_1}^{\mathrm{in}} = 0.018\,\ell/\mathrm{cm}$ $\mathrm{H_2O}$, $b_{i_1}^{\mathrm{in}} = 0.0233$, $a_{i_2}^{\mathrm{in}} = 0.025\,\ell/\mathrm{cm}$ $\mathrm{H_2O}$, $a_{i_3}^{\mathrm{in}} = 0.2532\,\ell/\mathrm{cm}$ $\mathrm{H_2O}$, $b_{i_3}^{\mathrm{in}} = -0.01$, $x_{i_1}^{\mathrm{in}} = 0.3\,\ell$, $x_{i_2}^{\mathrm{in}} = 0.48\,\ell$, $a_{i_1}^{\mathrm{ex}} = 0.02\,\ell/\mathrm{cm}$ $\mathrm{H_2O}$, $b_{i_1}^{\mathrm{ex}} = 0.078$, $a_{i_2}^{\mathrm{ex}} = 0.038\,\ell/\mathrm{cm}$ $\mathrm{H_2O}$, $a_{i_3}^{\mathrm{ex}} = 0.1025\,\ell/\mathrm{cm}$ $\mathrm{H_2O}$, $b_{i_3}^{\mathrm{ex}} = -0.15$, $x_{i_1}^{\mathrm{ex}} = 0.23\,\ell$, $x_{i_2}^{\mathrm{ex}} = 0.43\,\ell$, $i = 1, 2$. Here, we assume that the bronchial tree has a dichotomy structure (see Section 5.4). The airway resistance varies with the branch generation and typical values can be found in [26]. Furthermore, the expiratory resistance will be higher than the inspiratory resistance by a factor 2 to 3. Here, we assume that the factor is 2.5. The initial conditions are set as $x_0 = [0.01,\ 0.05]^{\mathrm{T}}$ and $u_0 = 0$. The prediction time steps τ and δ are both set to be 0.1. We choose the control input constraints to be $\underline{u} = 0$ cm $\mathrm{H_2O}$ and $\overline{u} = 25$ cm $\mathrm{H_2O}$, and the control rate constraints to be $\underline{v} = -100$ cm $\mathrm{H_2O}$/sec and

$\overline{v} = 50$ cm H_2O/sec. Finally, we set $Q = 100$ and $R = 0$. Note that since $R = 0$, the optimal performance criterion (5.16) becomes $J_p^*(v(t)) = \frac{1}{2}\phi^{*\mathrm{T}}_p(t+\tau)Q\phi^*_p(t+\tau), p \in \mathcal{P}$ for almost every $t \geq 0$. Since $J_p^*(v(t))$ is strictly convex and $\mathcal{V}_t$ is convex, it follows that there exist an optimal control $v^*(t)$ and $J_p^*(v(t)) < \infty$ at every fixed $t \geq 0$ and $p \in \mathcal{P}$. Thus, $\phi_p^*(t), p \in \mathcal{P}$, for almost every $t \geq 0$, is bounded. Furthermore, since (5.11) is Hurwitz, the tracking error $e^*(t)$ is bounded for almost every $t \geq 0$. Specifically, if the optimal control rate $v^*(t), t \geq 0$, satisfies $\underline{v} < v^*(t) < \overline{v}, t \geq 0$, then it follows from Section 5.3 that the tracking error $e^*(t)$ asymptotically converges to zero for almost every $t \geq 0$.

First, we use a reference trajectory $r_{\mathrm{c}}(t), 0 \leq t \leq T_{\mathrm{in}} + T_{\mathrm{ex}}$, generated from the solution of an optimal airflow pattern problem given in [41]. Figure 5.3 shows that optimal driving pressure $u^*(t), t \geq 0$, which satisfies the input amplitude constrains. Figure 5.4 shows the optimal control rate $v^*(t), t \geq 0$, which satisfies the input rate constraints. Figure 5.7 shows the total lung compartment volume versus the reference lung volume. In Figure 5.7, we can see that there exists a bounded trajectory tracking error. This is because the reference trajectory given in [41] is generated by a driving pressure with peak values greater than $\overline{u}$. Thus, the control input $u^*(t)$ and the control rate $v^*(t), t \geq 0$ are both saturated over certain time intervals as shown in Figure 5.3 and Figure 5.4, respectively.

Next, we change the control input constraints to $\underline{u} = 0$ cm H_2O and $\overline{u} = 35$ cm H_2O, and the control rate constraints to $\underline{v} = -100$ cm H_2O/sec and $\overline{v} = 100$ cm H_2O/sec. Figures 5.5 and 5.6 show that the optimal control input $u^*(t), t \geq 0$, and the control rate $v^*(t), t \geq 0$, satisfy the amplitude and rate constraints and are not saturated. Figure 5.8 shows that controller drives the total lung compartment volume to the reference trajectory asymptotically, which agrees with the analysis in Section 5.3.

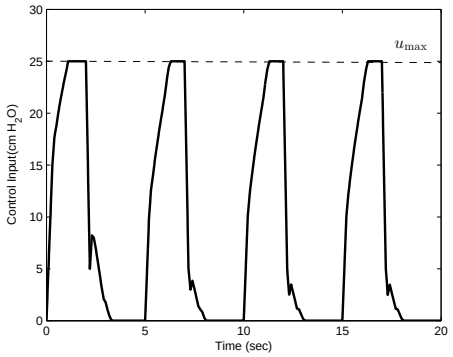

Figure 5.3: The constrained control input $u^*(t)$ versus time (saturated).

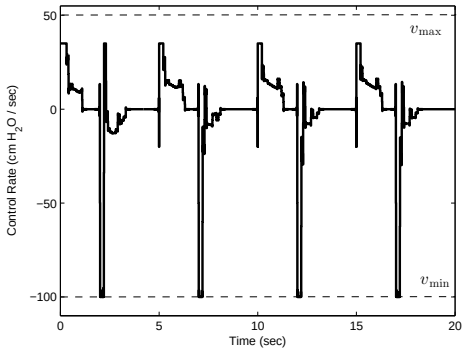

Figure 5.4: The constrained control rate $v^*(t)$ versus time (saturated).

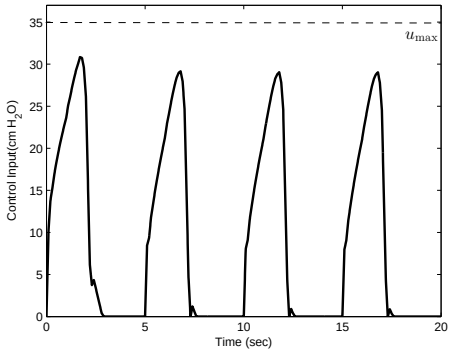

Figure 5.5: The constrained control input $u^*(t)$ versus time (non-saturated).

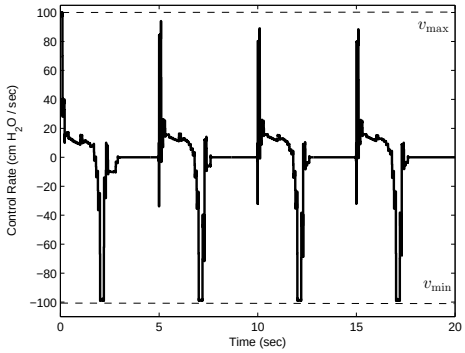

Figure 5.6: The constrained control rate $v^*(t)$ versus time (non-saturated).

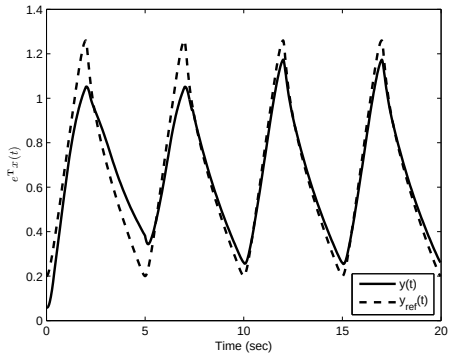

Figure 5.7: The output for the total lung volume driven by saturated controller.

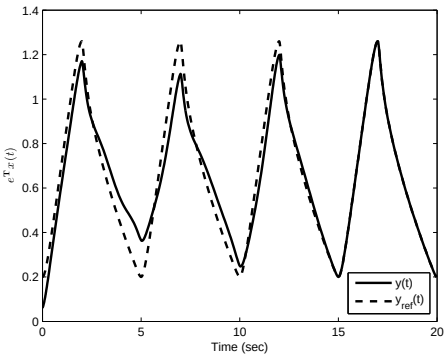

Figure 5.8: The output for the total lung volume driven by non-saturated controller.

Chapter 6

Conclusion and Ongoing Research

6.1. Conclusion

In this dissertation we developed an analysis and control synthesis framework for a pressure-limited respirator and lung mechanics system using a multicompartment model. Respiratory failure, the inadequate exchange of carbon dioxide and oxygen by the lungs, is a common clinical problem in critical care medicine, and patients with respiratory failure frequently require support with mechanical ventilation while the underlying cause is identified and treated. At its simplest, mechanical ventilation is accomplished by the application of cyclically varying positive gas pressure to the trachea. In the absence of patient respiratory effort, it is commonly observed that the lung volumes at end-inspiration and end-expiration rapidly converge to stable steady-state values. However, this does not guarantee that the lungs, viewed as a dynamical system, are stable. Anatomically the lungs are a tree-like structure with repetitive branching into smaller and smaller airways, culminating in the functional units of gas exchange, the alveoli. Stability of end-inspiratory and end-expiratory lung volume does not guarantee that the volumes of individual functional units (the alveoli) are stable.

In this dissertation, we developed a general mathematical model to analyze the

behavior of a multicompartment respirator and lung mechanics system. In particular, we used compartmental dynamical system theory and Poincaré maps to show that a general multicompartment dichotomous lung model converges to a stable limit cycle. Furthermore, we extended the analysis to models with a general tree architecture using graph theory. This extension is particularly important since the anatomy of the lungs is significantly more complex than a regular dichotomous model. Then, we developed an adaptive control framework for the multicompartmental model of a pressure-limited respirator and lung mechanics system. Specifically, we developed a model reference direct adaptive controller framework where the plant and reference models involve switching and time-varying dynamics. Next, we applied the proposed adaptive feedback controller framework to stabilize a given limit cycle corresponding to a clinically plausible respiratory pattern.

Furthermore, we developed an optimal respiratory air flow pattern using a nonlinear multicompartment model for a lung mechanics system. The determination of the optimal air volume trajectories are derived using classical calculus of variations techniques and involve optimization criteria that account for oxygen expenditure of the respiratory lung muscles, lung volume acceleration, and elastic potential energy of the lung. Since sedation in intensive care units is often administered to prevent the patient from fighting the ventilator, it seems plausible to use respiratory parameters as a performance variable for closed-loop control. Calculation of patient work of breathing requires measurement of a patient-generated pressure/volume loop or work of breathing. Since work of breathing can be measured using a commercially available esophageal balloon [31], work of breathing can serve as a performance variable for closed-loop control of sedation. Furthermore, patient-ventilator dyssynchrony can be identified by analysis of pressure/flow wave forms [52].

Closed-loop control algorithms can use either work-of-breathing as measured by an

esophageal balloon or patient respiratory rate as a performance variable for closed-loop control of sedation. The need for optimal control algorithms is necessary for achieving a target performance value while satisfying certain constraints. For example, we could seek to design a control algorithm that seeks to minimize the patient respiratory rate (above the set ventilator rate) but which does not result in hypotension. This requires the development of a constrained optimal control framework that seeks to minimize a given performance measure (e.g., patient respiratory rate) within a class of fixed-architecture controllers satisfying internal controller constraints (e.g., controller order, control signal nonnegativity, etc.) as well as system constraints (e.g., blood pressure, system state nonnegativity, etc.). To this end, in this dissertation, we considered a model predictive controller for a multicompartment respiratory system to guarantee asymptotic tracking for a given periodic reference lung volume pattern. Specifically, since both the reference trajectory and system dynamics are periodic, we merged the features of repetitive control and model predictive control to achieve periodic tracking in the face of system input constraints.

Finally, to account for the fact that the compliance of the lung units vary with lung volume, we designed a predictive tracking controller for a *nonlinear* multicompartment respiratory system to track a given reference lung volume pattern that accounts for amplitude and rate control constraints. The predictive control law is derived by minimizing a quadratic performance criterion involving a prediction of the system response over a prescribed time step. This proposed approach gives an explicit form of the control law, and thus, avoids online optimization.

6.2. Recommendations for Future Research

Floquet theory has a wide range of uses in studying linear systems with periodic coefficients. Thus, as an alternative to the framework in Chapter 2, we can use

Floquet theory for the stability analysis of the breathing limit cycle generated by the switched linear dynamical system (2.19). In addition, Floquet theory can be used to analyze the stability of the nonlinear multicompartment respiratory system given by (5.38) and (5.39). Specifically, if we linearize the nonlinear system model (5.38) and (5.39) about a periodic limit cycle, then, extended Floquet theory [61] can be used to analyze the stability of the first variation of the system states using Floquet multipliers.

To see this, we consider the nonlinear multicompartment system model given by

$$\dot{x}(t) = f(x(t), u(t)), \quad x(0) = x_0, \quad 0 \leq t \leq T, \tag{6.1}$$

where

$$f(x(t), u(t)) = \begin{cases} A_{\rm in}(x(t))x(t) + B_{\rm in}u(t), & 0 \leq t \leq T_{\rm in} \\ A_{\rm ex}(x(t))x(t) + B_{\rm ex}u(t), & T_{\rm in} \leq t \leq T \end{cases} . \tag{6.2}$$

Now, let $x_{\rm r}(t), t \geq 0$, denote a stable limit cycle generated by the switched linear system (2.19) with a given periodic input $u_{\rm r}(t), t \geq 0$, and let $u(t) = u_{\rm r}(t), t \geq 0$. Then, it follows from a first-order Taylor expansion that

$$\dot{x}_{\rm r}(t) + \delta x(t) = f(x_{\rm r}(t), u_{\rm r}(t)) + \frac{\partial f(x(t), u(t))}{\partial x}|_{x_{\rm r}(t), u_{\rm r}(t)} \delta x(t). \tag{6.3}$$

Since $x_{\rm r}(t)$ and $u_{\rm r}(t)$ satisfy the linear system model (2.19), it follows that the first variation $\delta x(t), t \geq 0$, satisfies

$$\delta\dot{x}(t) = A(t)\delta x(t) + g(t), \tag{6.4}$$

where $A(t) = \frac{\partial f(x(t), u(t))}{\partial x}|_{x_{\rm r}(t), u_{\rm r}(t)}$ and $g(t) = f(x_{\rm r}(t), u_{\rm r}(t)) - \dot{x}_{\rm r}(t)$. Since $x_{\rm r}(t)$ and $u_{\rm r}(t)$ are both periodic, $A(t+T) = A(t)$ and $g(t+T) = g(t)$.

Next, it follows from Theorem 4.1 in [61] that the solution $\delta x(t)$ at nT given by

$$\delta x(nT) = X^n(T)x(0) + [X^n(T) + \ldots + X^2(T) + X(T)] \int_0^T X^{-1}(\tau)g(\tau)\mathrm{d}\tau, \tag{6.5}$$

where $X(T)$ is a monodromy matrix calculated from the homogenous portion of the differential equation (6.4), that is, $\delta\dot{x}(t) = A(t)\delta x$, with initial conditions $X(0) = I_n$. The eigenvalues of $X(T)$ are known as Floquet multipliers, which determine the stability of the solution $\delta x(t), t \geq 0$. Specifically, if the radius of Floquet multipliers are less than one, that is, $\rho(X(T)) < 1$, it can be shown that

$$\lim_{n\to\infty} \delta x(nT) = [I - X(T)]^{-1} X(T) \int_0^T X^{-1}(\tau) g(\tau) \mathrm{d}\tau. \tag{6.6}$$

Thus, the stability of the solution to the nonlinear system model (6.1) depends on the monodromy matrix. However, the monodromy matrix $X(T)$ has to be determined numerically. These ideas can be further explored as a viable direction for future research.

The model predictive control frameworks presented in Chapters 4 and 5 of this dissertation are based on a nominal lung mechanics model. However, physiological variables vary from patient to patient, as well as within the same patient under different conditions, making it very challenging to develop models and effective control law architectures for active mechanical ventilation. Adaptive control [35, 51] has focused on achieving system stability and performance without excessive reliance on system models. In future research, we propose to extend the nonlinear model predictive control framework developed in Chapter 5 to address system uncertainty. While there exist some results on linear adaptive model predictive control [12, 18], very few adaptive model predictive control frameworks have been developed for nonlinear systems [47]. Specifically, one possible approach for mechanical ventilation control is to extend the single-step-ahead scheme developed in Chapter 5, such that the computational effort will be reduced for a nonlinear lung mechanics system. In addition, a system parametric identification mechanism needs to be added to the architecture such that the controller can be tuned online (see Figure 6.1). Furthermore, robust stability conditions need to be developed to guarantee that the system tracking errors

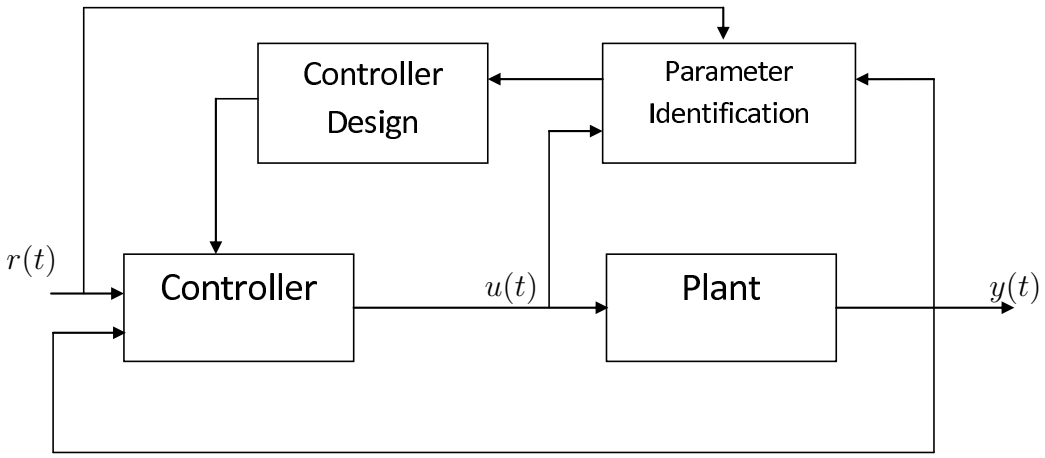

Figure 6.1: Adaptive model predictive control framework.

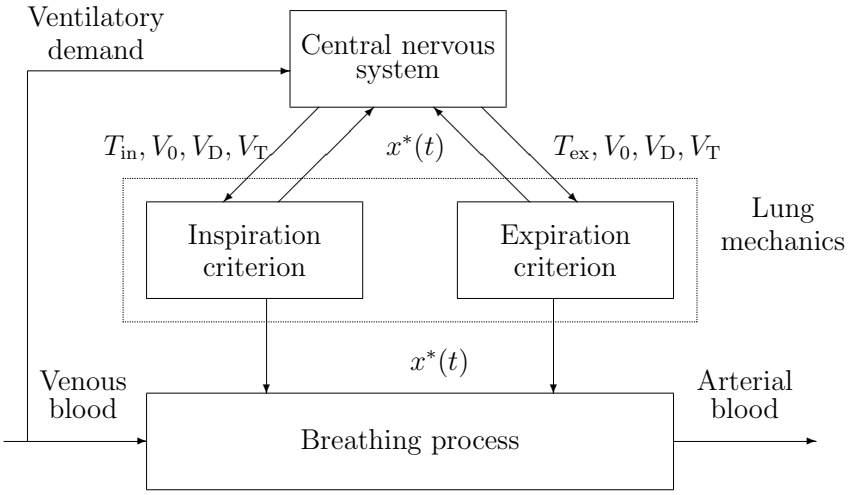

Figure 6.2: A respiratory system model.

converge asymptotically over a prescribed system uncertainty envelope.

Another area related to this research is that the human respiratory system is composed of three components; namely, ventilation, gas exchange at the lungs and the cells, and the transport of gases in the blood [43]. Specifically, as stated in Chapter 3, respiration is regulated by three chemical factors; carbon dioxide CO_2, oxygen O_2, and the pH value. Any changes in these three chemical factors can result in the changes in ventilation. For example, an increase in partial arterial

pressure of carbon dioxide $p\mathrm{CO}_2$ causes increased rate and depth of ventilation, thus increasing alveolar ventilation and removing CO_2 from the blood. Hence, to achieve better ventilation control, in future research, we propose to investigate the interactions between ventilation control and the aforementioned chemical factors for respiratory regulation.

Moreover, the process of ventilation is controlled by the central nervous system, which is a network of neurons in the brain stem. By monitoring the level of the three chemical factors CO_2, O_2, and pH through chemoreceptors, the central nervous system automatically generates rhythmic cycles of neuronal fires to stimulate respiratory activity. Thus, to better understand the mechanism for ventilation control, in future research we propose to build a more general mathematical respiratory system model (see Figure 6.2) that describes the interactions between respiratory parameter regulation in the central nervous system and muscle control in the lung mechanics system. This model can greatly benefit the study of the interaction between ventilation control and sedation control for the patients in intensive care units.

References

[1] J. M. Bailey and W. M. Haddad, "Drug-dosing control in clinical pharmacology: Paradigms, benefits, and challenges," *Contr. Syst. Mag.*, vol. 25, pp. 35–51, 2005.

[2] P. Barbini, "Nonlinear models of the mechanics of breathing applied to the use and design of ventilators," *J. Biomed. Eng.*, vol. 4, pp. 294–304, 1982.

[3] J. Barwing, M. Ambold, N. Linden, M. Quintel, and O. Moerer, "Evaluation of the catheter positioning for neurally adjusted ventilatory assist," *Intens. Care Med.*, vol. 35, no. 10, pp. 1809–1814, 2009.

[4] J. Beck, M. Reilly, G. Grasselli, L. Mirabella, A. Slutsky, M. S. Dunn, and C. Sinderby, "Patient-ventilator interaction during neutrally adjusted ventilatory assist in low birth weight infants," *Pedia. Res.*, vol. 65, no. 6, pp. 663–668, Jun. 2009.

[5] A. Bemporad, M. Morari, V. Dua, and E. Pistikopoulos, "The explicit linear quadratic regulator for constrained systems," *Automatica*, vol. 38, pp. 3–20, 2002.

[6] D. S. Bernstein, *Matrix Mathematics: Theory, Facts, And Formulas With Application to Linear Systems Theory*. Princeton, New Jersey: Princeton University Press, 2005.

[7] C. Boor, *A Practical Guide to Splines*. New York: Springer-Verlag, 1978.

[8] L. Bouadma, F. Lellouche, B. Cabello, S. Taille, J. Mancebo, M. Dojat, and L. Brochard, "Computer-driven management of prolonged mechanical ventilation and weaning: A pilot study," *Intens. Care Med.*, vol. 31, no. 10, pp. 1446–1450, 2005.

[9] D. Campbell and J. Brown, "The electrical analog of the lung," *Brit. J. Anaesth.*, vol. 35, pp. 684–693, 1963.

[10] V. Chellaboina, W. M. Haddad, H. Li, and J. M. Bailey, "Limit cycle stability analysis and adaptive control of a multi-compartment model for a pressure-limited respirator and lung mechanics system," *International Journal of Control*, vol. 83, pp. 940–955, 2010.

[11] H. Chen and F. Allgöwer, "A quasi-infinite horizon nonlinear model predictive

control scheme with guaranteed stability," *Automatica*, vol. 34, pp. 1205–1217, 1998.

[12] D. W. Clarke and R. Scattloni, "Constrained receding- horizon predictive control," *IEE Proceedings, Part D, Control Theory and Applications*, vol. 138, pp. 347–354, 2003.

[13] P. S. Crooke, J. D. Head, and J. J. Marini, "A general two-compartment model for mechanical ventilation," *Mathematical and Computer Modeling*, vol. 24, pp. 1–18, 1996.

[14] P. S. Crooke, J. J. Marini, and J. R. Hotchkiss, "Modeling recruitment maneuvers with a variable compliance model for pressure controlled ventilation," *Journal of Theoretical Medicine*, vol. 4, 2002.

[15] M. Dojat, L. Brochard, F. Lemaire, and A. Harf, "A knowledge-based system for assisted ventilation of patients in intensive care units," *Intern. Journal of Clinical Monitoring and Computing*, vol. 9, no. 4, pp. 239–250, 1992.

[16] J. Dombi and Z. Gera, "The approximation of piecewise linear membership functions and Lukasiewicz operators," *Fuzzy Sets and Systems*, vol. 154, pp. 275–286, 2005.

[17] M. A. Epstein and R. A. Epstein, "Airway flow patterns during mechanical ventilation of infants: A mathematical model," *IEEE Trans. Biomed. Eng.*, vol. 26, pp. 299–306, 1979.

[18] H. Fukushima, T. Kim, and T. Sugie *Automatica*, vol. 43, pp. 301–308, 2007.

[19] W. M. Haddad and V. Chellaboina, *Nonlinear Dynamical Systems and Control: A Lyapunov-Based Approach*. Princeton, New Jersey: Princeton University Press, 2008.

[20] W. M. Haddad, V. Chellaboina, and Q. Hui, *Nonnegative and Compartmental Dynamical Systems*. Princeton, NJ: Princetone Univ. Press, 2010.

[21] W. M. Haddad, V. Chellabonia, and S. G. Nersesov, *Impulsive and Hybrid Dynamical Systems*. Princeton, New Jersey: Princeton University Press, 2006.

[22] R. P. Hämäläinen and A. Sipilä, "Optimal control ofinspiratory airflow in breathing," *Optimal Control Applications & Methods*, vol. 5, pp. 177–191, 1984.

[23] R. P. Hämäläinen and A. A. Viljanen, "A hierarchical goal-seeking model of the control of breathing I-II," *Biological Cybernetics*, vol. 29, pp. 151–166, 1978.

[24] R. P. Hämäläinen and A. A. Viljanen, "Modelling the respiratory airflow pattern by optimization criteria," *Biological Cybernetics*, vol. 29, pp. 143–149, 1978.

[25] S. Hara, Y. Yamamoto, T. Omata, and N. Nakano, "Repetitive control system: A new type servo system for periodic exogenous signals," *IEEE Trans. Autom. Contr.*, vol. 33, pp. 659–668, 1988.

[26] W. F. Hofman and D. C. Meyer, *Essentials of Human Physiology*, ch. Respiratory Physiology. Gold Standard Media, Inc., 2 ed., 1999. `http://www.lib.mcg.edu/edu/eshuphysio/program/section4/4outline.htm`.

[27] K. Horsfield, "Diameters, generations, and orders of branches in the bronchial tree," *Journal of Applied Physiology*, vol. 68, pp. 457–461, 1990.

[28] K. Horsfield and G. Cumming, "Morphology of the bronchial tree in man," *Journal of Applied Physiology*, vol. 38, pp. 990–1975, 1975.

[29] J. R. Hotchkiss, P. S. Crooke, A. B. Adams, and J. J. Marini, "Implications of a biphasic two-compartment model of constant flow ventilation for the clinical setting," *Journal of Critical Care*, vol. 9, pp. 114–123, 1994.

[30] A. Huszcuzuk, "A respiratory pump controlled by phrenic nerve activity," *J. Physiol.*, vol. 210, no. 2, pp. 183–184, 1970.

[31] R. H. Kallet, A. R. Campell, R. A. Dicker, J. A. Katz, and R. C. Mackersie, "Effects of tidal volume on work of breathing during lung-protective ventilation in patients with acute lung injury and acute respiratory distress syndrome," *Crit. Care Med.*, vol. 34, pp. 8–14, 2006.

[32] H. B. Keller, *Numerical Solution of Two-Point Boundary Value Problems*. Society for Industrial Mathematics, 1987.

[33] D. Kirk, *Optimal Control Theory*. New Jersey: Prentice-Hall Inc., 1970.

[34] H. Kitaoka and B. Suki, "Branching design of the bronchial tree based on a diameter-flow relationship," *Journal of Applied Physiology*, vol. 82, pp. 968–976, 1997.

[35] K. A. KJ and B. Wittenmark, *Adaptive Control*. MA: Addison-Wesley: Reading, 1989.

[36] M. Kvasnica, P. Grieder, and M. Baotić, "Multi-Parametric Toolbox (MPT)," 2004.

[37] T. P. Laubscher, W. Heinrichs, and N. Weiler, "An adaptive lung ventilation controller," *IEEE Trans. Biomed. Eng*, vol. 41, no. 1, pp. 51–59, 1994.

[38] J. H. Lee, S. Natarajan, and K. S. Lee, "A model-base prediction control approach to repetitive control of continuous processes with periodic operations," *Journal of Process Control*, vol. 11, pp. 195–207, 2001.

[39] F. Lellouche, J. Mancebo, P. Jolliet, J. Roeseler, F. Shortgen, M. Dojat, B. Cabello, L. Bouadma, P. Rodriguez, S. maggiore, M. Reynaert, S. Mersmann, and L. Brochard, "A multicenter randomized trial of computer-driven protocolized weaning from mechanical ventilation," *Amer. J. Resp. Crit. Care Med.*, vol. 174, pp. 894–900, Jul. 2006.

[40] H. Li and W. M. Haddad, "Optimal determination of respiratory air flow patterns using a nonlinear multi-compartment model for a lung-rib-cage system," in *Proc. Amer. Contr. Conf.*, San Francisco, CA, pp. 3524–3529, 2010.

[41] H. Li and W. M. Haddad, "Optimal determination of respiratory airflow patterns using a nonlinear multicompartment model for a lung mechanics system," *Computational and Mathematical Methods in Medicine*, vol. 2012, pp. 1–11, 2012.

[42] P. Lu, "Constrained tracking control of nonlinear systems," *Sys. Contr. Lett.*, vol. 27, pp. 305–314, 1996.

[43] M. Mahfouf, *Intelligent Systems Modeling And Decision Support in Bioengineering (Engineering in Medicine & Biology)*. Artech House, 1 ed., 2006.

[44] J. J. Marini and P. S. Crooke, "A general mathematical model for respiratory dynamics relevant to the clinical setting," *American Review of Respiratory Disease*, vol. 147, pp. 14–24, 1993.

[45] L. Martin, *Pulmonary Physiology in Clinical Practice*. St. Louis, MO: Mosby, 1987.

[46] S. Martinez, G. Michon, and J. S. Martin, "Inverse of strictly ultrametric matrices are of Stieltjes type," *SIAM J. Matrix Anal. Appl.*, vol. 15, pp. 98–106, 1994.

[47] D. Q. Mayne and H. Michalska, "Adaptive receding horizon control for constrained nonlinear systems," in *Proc. IEEE Conf. Dec. Contr.*, San Antonio, Texas, pp. 1286–1291, 1993.

[48] D. Q. Mayne, J. B. Rawlings, C. V. Rao, and P. O. M. Scokaert, "Constrained model predictive control: Stability and optimality," *Automatica*, vol. 36, pp. 789–814, 2000.

[49] M. McGregor and M. R. Becklake, "The relationship of oxygen cost of breathing to respiratory mechanical work and respiratory force," *The Journal of Clinical Investigation*, vol. 40, pp. 971–980, 1961.

[50] O. Moerer, J. Beck, L. Brander, R. Costa, M. Quintel, A. S. Slutsky, F. Brunet, and C. Sinderby, "Subject-ventilator synchrony during neural versus pneumatically triggered non-invasive helmet ventilation," *Intens. Care Med.*, vol. 34, no. 9, pp. 1615–1623, 2008.

[51] K. S. Narendra and A. M. Annaswamy, *Stable Adaptive Systems*. Englewood Cliffs, NJ: Prentice-Hall, 1989.

[52] J. O. Nilsestuen and K. D. Hargett, "Using ventilator graphics to identify patient-ventilator asynchrony," *Respiratory Care*, vol. 50, pp. 202–234, 2005.

[53] A. B. Otis, W. O. Fenn, and H. Rahn, "Mechanics of the breathing in man," *Journal of Applied Phsiology*, vol. 2, pp. 592–607, 1950.

[54] S. P. Pilbeam and J. M. Cairo, *Mechanical Ventilation, Physiological and Clinical Applications*. St. Louis, MO: Mosby, 4 ed., 1987.

[55] D. F. Proctor, "Studies of respiratory air flow in measurement of ventilatory function," *Chest*, vol. 4, pp. 432–446, 1952.

[56] F. Rohrer, "Physilogie der atembewegung," *Handuch der Normalen und Pathologischen Physiologie*, vol. 2, pp. 70–127, 1925.

[57] L. F. Shampine, J. Kierzenka, and M. W. Reichelt, *Solving Boundary Value Problems for Ordinary Differential Equations in MATLAB with bvp4c*. Math Works Inc., 2000. `http://www.mathworks.com/bvp_tutorial`.

[58] T. Similowski and J. H. Bates, "Two-compartment modeling of respiratory system mechanics at low frequencies: Gas redistribution or tissue rheology," *European Respiratory Journal*, vol. 4, pp. 353–358, 1991.

[59] C. Sinderby, P. Navalesi, and J. Beck, "Neural control of mechanical ventilation in respiratory failure," *Natural Medicines*, vol. 5, no. 12, pp. 1433–1436, 1999.

[60] S. N. Singh, M. Steinberg, and R. D. DiGirolamo, "Nonlinear predictive control of feedback linearizable systems and flight control system design," *J. Guidance, Control, and Dynamics*, vol. 18, pp. 1023–1028, 1995.

[61] J. Slane and S. Tragesser, "Analysis of periodic nonautonomous inhomogeneous systems," *Nonlinear Dynamics and Systems Theory*, vol. 11, pp. 183–198, 2011.

[62] M. Soroush and C. Kravaris, "A continuous-time formulation of nonlinear model predictive control," *Int. J. Contr.*, vol. 63, pp. 121–146, 1996.

[63] F. T. Tehrani, "Automatic control of an artificial respirator," in *Proc. Int. Conf. IEEE Eng. Med. Biol. Soc.*, vol. 13, pp. 1738–1739, Nov., 1991.

[64] K. Thulasiraman and M. N. S. Swamy, *Graphs: Theory and Algorithms*. Wiley-Interscience, 1992.

[65] M. J. Tobin, *Principles and Practice of Mechanical Ventilation*. New York: McGraw-Hill, 1994.

[66] K. Y. Volyanskyy, W. M. Haddad, and J. M. Bailey, "Pressure- and work-limited neuroadaptive control for mechanical ventilation of critical care patients," *IEEE Trans. Neural Networks*, vol. 22, pp. 614–626, 2011.

[67] A. A. Wald, T. W. Murphy, and V. D. Mazzia, "A theoretical study of controlled ventilation," *IEEE Trans. Biomed. Eng.*, vol. 15, pp. 237–248, 1968.

[68] E. R. Weibel, *Morphometry of the Human Lung*. New York: Academic Publishers, 1963.

[69] J. B. West, *Respiratory Physiology*. Baltimore, MD: Williams & Wilkins, 2008.

[70] S. Wiggins, *Introduction to Applied Nonlinear Dynamical Systems and Chaos*. New York: Springer, 2 ed., 2003.

[71] S. M. Yamashiro and F. S. Grodins, "Optimal regulation of respiratory airflow," *Journal of Applied Physiology*, vol. 30, pp. 597–602, 1971.

[72] M. Younes, "Proportional assist ventilation, a new approach to ventilatory support: Theory," *Amer. Rev. Resp. Des.*, vol. 145, no. 1, pp. 114–120, 1992.

[73] M. Younes, *Principles and Practice of Mechanical Ventilation*, ch. Proportional Assist Ventilation. In Tobin M. J. (ed.), pp. 349–369. New York: McGraw-Hill, 1994.

[74] M. Younes, A. Puddy, and D. Roberts, "Proportional assist ventilation. Results of an initial clinical trial," *American Review of Respiratory Desease*, vol. 145, pp. 121–129, 1992.

Vita

Hancao Li received Bachelors of Science and Masters of Science degrees in Automation Engineering with specialization in testing measure technology and instrumentation from Shanghai University, China in 2001 and 2004, respectively. After working in Hyron Software Inc. for one year as a software engineer, in 2005 she was admitted to the University of Tennessee, Knoxville, TN, to pursue her Masters of Science degree in Mechanical Engineering, which she received in May 2008. In 2008, she joined the School of Aerospace Engineering at Georgia Institute of Technology, Atlanta, GA, to pursue here Doctoral degree in Aerospace Engineering, with specialization in dynamical systems and control. In 2011 she obtained Masters of Science degree in Mathematics from the Georgia Institute of Technology.

Her research interests include stability theory for linear and nonlinear dynamical systems, model predictive control, adaptive control, and optimal control theory. Her applied areas of interests are in the analysis and control design of automated mechanical ventilation systems for patients in the intensive care units. She also has a strong interest in the areas of the analysis and control design of biomedical and biological systems.